NASA TM X-1075

TRANSONIC AERODYNAMIC CHARACTERISTICS OF A SUPERSONIC TRANSPORT MODEL WITH VARIABLE-SWEEP AUXILIARY WING PANELS, OUTBOARD TAIL SURFACES, AND A DESIGN MACH NUMBER OF 2.6

By Roy V. Harris, Jr., and William A. Corlett

Langley Research Center
Langley Station, Hampton, Va.

NATIONAL AERONAUTICS AND SPACE ADMINISTRATION

TRANSONIC AERODYNAMIC CHARACTERISTICS OF A SUPERSONIC TRANSPORT MODEL WITH VARIABLE-SWEEP AUXILIARY WING PANELS, OUTBOARD TAIL SURFACES, AND A DESIGN MACH NUMBER OF 2.6*

By Roy V. Harris, Jr., and William A. Corlett
Langley Research Center

SUMMARY

The investigation was made in the Langley 8-foot transonic pressure tunnel at Mach numbers from 0.50 to 1.30 to determine the longitudinal aerodynamic characteristics of the SCAT 15-2.6 configuration at transonic speeds. The configuration, which was developed to explore the design requirements for an acceptable supersonic transport aircraft, has a blended wing-body, variable-sweep auxiliary wing panels, outboard tail surfaces, four engine nacelles, and a design Mach number of 2.6. Tests were made for auxiliary wing sweep angles of 35°, 45°, 55°, and 75°.

The results indicate that throughout the transonic speed range, the effect of the drag rise on the aerodynamic efficiency of the configuration can be minimized and the relatively high values of untrimmed lift-drag ratio can be obtained by varying the sweep angle of the auxiliary wing panels from 35° to 55°. The total rearward shift of the aerodynamic center is about 13 percent of the mean geometric chord between a Mach number of 0.80 at a sweep angle of 35° and a Mach number of 1.20 at a sweep angle of 55°. The configuration has a relatively large positive zero-lift pitching moment for all the Mach numbers and auxiliary wing sweep angles investigated. Deflection of the horizontal tails provides a linear variation in pitch control effectiveness which is generally constant throughout the range of lift coefficients.

[redacted] AUTHOR →

INTRODUCTION

As part of an extensive research program to define and meet the design requirements of a commercially acceptable supersonic transport aircraft, the National Aeronautics and Space Administration is continuing its study of configuration concepts which indicate a potential for high aerodynamic efficiency. One of the configuration concepts under study (SCAT 15) has a highly swept wing

---

*[redacted]

which is twisted and cambered to produce a near-optimum loading at the design Mach number and which is blended with the fuselage to minimize the drag. The configuration also has variable-sweep auxiliary wing panels that can be either fully retracted to form part of the basic fixed wing for high-speed flight or swept forward to increase the aerodynamic efficiency for low-speed flight. Both the horizontal and vertical tail surfaces are mounted on the wing at the tips of the fixed panels with the horizontal surfaces outboard of the vertical surfaces. The four engine nacelles are mounted on the wing lower surface near the trailing edge.

The SCAT 15-A, an early version of the SCAT 15 concept, had a design Mach number of 3.0 but did not employ wing twist and camber. This model has been tested at subsonic, transonic, and supersonic speeds, and the results of these tests are presented in references 1, 2, and 3. A second version of the concept which was optimized for a Mach number of 2.2 (SCAT 15-2.2) has been tested at supersonic speeds with the auxiliary wing panels fully retracted, and these results are presented in reference 4. An additional version of the SCAT 15 concept which was optimized for a Mach number of 2.6 (SCAT 15-2.6) has also been tested. The results of the tests at supersonic speeds for the configuration with the auxiliary wing panels fully retracted are presented in reference 5. Results of the low-subsonic-speed tests on the same configuration are presented in reference 6. This report presents the results of the tests on the SCAT 15-2.6 configuration at transonic speeds.

SYMBOLS

All data presented herein are referred to the stability-axis system. The moment center is on the model reference line at a longitudinal station corresponding to 75.91 percent of the body length. The coefficients and symbols are defined as follows:

C_D	drag coefficient, $\frac{\text{Drag}}{qS}$
C_L	lift coefficient, $\frac{\text{Lift}}{qS}$
C_{L_α}	lift-curve slope, per deg
C_m	pitching-moment coefficient, $\frac{\text{Pitching moment}}{qS\bar{c}}$
$\partial C_m/\partial C_L$	longitudinal stability parameter
$\bar{c}$	mean geometric chord of reference wing, 15.666 in.
L/D	lift-drag ratio

M	free-stream Mach number
q	free-stream dynamic pressure, lb/sq ft
R	radius, in.
S	reference wing area, 219.464 sq in.
α	angle of attack of model reference line, deg
δ_h	horizontal-tail deflection angle relative to model reference line (positive when trailing edge is down)
Λ	sweep angle of auxiliary wing panels, deg

Subscripts:

b	base
i	internal
max	maximum
min	minimum

MODELS AND APPARATUS

The model details and dimensions are shown in figure 1, and the geometric characteristics are given in table I. Photographs of the models are shown in figures 2 and 3. The two models were identical except that the auxiliary wing panels were fixed in the 75° sweep positions and the wing surfaces were smoothly faired on the first model, while the auxiliary wing panels were movable through a sweep-angle range from 25° to 75° on the second model. The first model was constructed with fixed auxiliary wing panels to get an early determination of the aerodynamic characteristics of the SCAT 15-2.6 with the wings fully swept. The surface discontinuities produced by the overlapping wing surfaces were unfaired on the model with movable auxiliary wing panels. Both models were constructed so that the horizontal-tail surfaces could be adjusted to various deflection angles. A conical inlet spike was mounted in each of the nacelles in order to simulate the transonic spillage requirements of the supersonic engine installation. (See fig. 1(d).)

The models were mounted on a remotely controlled sting in the Langley 8-foot transonic pressure tunnel, and the force and moment data were measured with a six-component internal strain-gage balance. In order to minimize the model base and sting interference effects on the highly swept wing and tail surfaces, a fairing was attached to the sting about 1/8 inch aft of each model base. (See figs. 2 and 3.) The fairing was contoured so that the model lines at the fuselage base were continued to a point where they intercepted the sting.

TESTS AND CORRECTIONS

The tests were conducted at Mach numbers of 0.50, 0.80, 0.90, 0.94, 1.03, 1.20, and 1.30. Data were obtained at auxiliary-wing sweep angles of 35°, 45°, and 55° on the model with movable auxiliary wing panels and 75° on the model with fixed auxiliary wing panels. The horizontal-tail deflection angle was varied from -2° to -10°. In order to provide turbulent boundary layers on the models at the test conditions, transition strips were applied of No. 60 carborundum grit near the nose of the fuselage and No. 80 grit near the leading edges of the wing, tails, nacelles, and spikes. The Reynolds number based on the wing mean geometric chord was 2.87×10^6. A constant stagnation temperature of 120° F was maintained throughout the tests, and the dewpoint was held sufficiently low to prevent condensation effects in the test section. The stagnation pressure for each Mach number is shown in the following table:

Mach number	Stagnation pressure, lb/sq ft
0.50	1689
.80	1235
.90	1174
.94	1154
1.03	1131
1.20	1104
1.30	1109

The tests were made through an angle-of-attack range from about -4° to 6° at the highest Mach number and from about -4° to 9° at the lowest Mach number. The angles of attack have been corrected for the deflections of the balance and sting under load and for the test-section flow angularity. The balance chamber pressure and the fuselage, nacelle, and spike base pressures were measured and the drag data have been adjusted to a base pressure equal to free-stream static pressure. An additional buoyancy correction was made to the drag data at a Mach number of 1.30. This correction was necessary because at this Mach number about 18 inches of the model nose extended into the tunnel Mach number gradient upstream of the test section. A drag-coefficient reduction of 0.0005 resulted from this additional buoyancy correction.

The interference effects of the tunnel boundary on the flow over the models in the slotted test section of the Langley 8-foot transonic pressure tunnel are believed to be negligible at all the test Mach numbers. (See ref. 7.) Although the results of reference 7 and other unpublished data indicate the probability that at $M = 1.20$ a reflected shock from the nose of the model may have impinged on a small region of the model near the wing tips, based on Schlieren observations made during the tests, these effects are believed to be negligible.

Total-pressure and static-pressure measurements were taken at each duct exit to determine the mass flow through the spiked nacelles and the internal

drag. All the internal total-pressure measurements were taken outside the duct boundary layer so that the internal drag based on the pressure measurements alone would not account for the internal skin friction. The internal skin friction was estimated by means of the Kármán-Schoenherr incompressible formula and the Sommer and Short T' method. (See ref. 8.) The internal drag of the nacelles has been subtracted from the drag data and the net external drag is presented. Figure 4 shows the variation of the total base drag and internal drag coefficients with angle of attack. (The internal drag is the sum of the measured and calculated values.)

RESULTS AND DISCUSSION

The effects of auxiliary wing sweep angle on the longitudinal aerodynamic characteristics of the configuration at transonic speeds are shown in figures 5 to 11. For this portion of the tests, the horizontal-tail deflection angle was set at -2°, and was alined approximately with the tip chord of the fixed wing panel. With this horizontal-tail setting, the configuration has a relatively large positive zero-lift pitching moment for all the Mach numbers and auxiliary wing sweep angles investigated. The variations of the pitching-moment coefficient at the lowest Mach number ($M = 0.50$) indicate a tendency toward longitudinal instability at a sweep angle of 35° which generally diminishes with increasing auxiliary wing sweep angle. At the higher Mach numbers (M greater than about 0.80), the tendency toward instability disappears at the three lowest auxiliary wing sweep angles. The slight tendency toward instability which remains for the configuration at an auxiliary wing sweep angle of 75° is generally confined to a range of lift coefficients above that for maximum lift-drag ratio.

The variations of untrimmed $(L/D)_{max}$ and $C_{D,min}$ with Mach number shown in figure 12 indicate one of the primary advantages of the variable-sweep auxiliary wing panels. As was the case with the SCAT 15-A configuration (ref. 2), the effect of the transonic drag rise on the aerodynamic efficiency of the SCAT 15-2.6 can be minimized and relatively high values of untrimmed lift-drag ratio can be obtained throughout the transonic speed range by varying the sweep angle of the auxiliary wing panels from 35° to 55°.

The characteristic increase in the effect of wing sweep angle on minimum drag as the Mach number becomes supersonic can be seen in figure 13. The relatively small increase in the minimum drag coefficient with decreasing auxiliary wing sweep angle at the lower Mach numbers is due primarily to the increasing amount of surface area that is exposed to the free stream as the auxiliary wing panels are swept forward. As the supersonic speeds are approached, however, the more pronounced effect is due primarily to the additional increase in wave drag as the auxiliary wing panels are extended.

The effect of Mach number on the longitudinal stability parameter $\partial C_m / \partial C_L$ and the lift-curve slope C_{L_α} is shown in figure 14 for the various auxiliary wing sweep angles. As would be expected, the longitudinal stability of the

SCAT 15-2.6 model is increased because of the rearward shift in aerodynamic center as Mach number is increased through the transonic speed range. The total rearward shift of the aerodynamic center is about 13 percent of the mean geometric chord between a Mach number of 0.80 at a sweep angle of 35° and a Mach number of 1.20 at a sweep angle of 55°. The variation of $\partial C_m/\partial C_L$ with auxiliary wing sweep angle shown in figure 15 indicates increases in the stability level with increasing sweep angle throughout the Mach number range. The characteristically large change in C_{L_α} with wing sweep can also be seen.

The effects of horizontal-tail deflection on the longitudinal aerodynamic characteristics at transonic speeds for the configuration with the auxiliary wing panels at various sweep angles are shown in figures 16 to 43. At each test condition, deflection of the horizontal tails results in a linear variation in pitch control effectiveness which is generally constant throughout the range of lift coefficients. Also, as a result of the relatively large values of zero-lift pitching moment, the configuration requires a positive horizontal-tail deflection angle in order to trim at lift coefficients corresponding to $(L/D)_{max}$ for low Mach numbers and low sweep angles. (For example, see fig. 17 where $M = 0.80$ and $\Lambda = 35°$.) At the high Mach numbers and low sweep angles, however, a large negative horizontal-tail deflection angle is required in order to trim near the maximum lift-drag ratio. (For example, see fig. 28 where $M = 1.20$ and $\Lambda = 45°$.) As a result the trim penalty is severe. However, the trim requirement is reduced with increasing sweep angle. (For example, see fig. 43 where $M = 1.30$ and $\Lambda = 75°$.)

CONCLUDING REMARKS

The investigation was made in the Langley 8-foot transonic pressure tunnel at Mach numbers from 0.50 to 1.30 to determine the longitudinal aerodynamic characteristics of the SCAT 15-2.6 model. The configuration, which was developed to explore the design requirements for an acceptable supersonic transport aircraft, has a blended wing-body, variable-sweep auxiliary wing panels, outboard tail surfaces, four engine nacelles, and a design Mach number of 2.6. The tests were made over the transonic speed range for auxiliary wing sweep angles of 35°, 45°, 55°, and 75°.

The results indicate that throughout the transonic speed range the effect of the drag rise on the aerodynamic efficiency of the configuration can be minimized and the relatively high values of untrimmed lift-drag ratio can be obtained by varying the sweep angle of the auxiliary wing panels from 35° to 55°. The total rearward shift of the aerodynamic center is about 13 percent of the mean geometric chord between a Mach number of 0.80 at a sweep angle of 35° and a Mach number of 1.20 at a sweep angle of 55°. The configuration has a relatively large positive zero-lift pitching moment for all the Mach numbers and auxiliary wing sweep angles investigated. Deflection of the horizontal

tails provides a linear variation in pitch control effectiveness which is generally constant throughout the range of lift coefficients.

Langley Research Center,
National Aeronautics and Space Administration,
Langley Station, Hampton, Va., December 22, 1964.

REFERENCES

1. Spearman, M. Leroy; Driver, Cornelius; and Robins, A. Warner: Aerodynamic Characteristics at Mach Numbers of 2.30, 2.96, and 3.50 of a Supersonic Transport Model With a Blended Wing-Body, Variable-Sweep Auxiliary Wing Panels, and Outboard Tail Surfaces. NASA TM X-803, 1963.

2. Harris, Roy V., Jr.; and Corlett, William A.: Longitudinal Aerodynamic Characteristics at Mach Numbers From 0.50 to 1.20 of a Supersonic Transport Model With a Blended Wing-Body, Variable-Sweep Auxiliary Wing Panels, and Outboard Tail Surfaces. NASA TM X-837, 1963.

3. Alford, William J., Jr.; Hammond, Alexander D.; and Henderson, William P.: Low-Speed Stability Characteristics of a Supersonic Transport Model With a Blended Wing-Body, Variable-Sweep Auxiliary Wing Panels, Outboard Tail Surfaces, and Simplified High-Lift Devices. NASA TM X-802, 1963.

4. Driver, Cornelius; Spearman, M. Leroy; and Corlett, William A.: Aerodynamic Characteristics at Mach Numbers From 1.61 to 2.86 of a Supersonic Transport Model With a Blended Wing-Body, Variable-Sweep Auxiliary Wing Panels, Outboard Tail Surfaces, and a Design Mach Number of 2.2. NASA TM X-817, 1963.

5. Robins, A. Warner; Spearman, M. Leroy; and Harris, Roy V., Jr.: Aerodynamic Characteristics at Mach Numbers of 2.30, 2.60, and 2.96 of a Supersonic Transport Model With a Blended Wing-Body, Variable-Sweep Auxiliary Wing Panels, Outboard Tail Surfaces, and a Design Mach Number of 2.6. NASA TM X-815, 1963.

6. Henderson, William P.: Low-Speed Aerodynamic Characteristics of a Supersonic Transport Model With a Blended Wing-Body, Variable-Sweep Auxiliary Wing Panels, and Outboard Tail Surfaces. NASA TM X-993, 1964.

7. Wright, Ray H.; Ritchie, Virgil S.; and Pearson, Albin O.: Characteristics of the Langley 8-Foot Transonic Tunnel With Slotted Test Section. NACA Rep. 1389, 1958. (Supersedes NACA RM L51H10 by Wright and Ritchie and RM L51K14 by Ritchie and Pearson.)

8. Sommer, Simon C.; and Short, Barbara J.: Free-Flight Measurements of Turbulent-Boundary-Layer Skin Friction in the Presence of Severe Aerodynamic Heating at Mach Numbers From 2.8 to 7.0. NACA TN 3391, 1955.

TABLE I.- GEOMETRIC CHARACTERISTICS OF MODELS

Wing:	
Sweep angle of leading edge (fixed portion), deg	75
Sweep angle of trailing edge, deg	56.18
Aspect ratio ($\Lambda = 75^\circ$)	1.166
Span ($\Lambda = 75^\circ$), in.	16.0
Reference area, sq in.	219.464
Root chord, in.	22.674
Tip chord (including auxiliary wing panel at $\Lambda = 75^\circ$), in.	4.759
Mean aerodynamic chord, in.	15.666
Pivot location:	
Longitudinal distance from nose of model to pivot, in.	30.50
Lateral distance from model center line to pivot, in.	3.00
Fuselage:	
Length, in.	40.842
Balance-chamber area, sq in.	2.680
Horizontal tail:	
Area (both), sq in.	16.570
Thickness ratio	0.03
Airfoil section	Circular arc
Vertical tail:	
Area (both), sq in.	16.124
Thickness ratio	0.02
Airfoil section	Half circular arc
Nacelles:	
Length, in.	7.500
Base area (each), sq in.	0.749
Spike half-angle, deg	12.5
Spike base area (each), sq in.	0.0951
Inboard nacelle location:	
Cant angle	$0^\circ45'$
Longitudinal distance from model nose to lip of nacelle, in.	32.6
Lateral distance from model reference line to center line of nacelle lip, in.	2.500
Vertical distance from model reference line to nacelle center line, in.	0.937
Outboard nacelle location:	
Cant angle	$1^\circ30'$
Longitudinal distance from model nose to lip of nacelle, in.	38.1
Lateral distance from model reference line to center line of nacelle lip, in.	5.000
Vertical distance from model reference line to nacelle center line, in.	0.462

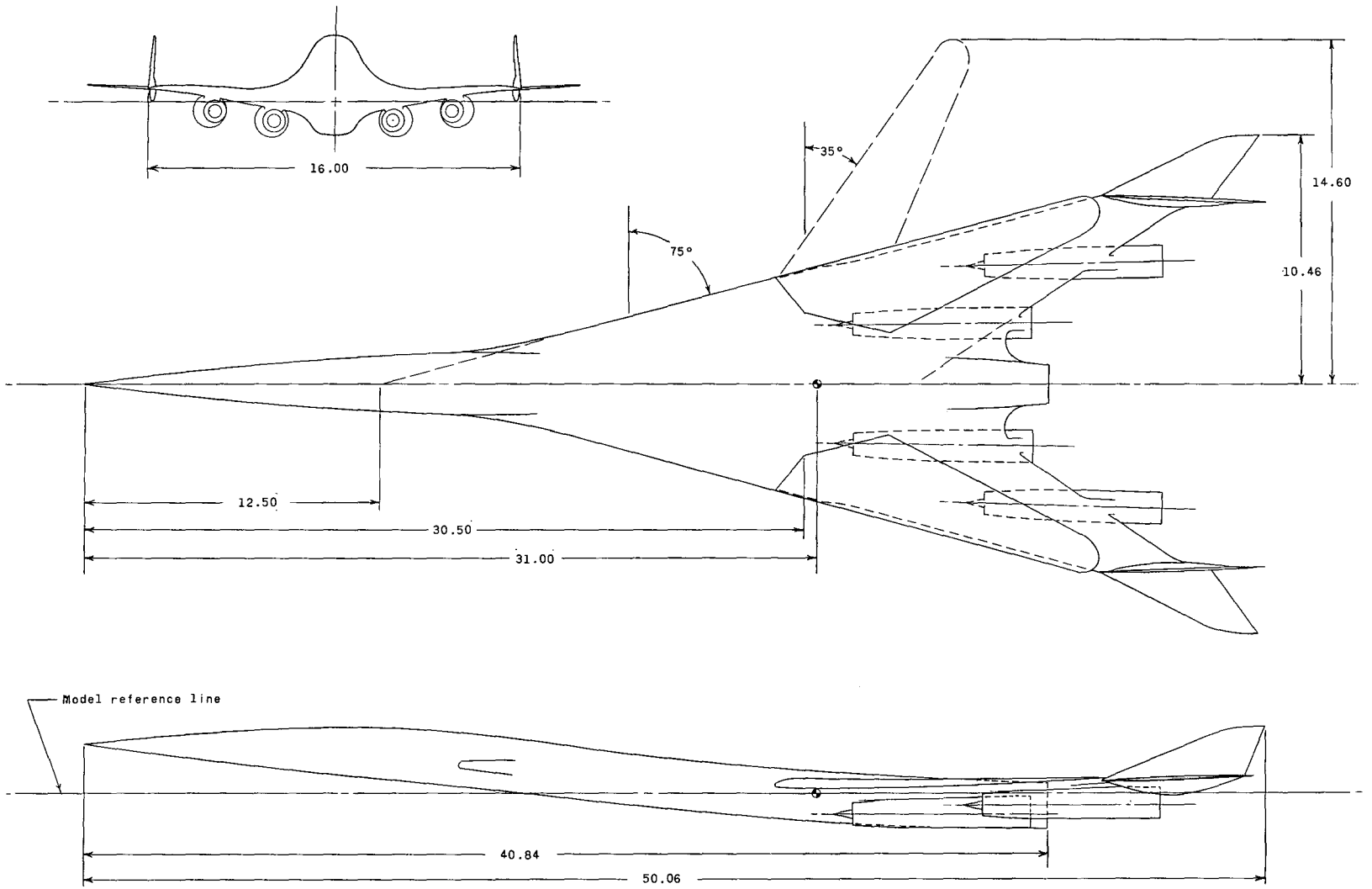

(a) Complete configuration.

Figure 1.- Details of model. All dimensions are in inches unless otherwise noted.

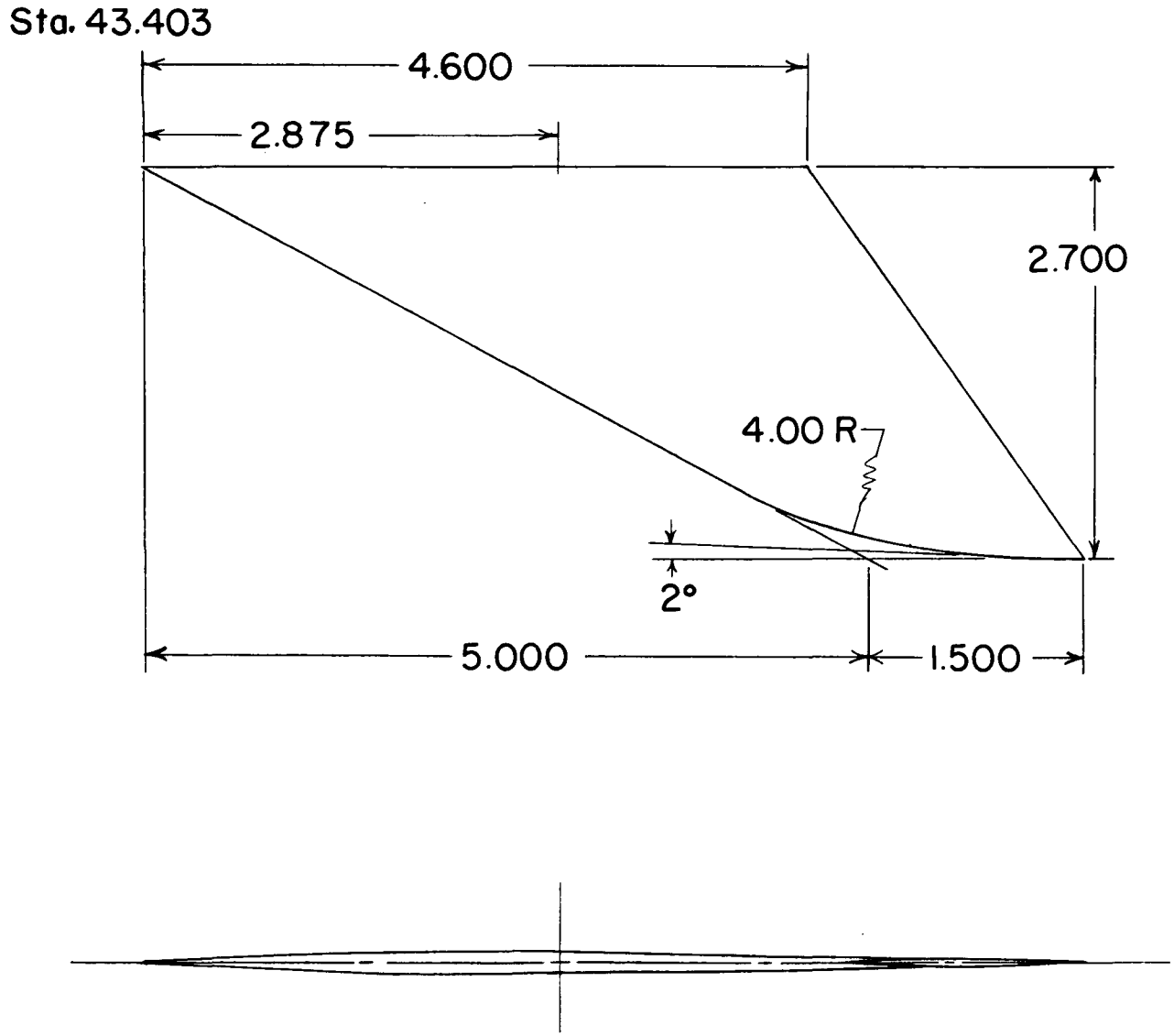

(b) Details of horizontal tail.

Figure 1.- Continued.

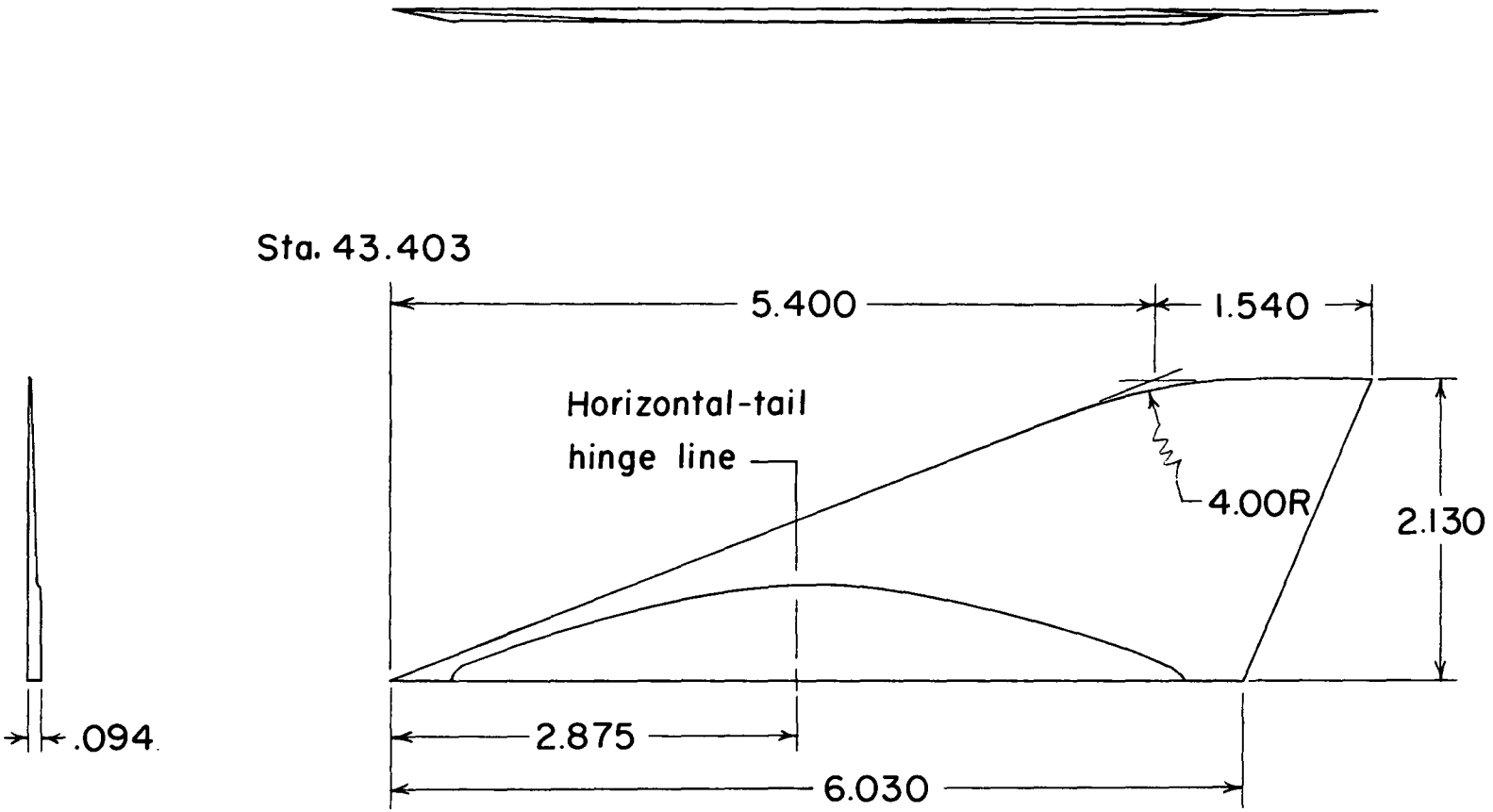

(c) Details of vertical tail.

Figure 1.- Continued.

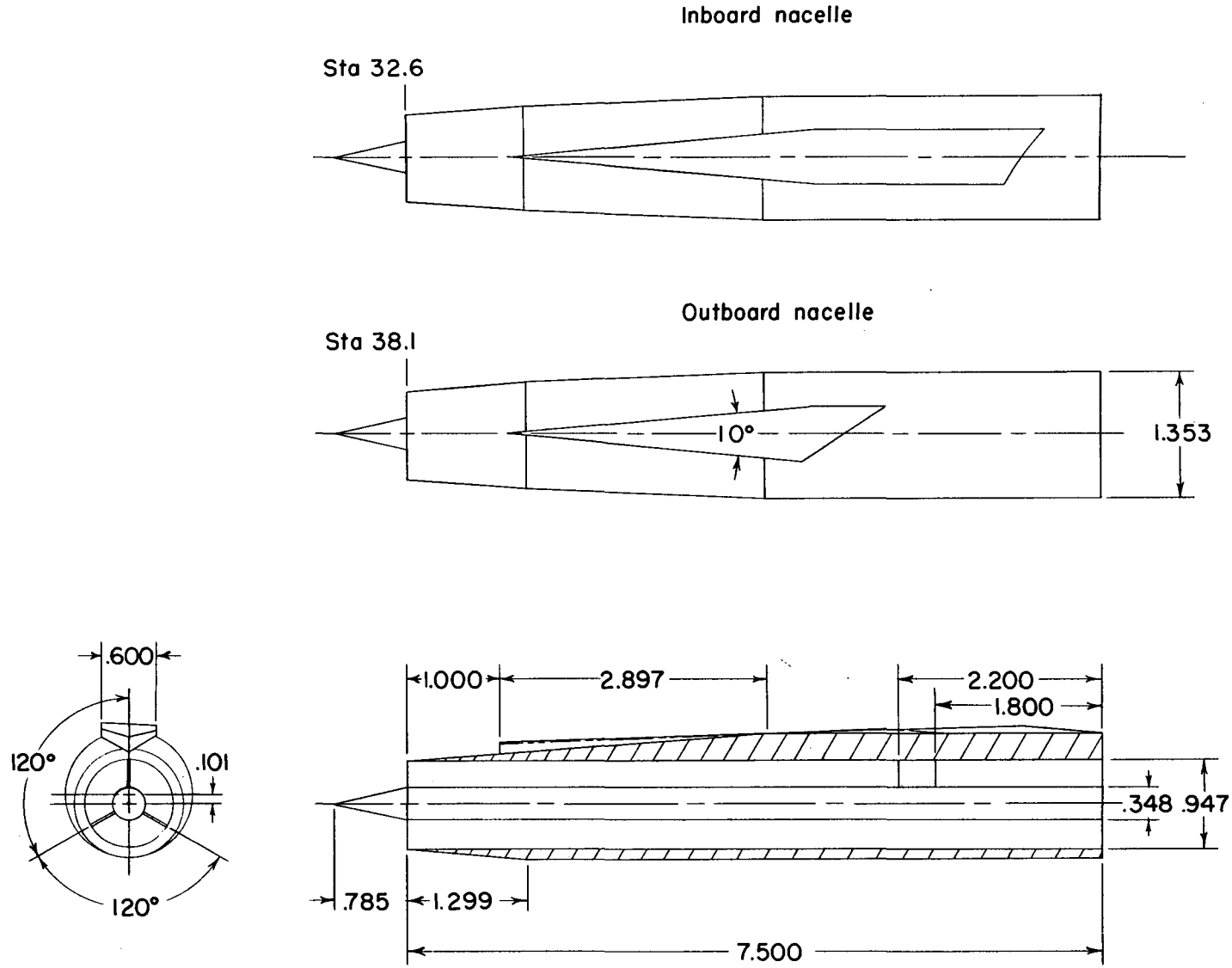

(d) Details of nacelles.

Figure 1.- Concluded.

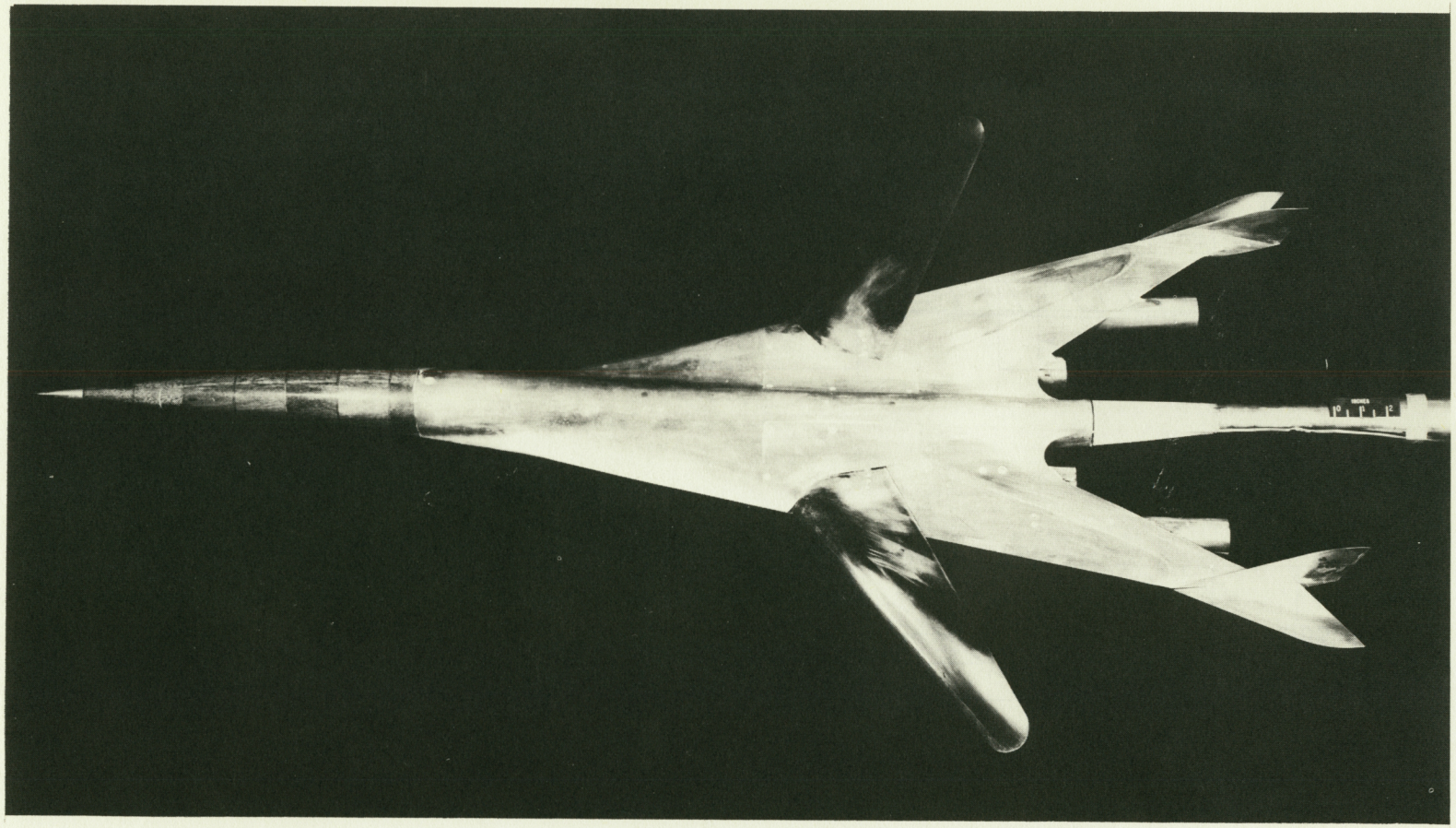

(a) $\Lambda = 35^{\circ}$.

Figure 2.- Photographs of model with movable auxiliary wing panels. L-63-2488

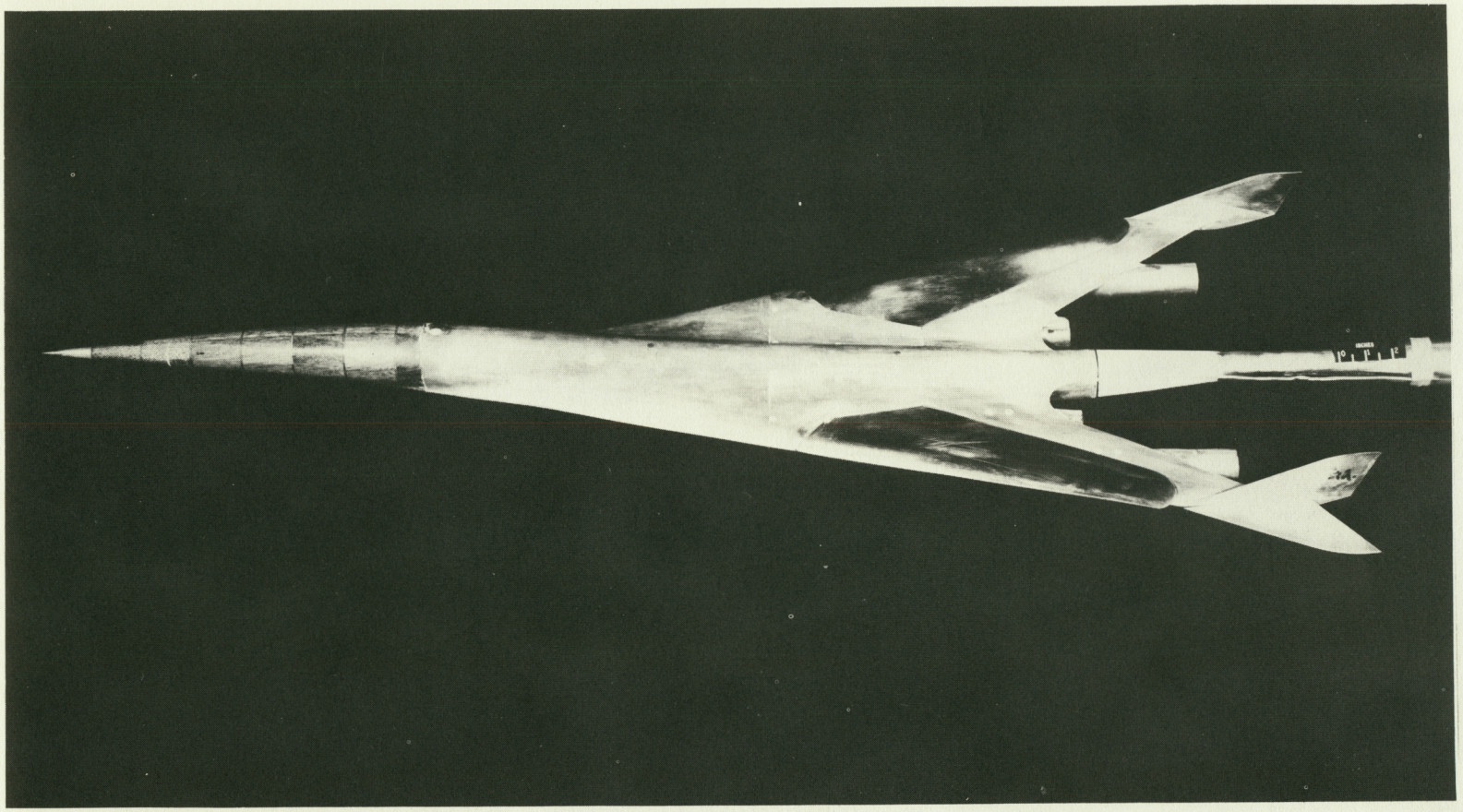

(b) $\Lambda = 75^{\circ}$.

Figure 2.- Concluded.

L-63-2491

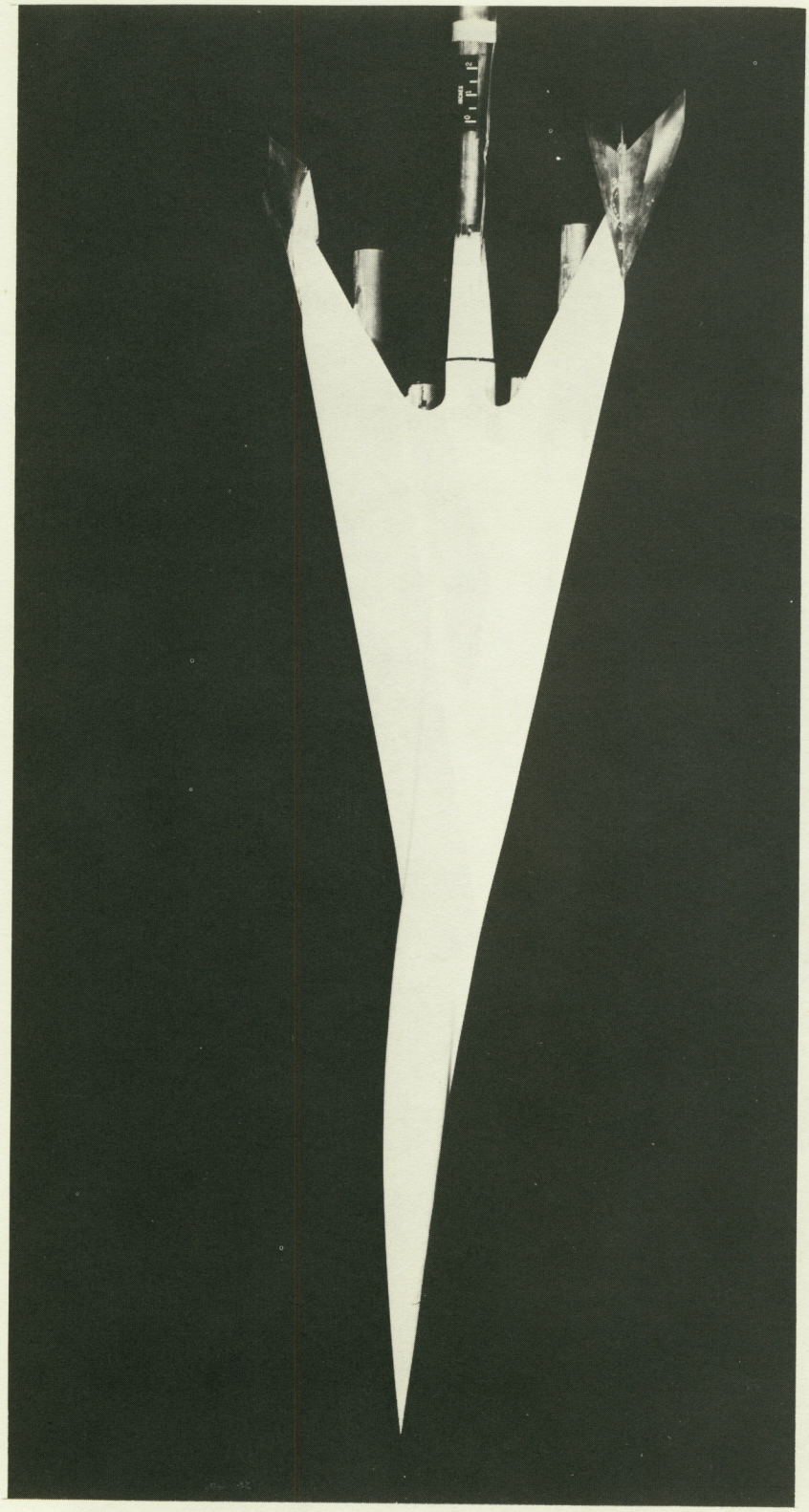

L-63-2489

Figure 3.- Photograph of model with fixed auxiliary wing panels.

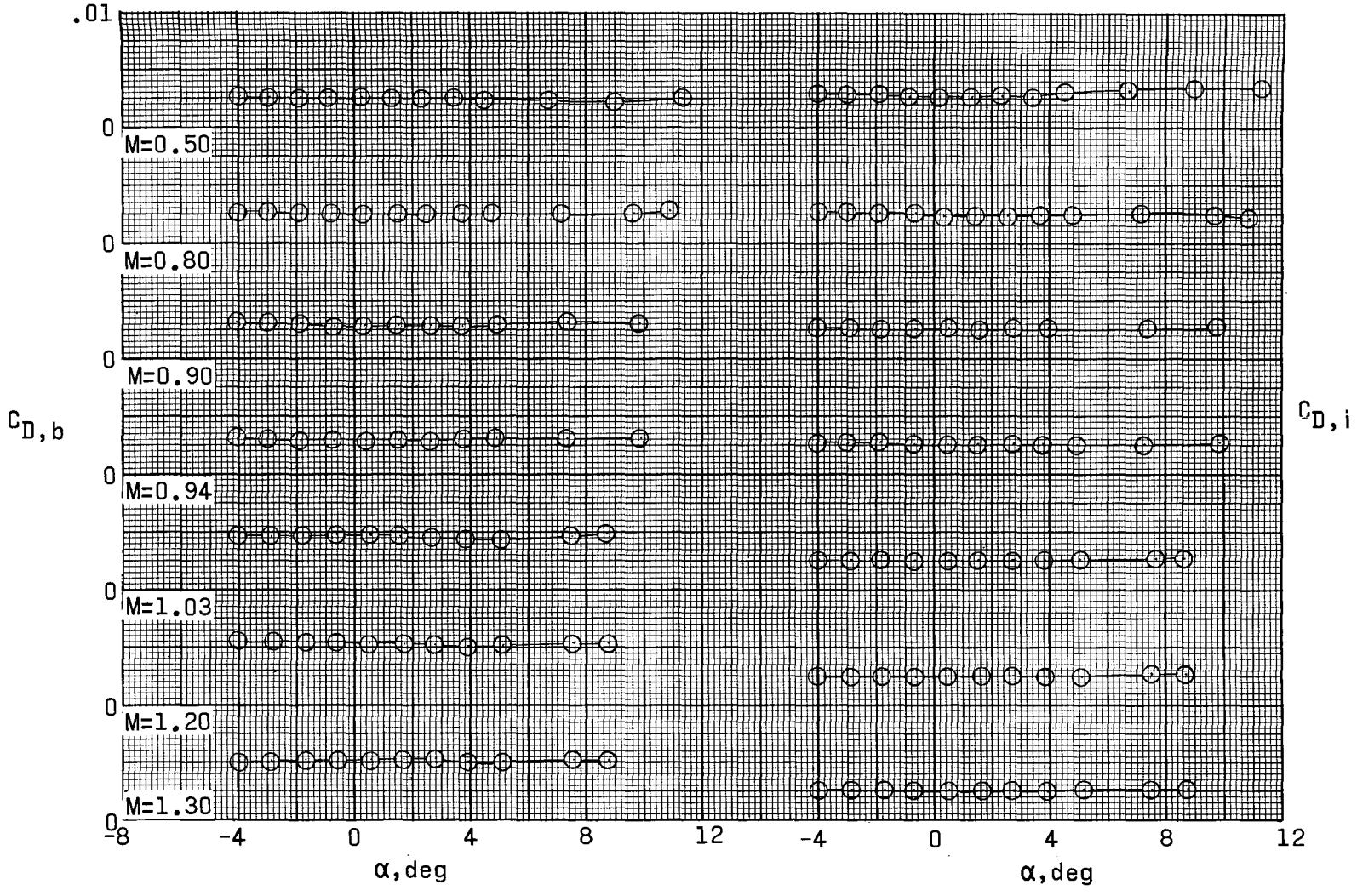

Figure 4.- Variation of total base drag and internal drag coefficients with angle of attack.

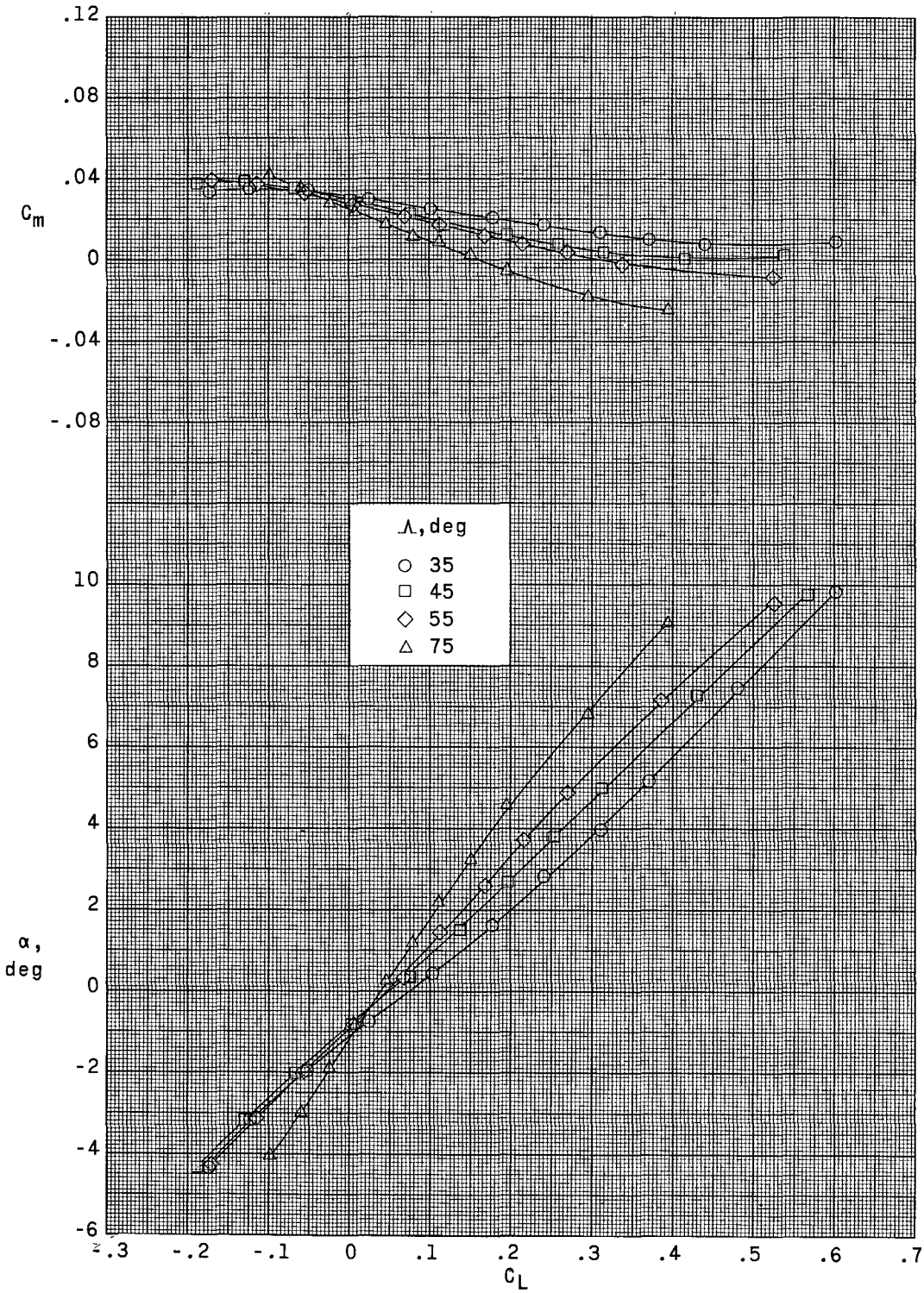

Figure 5.- Effect of auxiliary wing sweep angle on longitudinal aerodynamic characteristics at Mach number 0.50. $\delta_h = -2^o$.

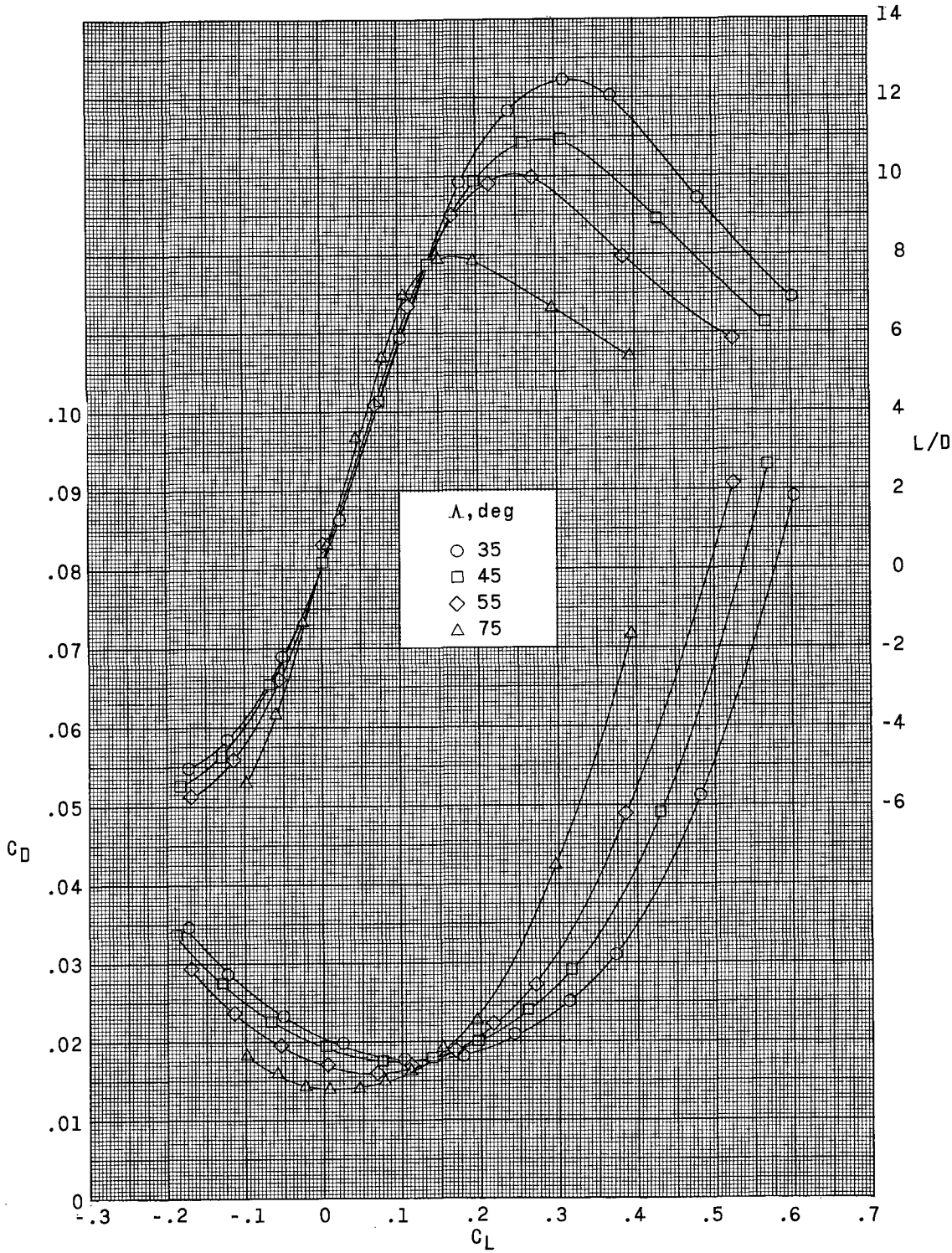

Figure 5.- Concluded.

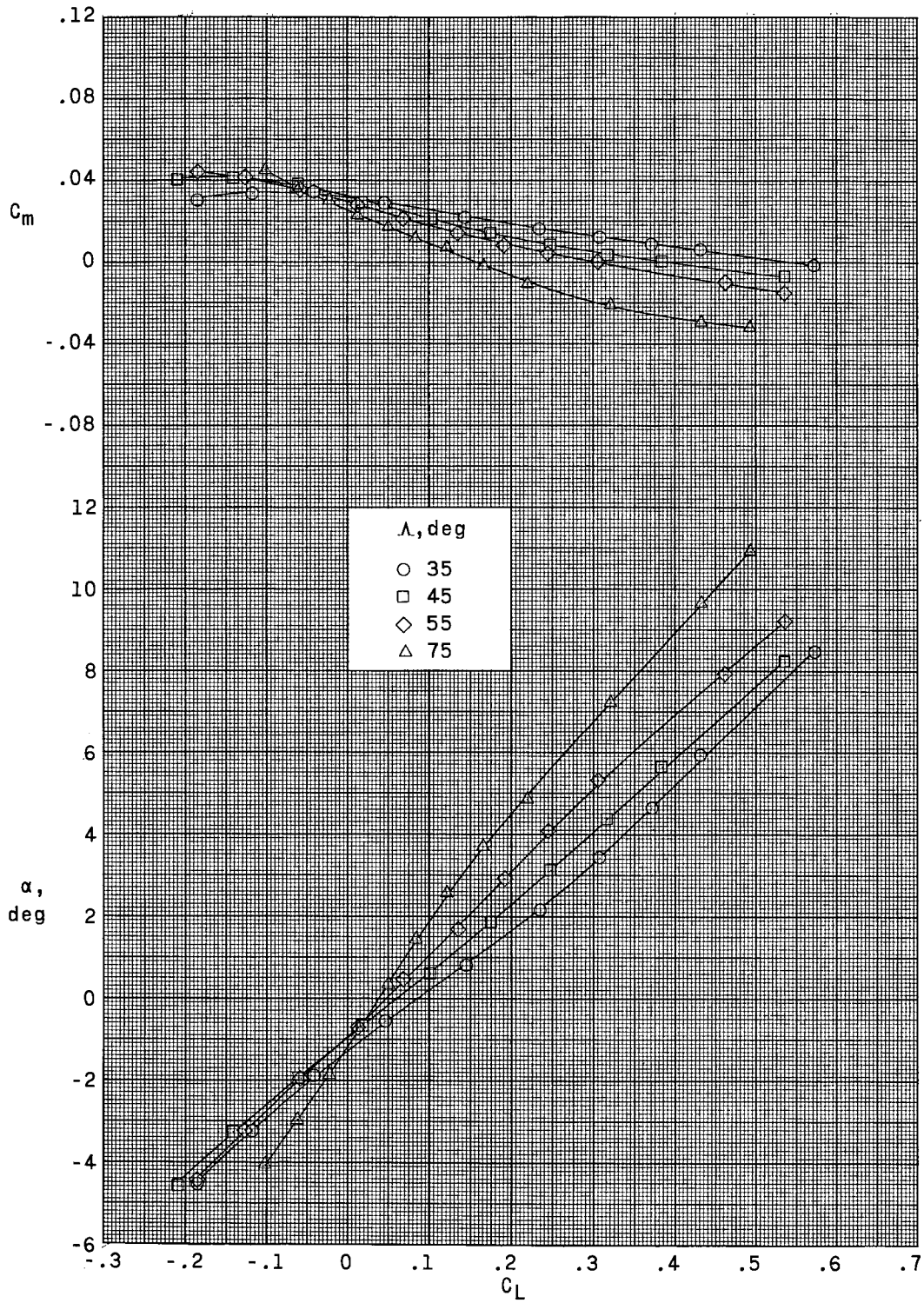

Figure 6.- Effect of auxiliary wing sweep angle on longitudinal aerodynamic characteristics at Mach number 0.80. $\delta_h = -2^\circ$.

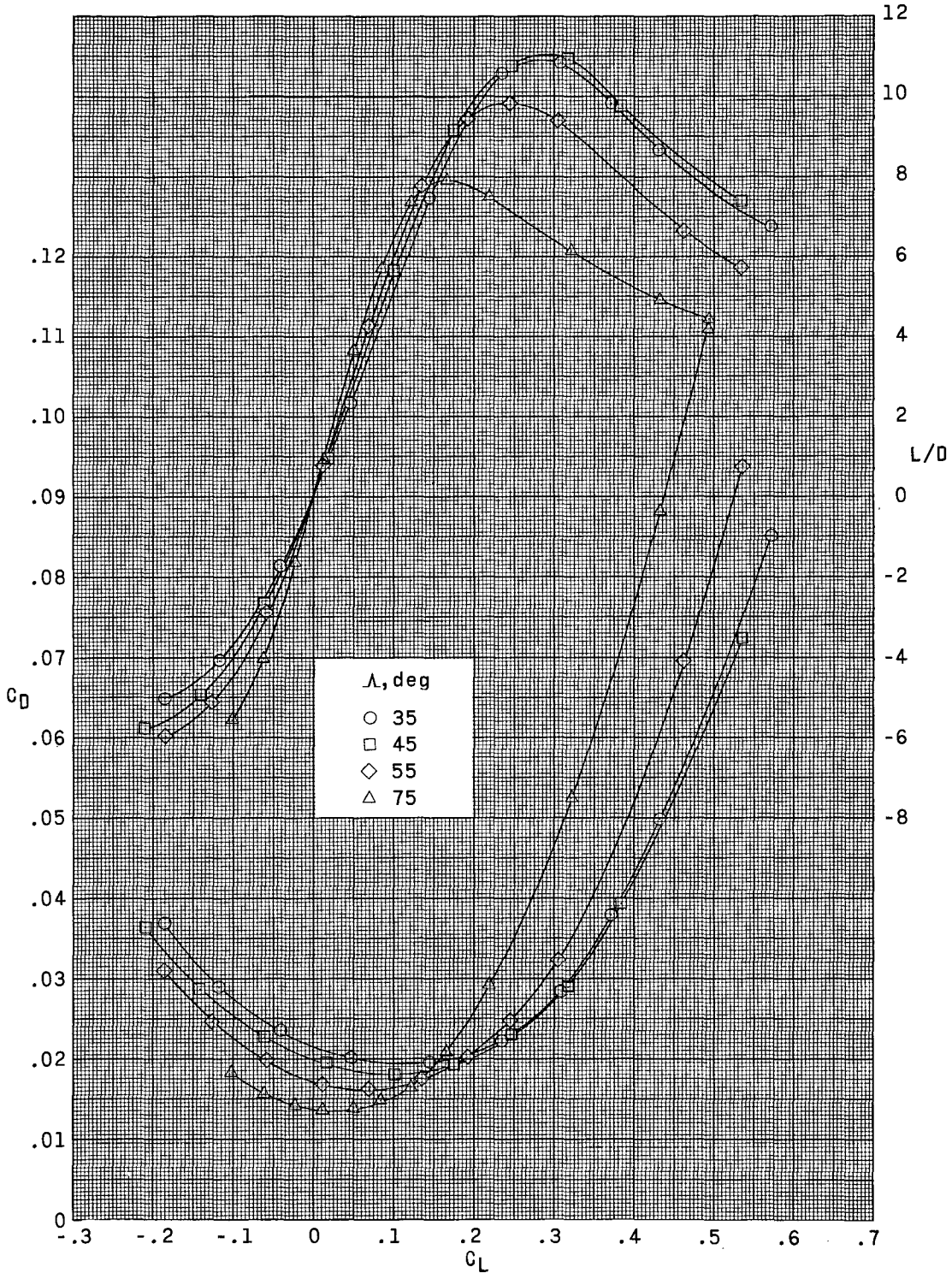

Figure 6.- Concluded.

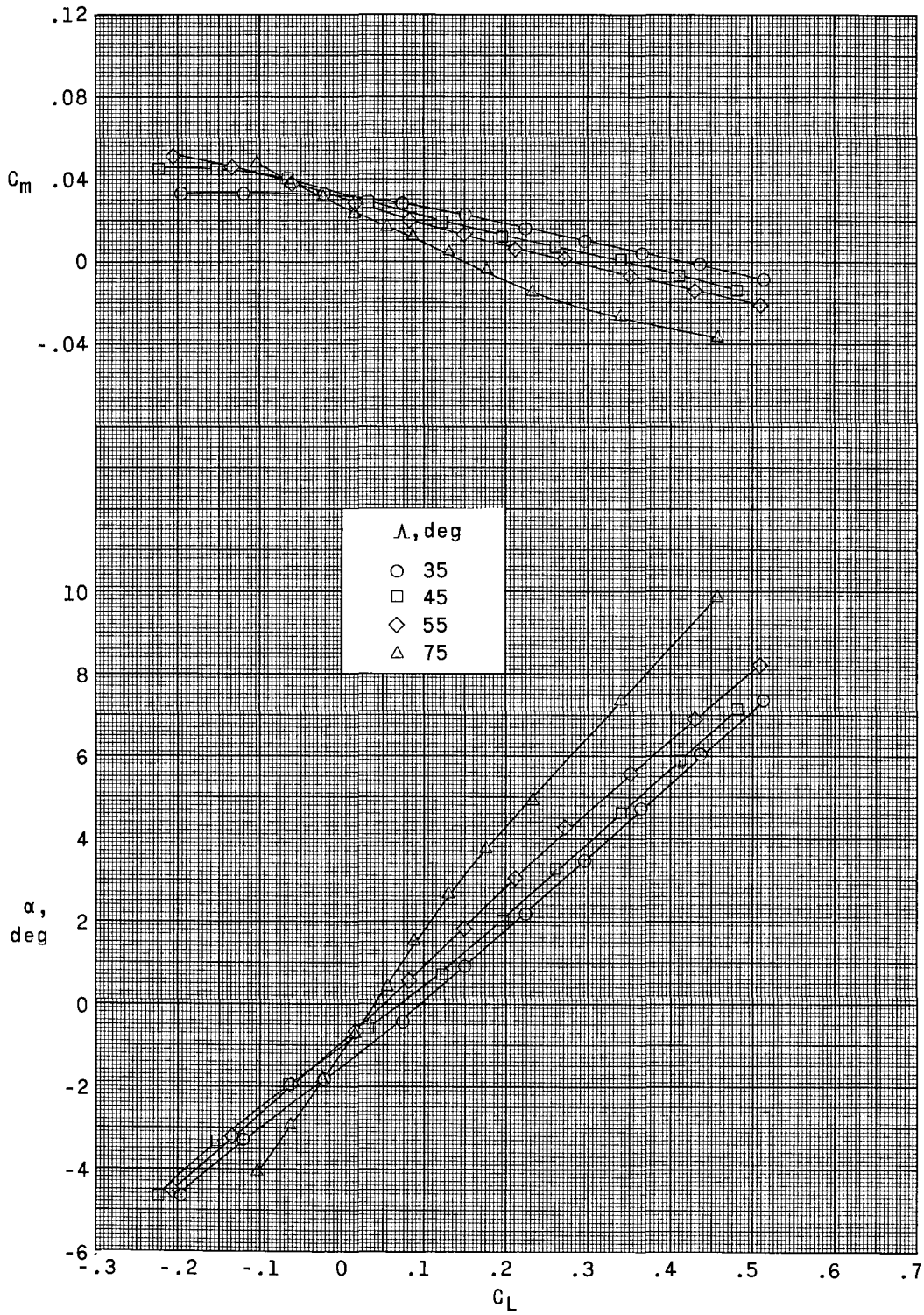

Figure 7.- Effect of auxiliary wing sweep angle on longitudinal aerodynamic characteristics at Mach number 0.90. $\delta_h = -2^\circ$.

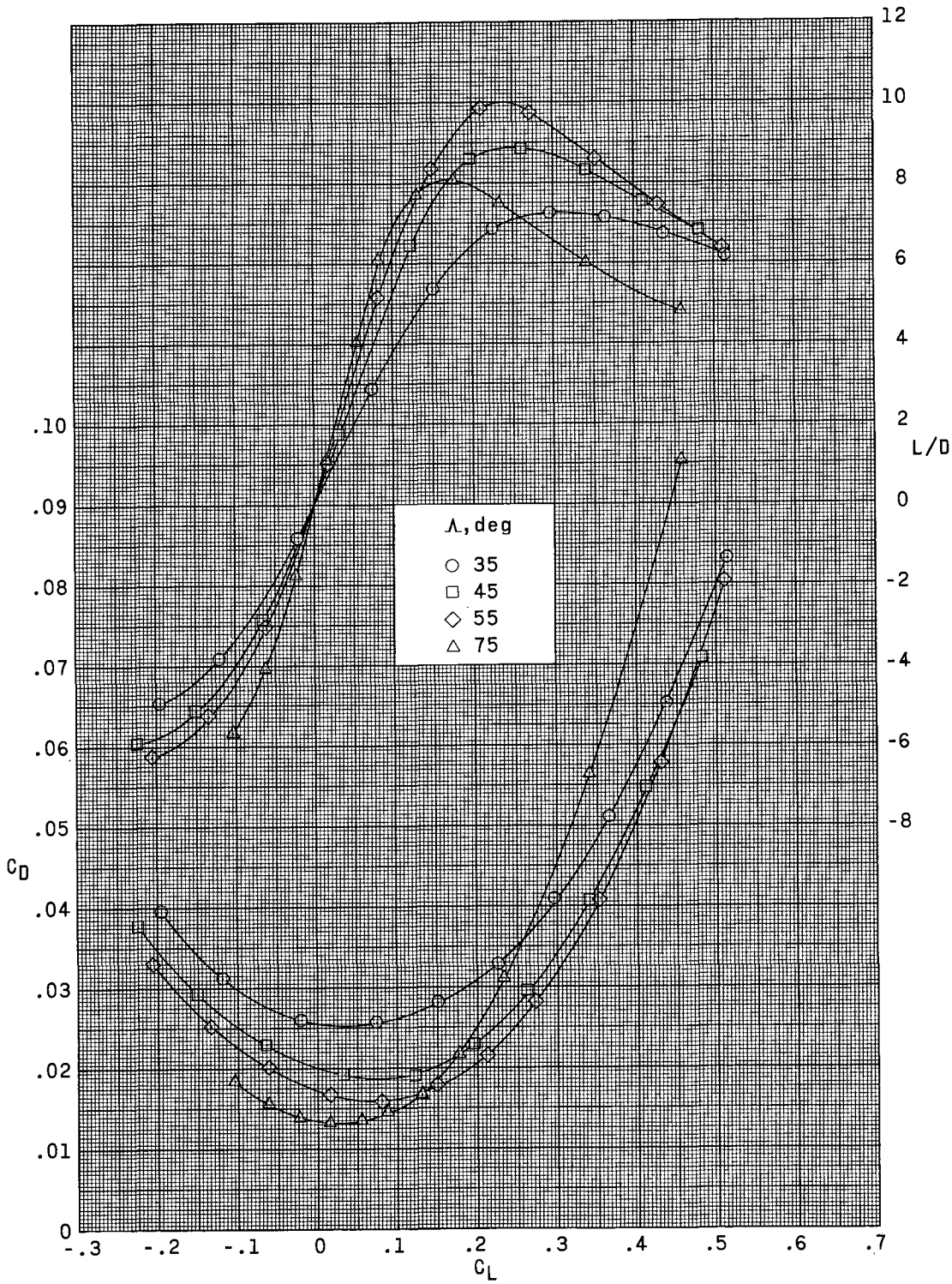

Figure 7.- Concluded.

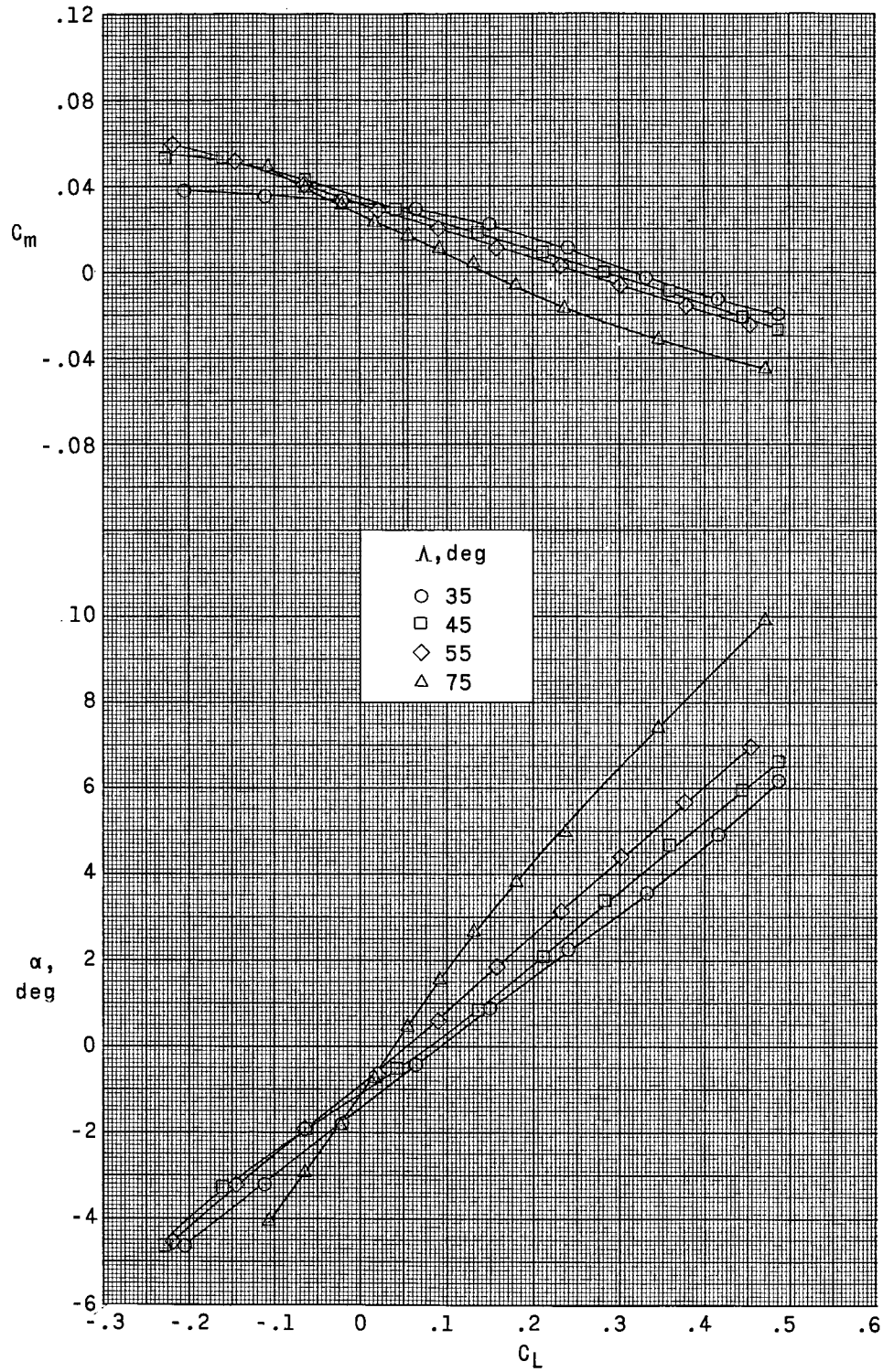

Figure 8.- Effect of auxiliary wing sweep angle on longitudinal aerodynamic characteristics at Mach number 0.94. $\delta_h = -2^\circ$.

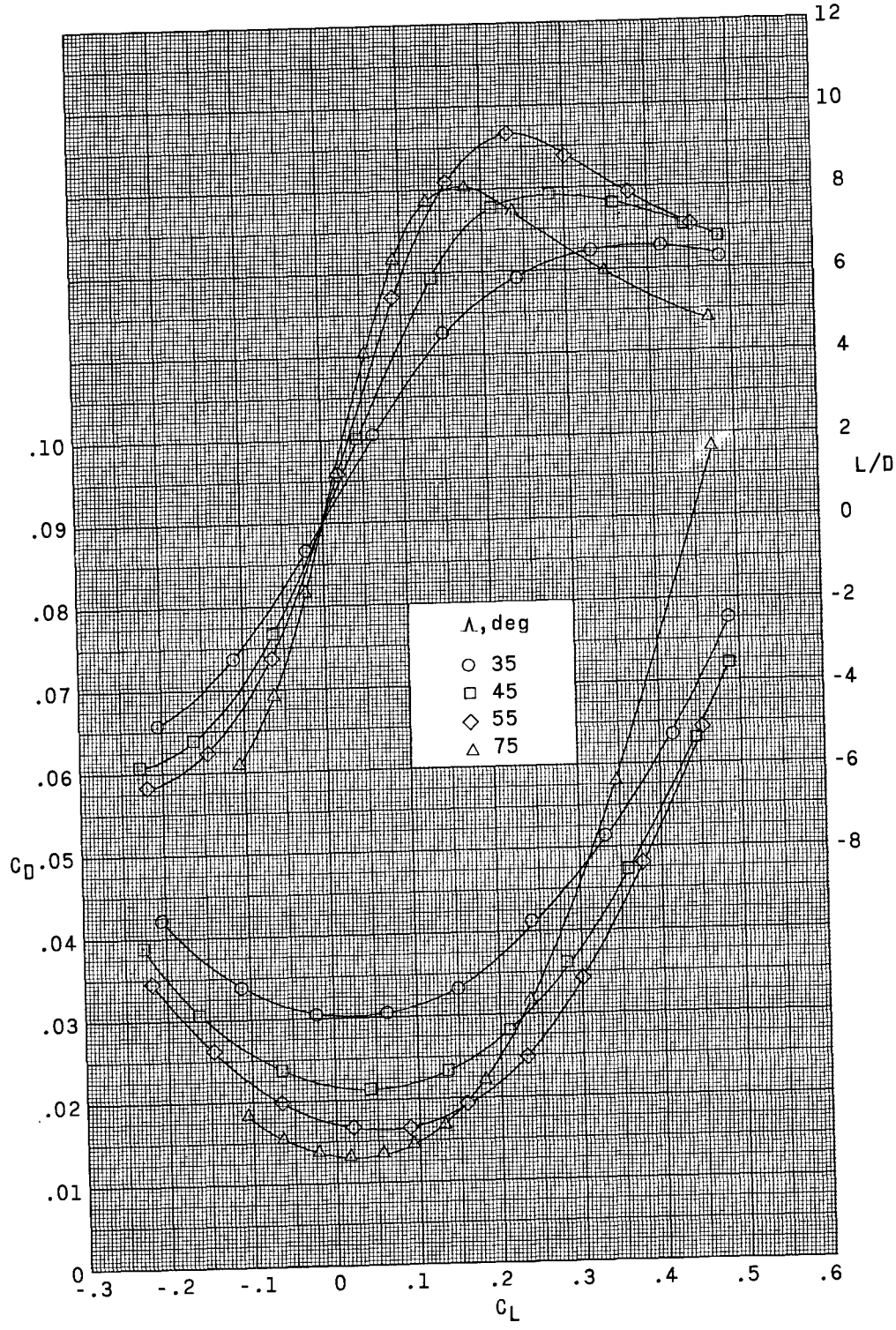

Figure 8.- Concluded.

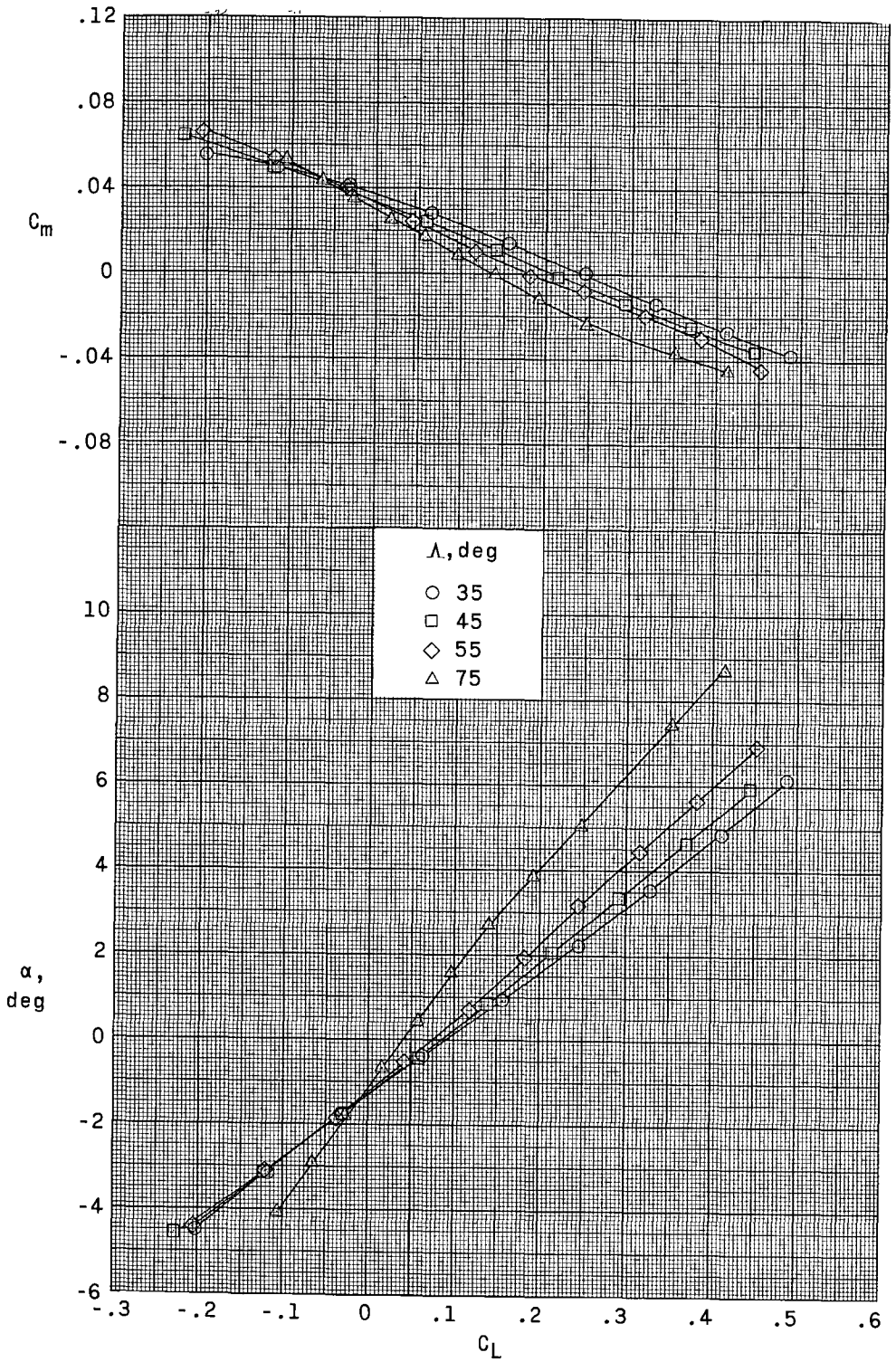

Figure 9.- Effect of auxiliary wing sweep angle on longitudinal aerodynamic characteristics at Mach number 1.03. $\delta_h = -2^o$.

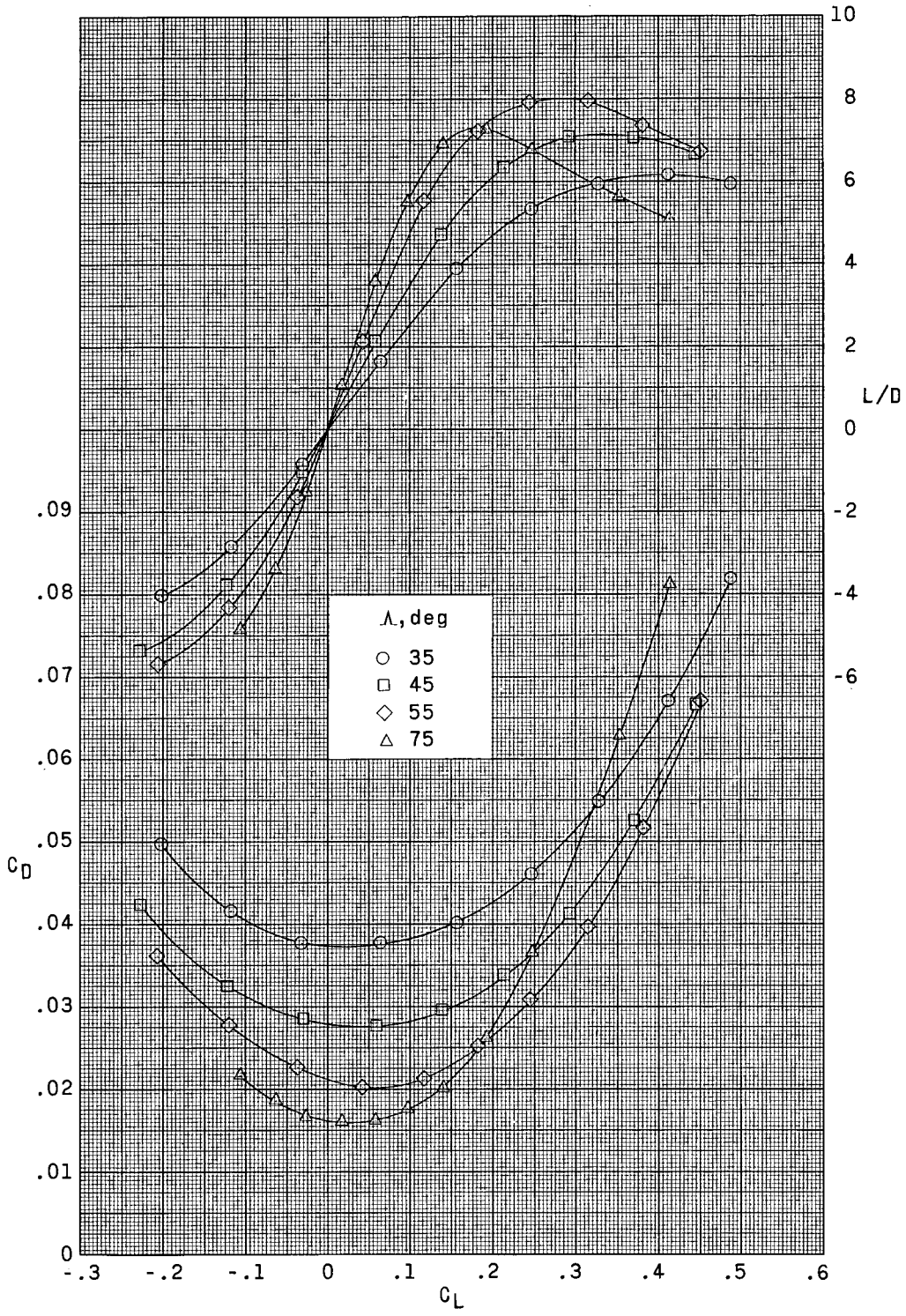

Figure 9.- Concluded.

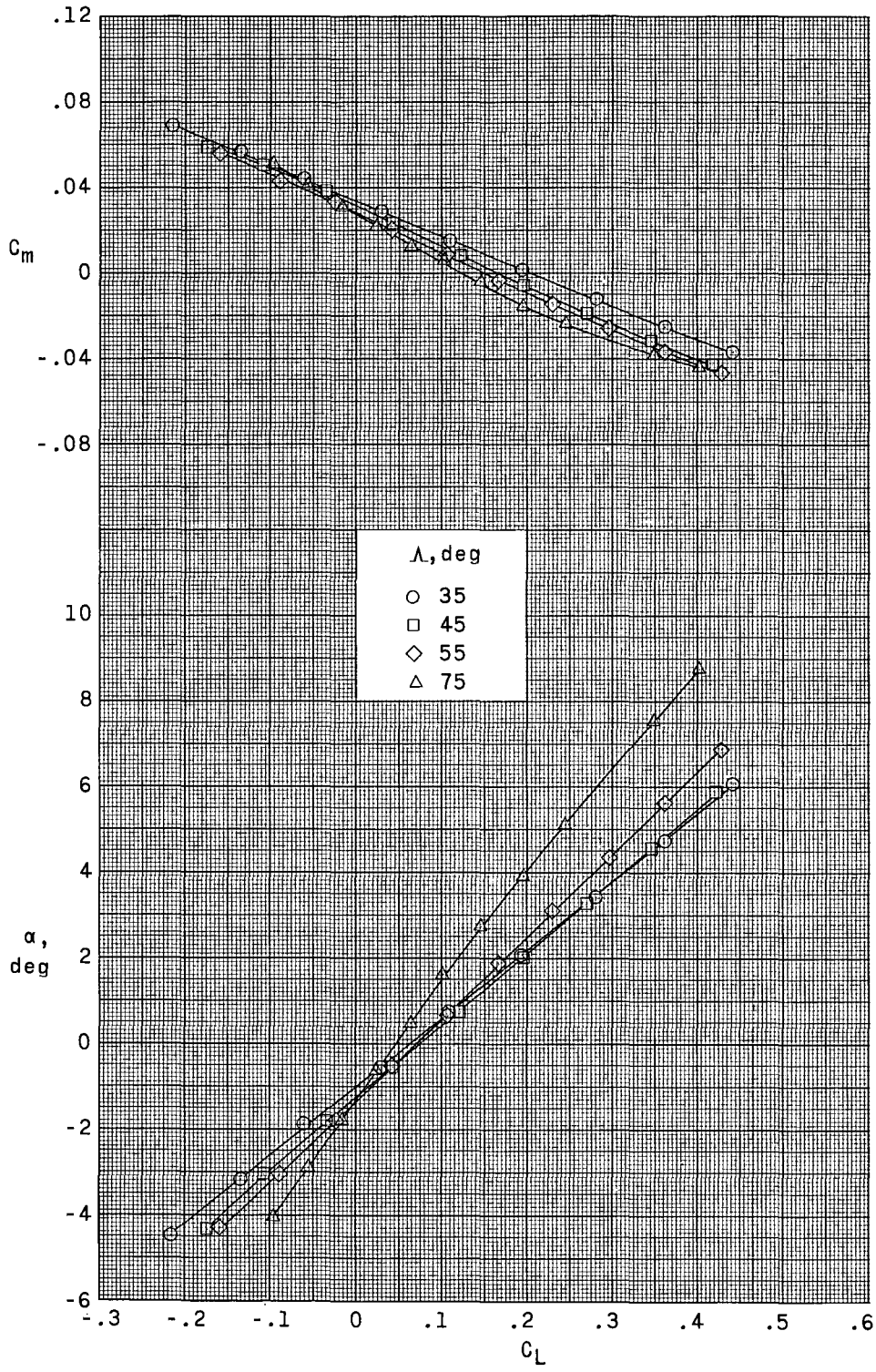

Figure 10.- Effect of auxiliary wing sweep angle on longitudinal aerodynamic characteristics at Mach number 1.20. $\delta_h = -2^o$.

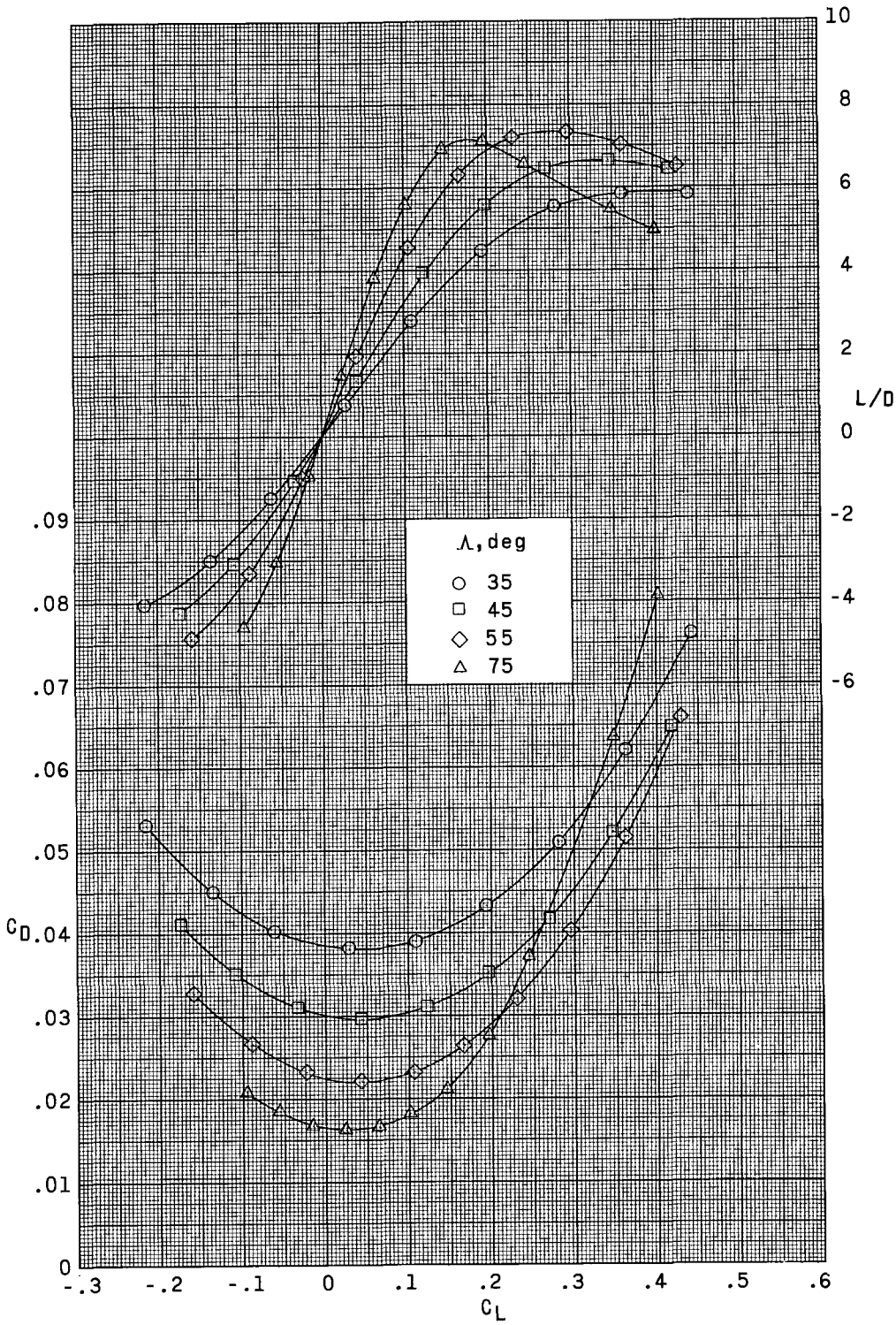

Figure 10.- Concluded.

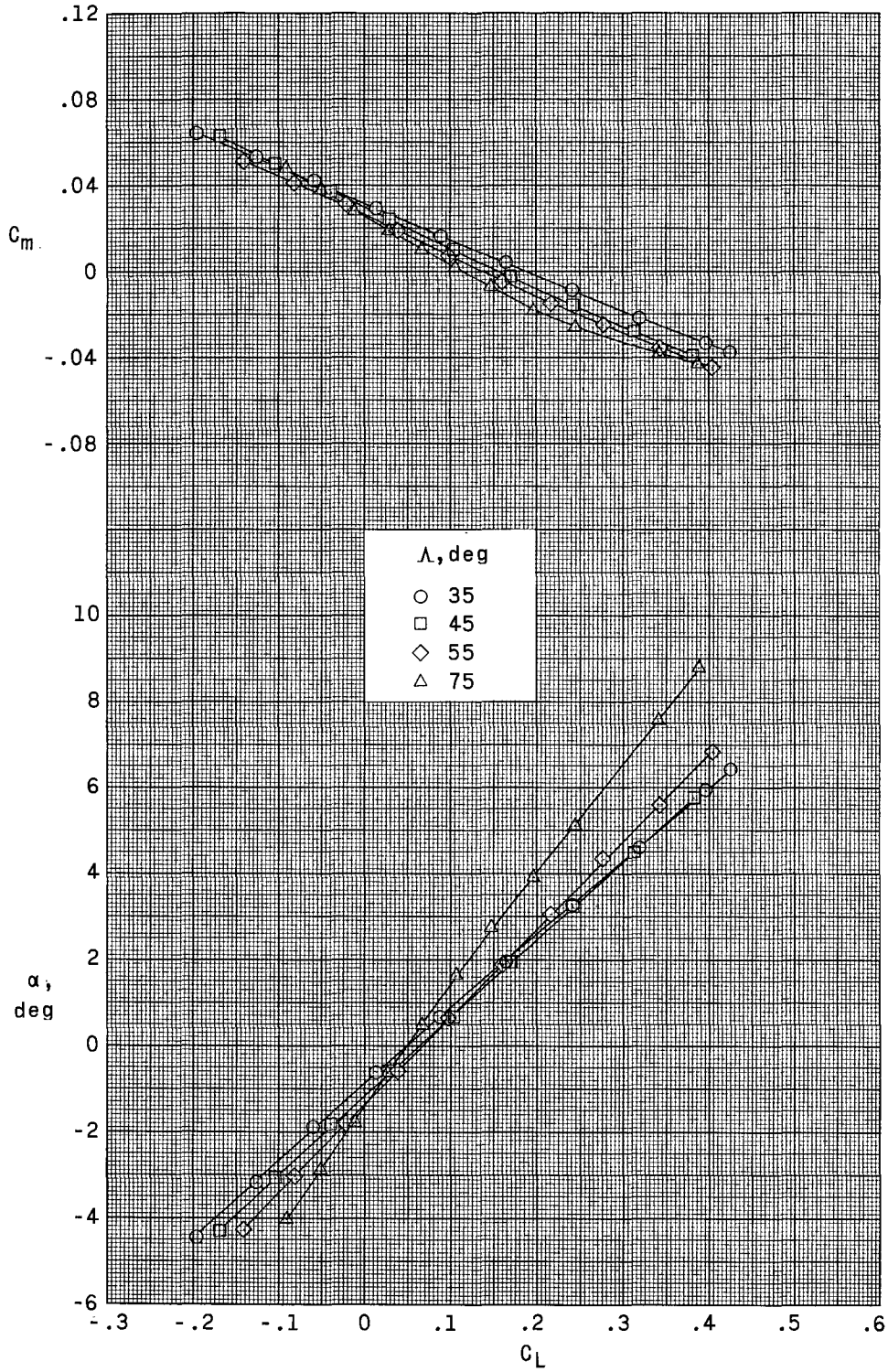

Figure 11.- Effect of auxiliary wing sweep angle on longitudinal aerodynamic characteristics at Mach number 1.30. $\delta_h = -2^o$.

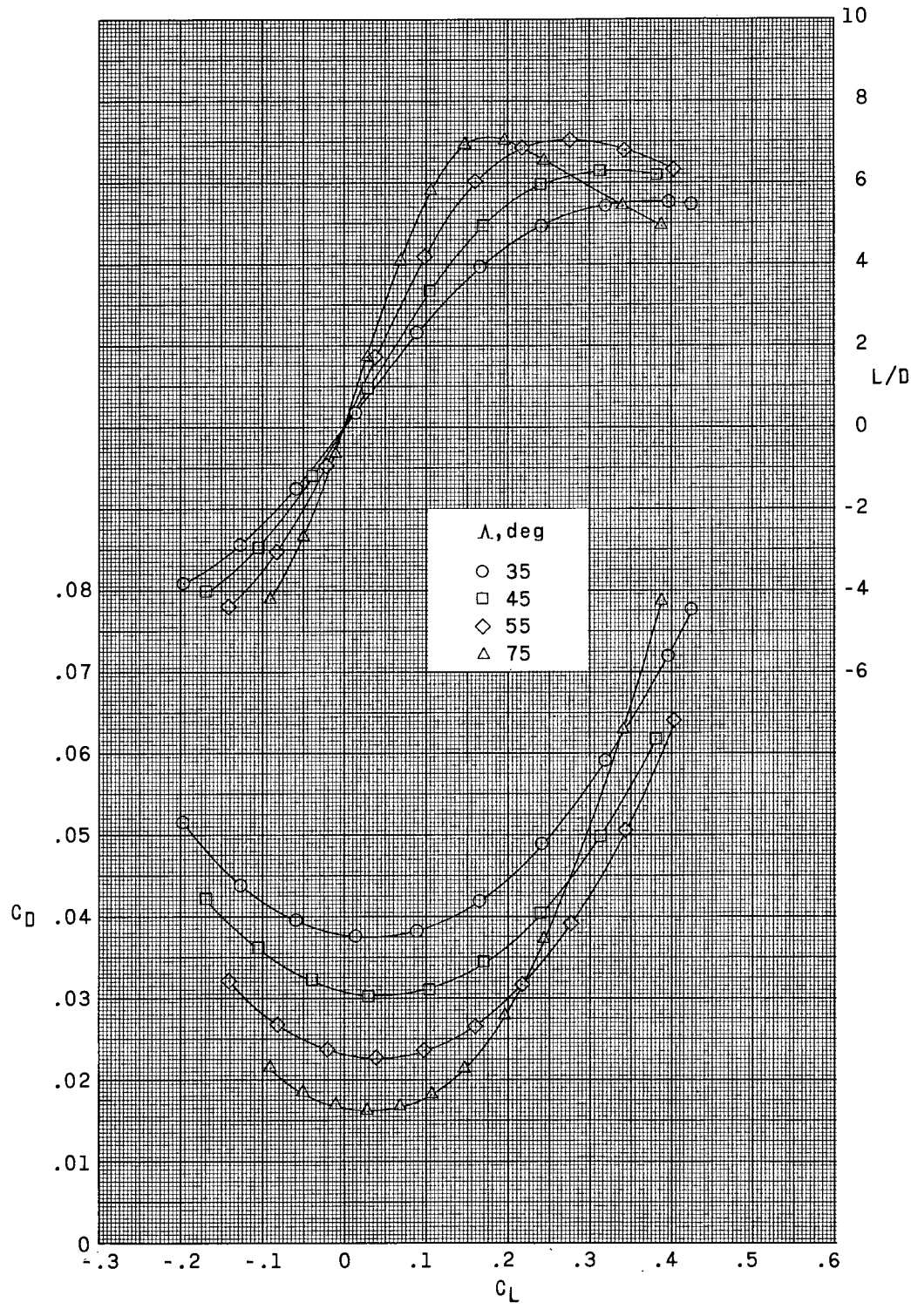

Figure 11.- Concluded.

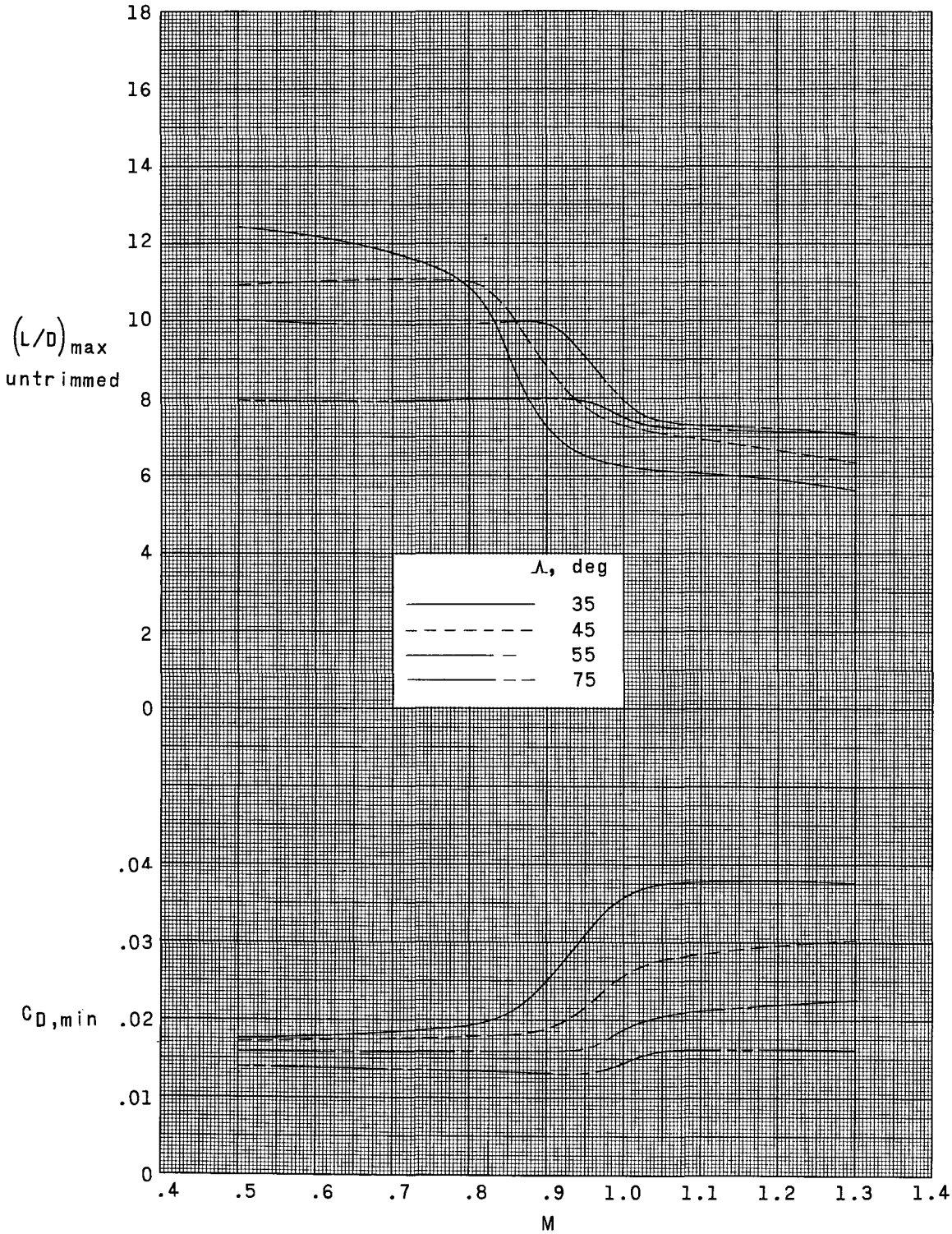

Figure 12.- Variations of untrimmed $(L/D)_{max}$ and $C_{D,min}$ with Mach number for various auxiliary wing sweep angles.

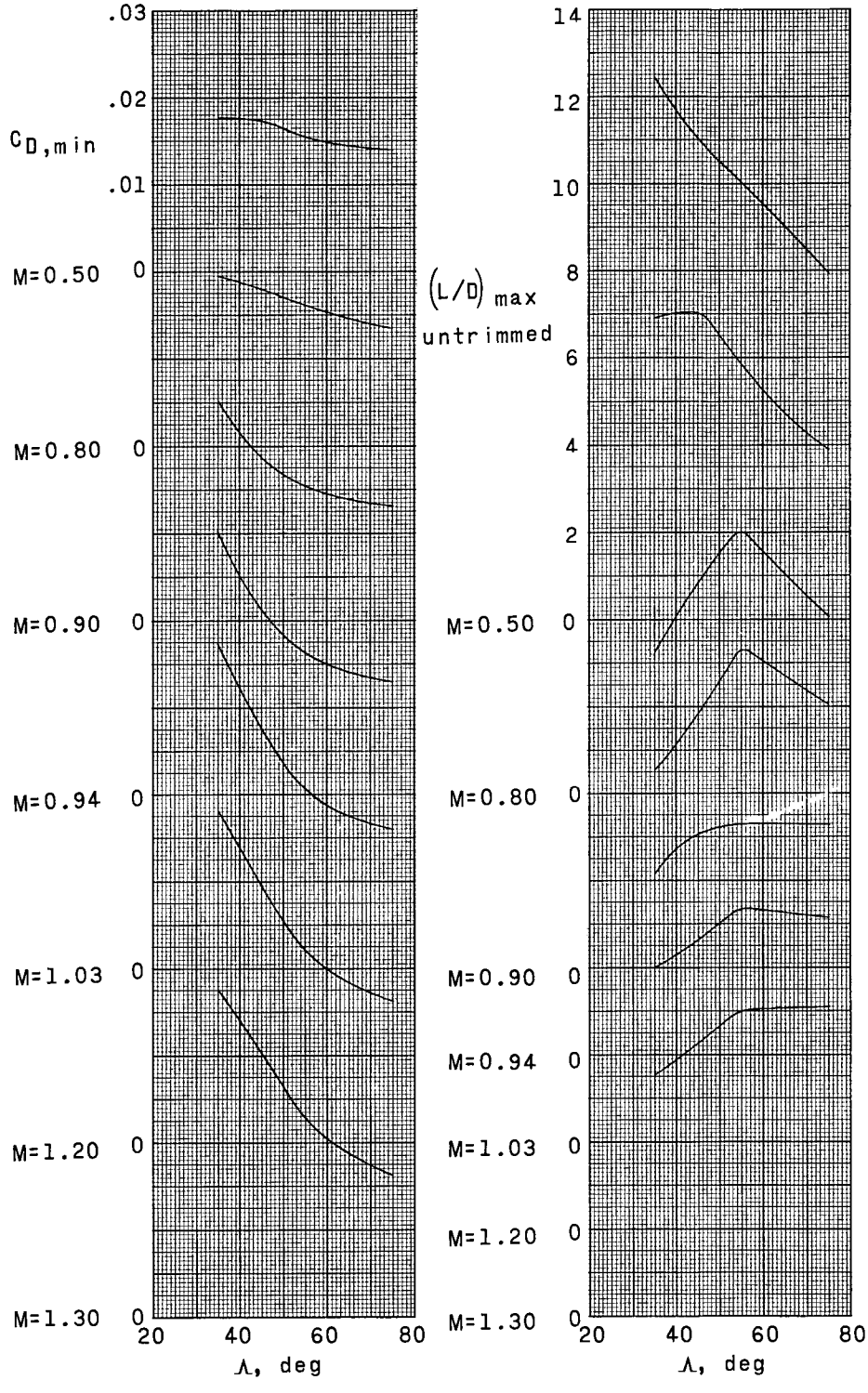

Figure 13.- Variation of $(L/D)_{max}$ and $C_{D,min}$ with auxiliary wing sweep angle for various Mach numbers.

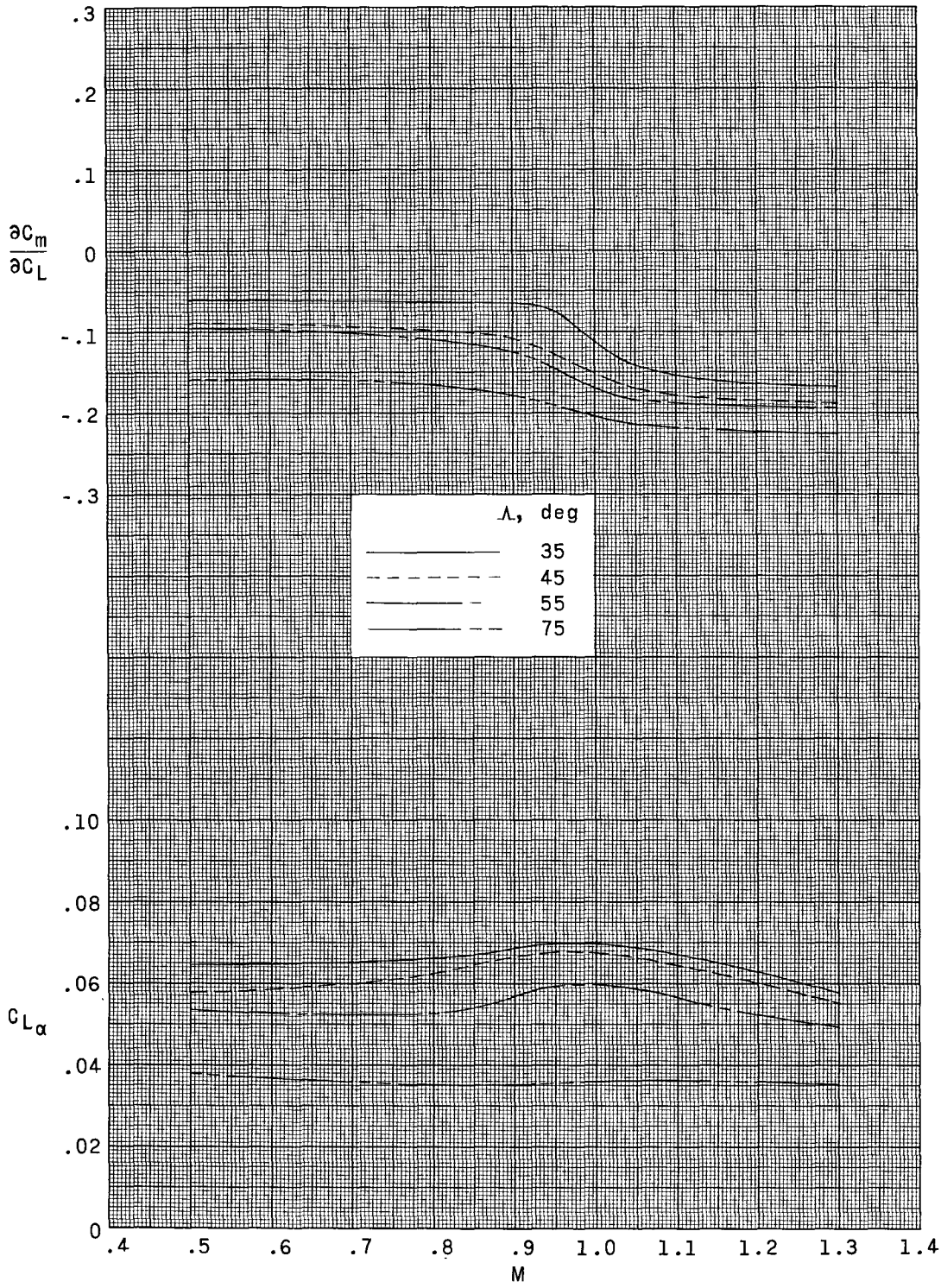

Figure 14.- Variation of $\partial C_m/\partial C_L$ and C_{L_α} with Mach number for various auxiliary wing sweep angles.

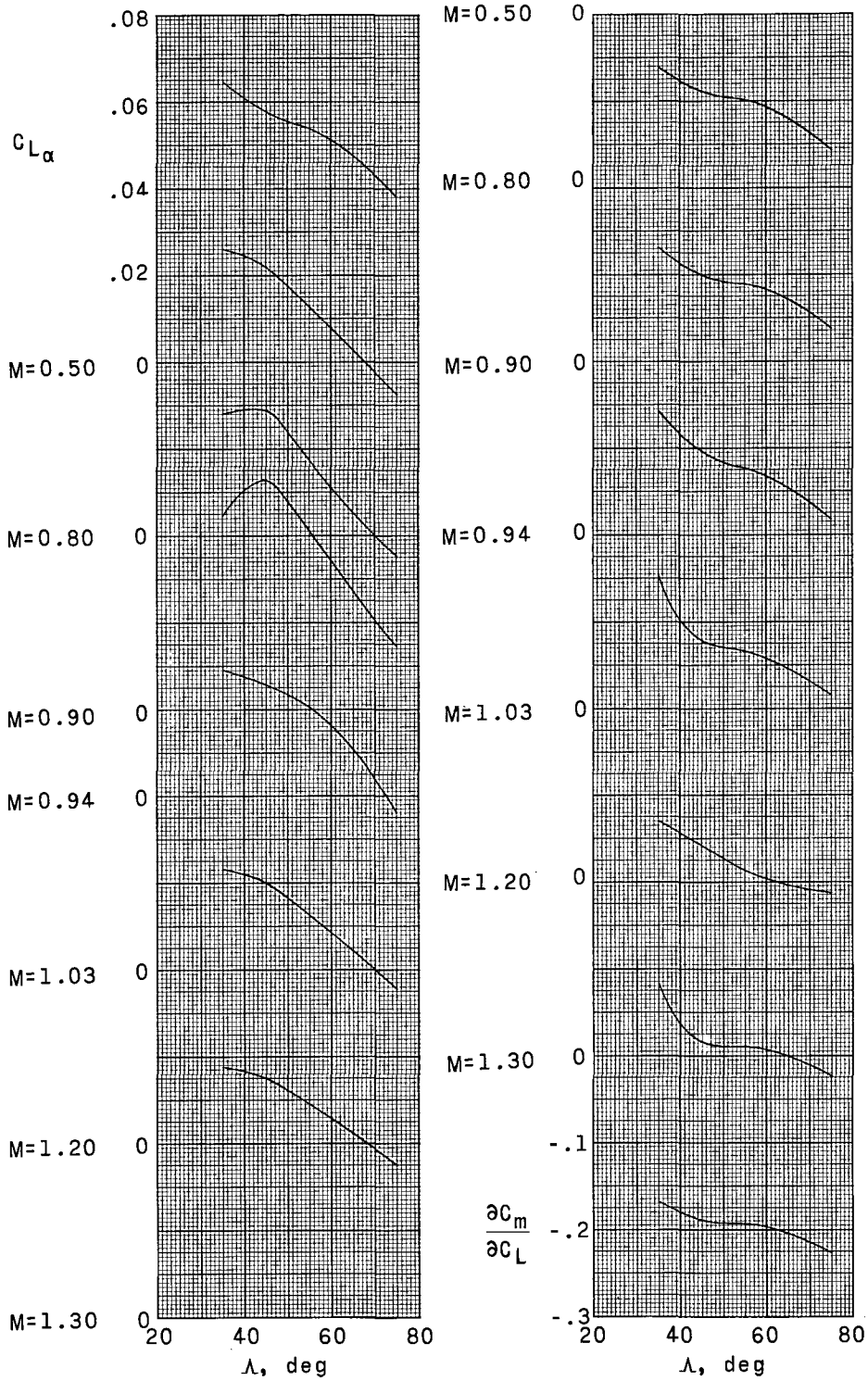

Figure 15.- Variation of $\partial C_m/\partial C_L$ and C_{L_α} with auxiliary wing sweep angle for various Mach numbers.

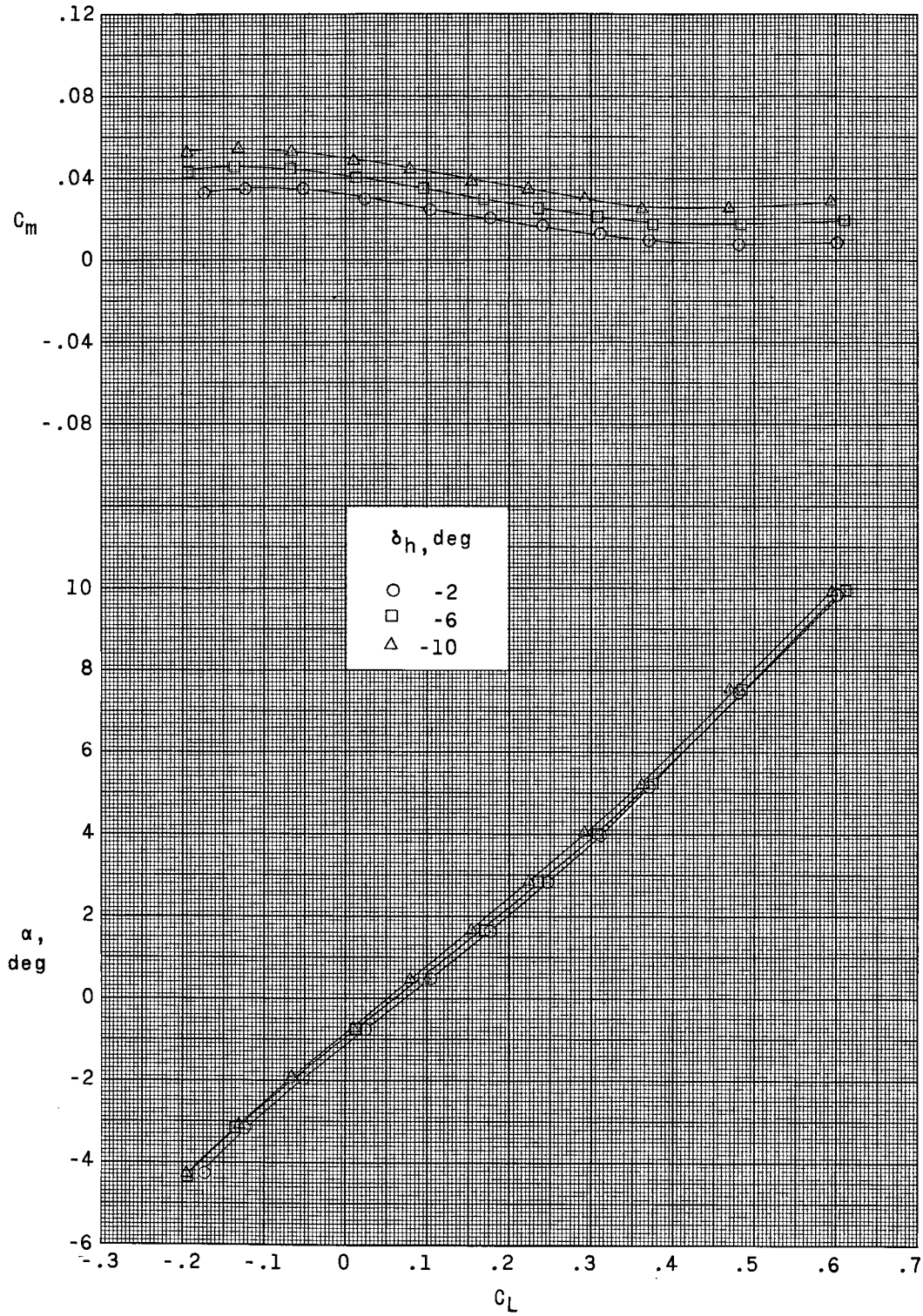

Figure 16.- Effect of horizontal-tail deflection on longitudinal aerodynamic characteristics at Mach number 0.50. $\Lambda = 35^{\circ}$.

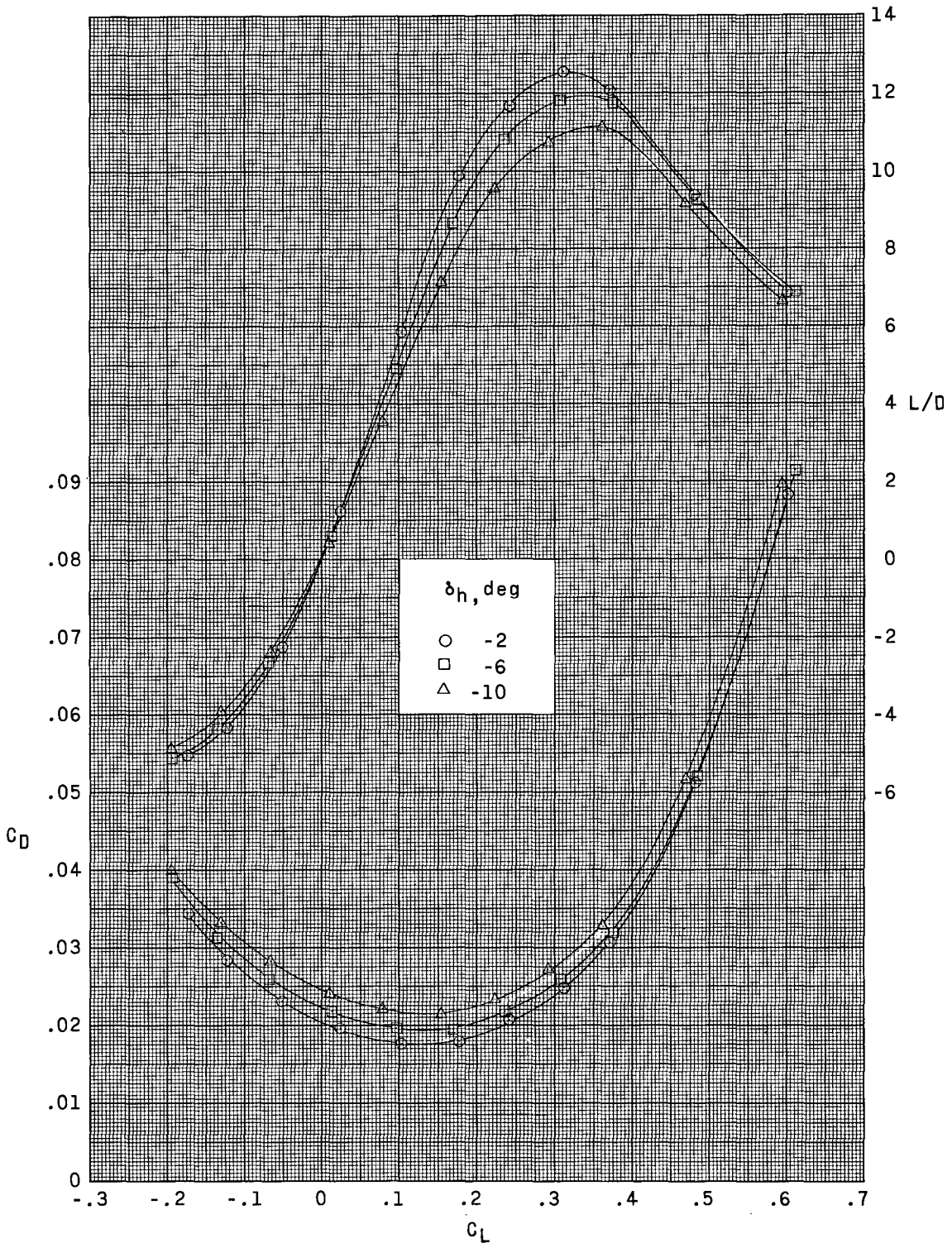

Figure 16.- Concluded.

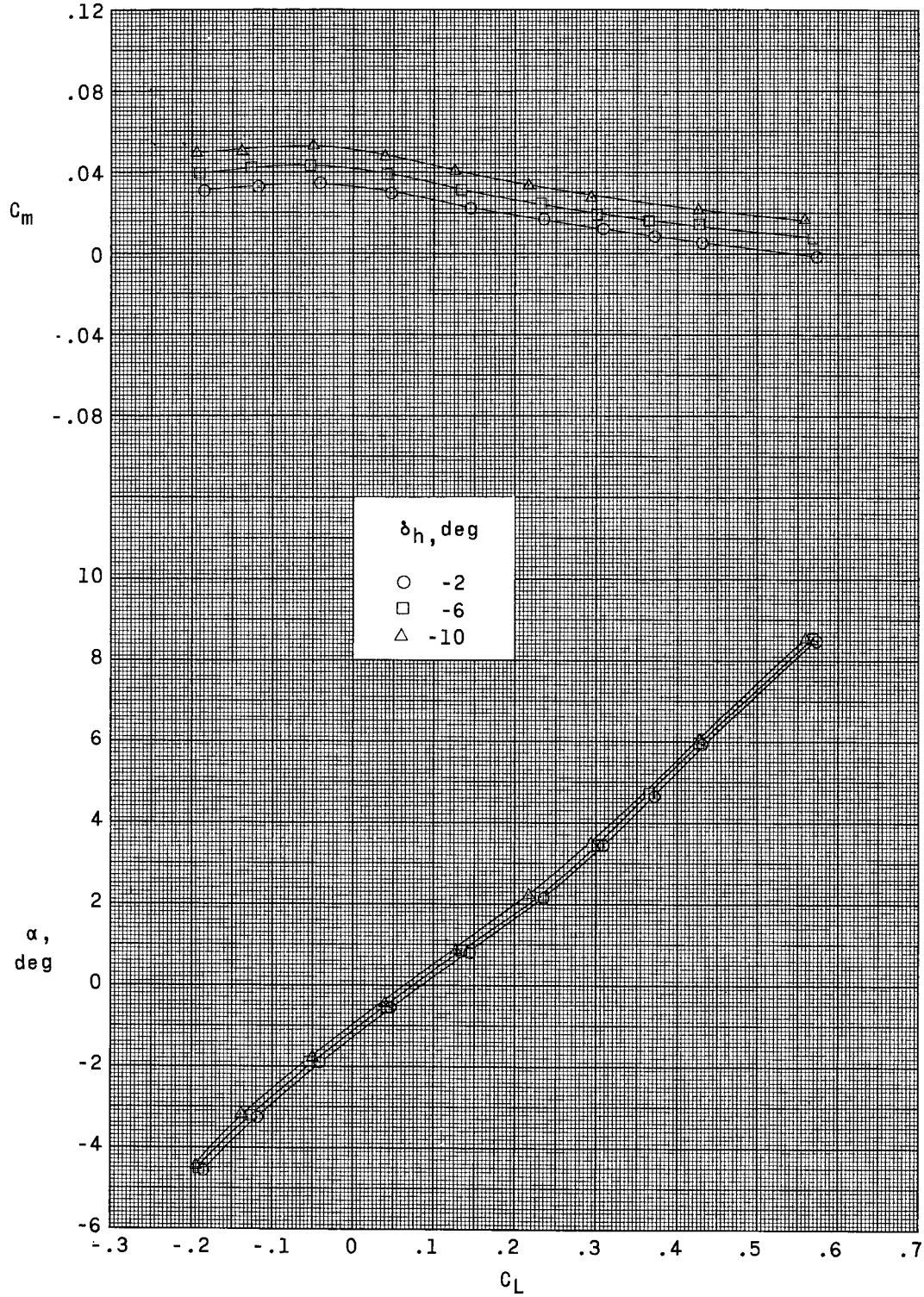

Figure 17.- Effect of horizontal-tail deflection on longitudinal aerodynamic characteristics at Mach number 0.80. $\Lambda = 35^\circ$.

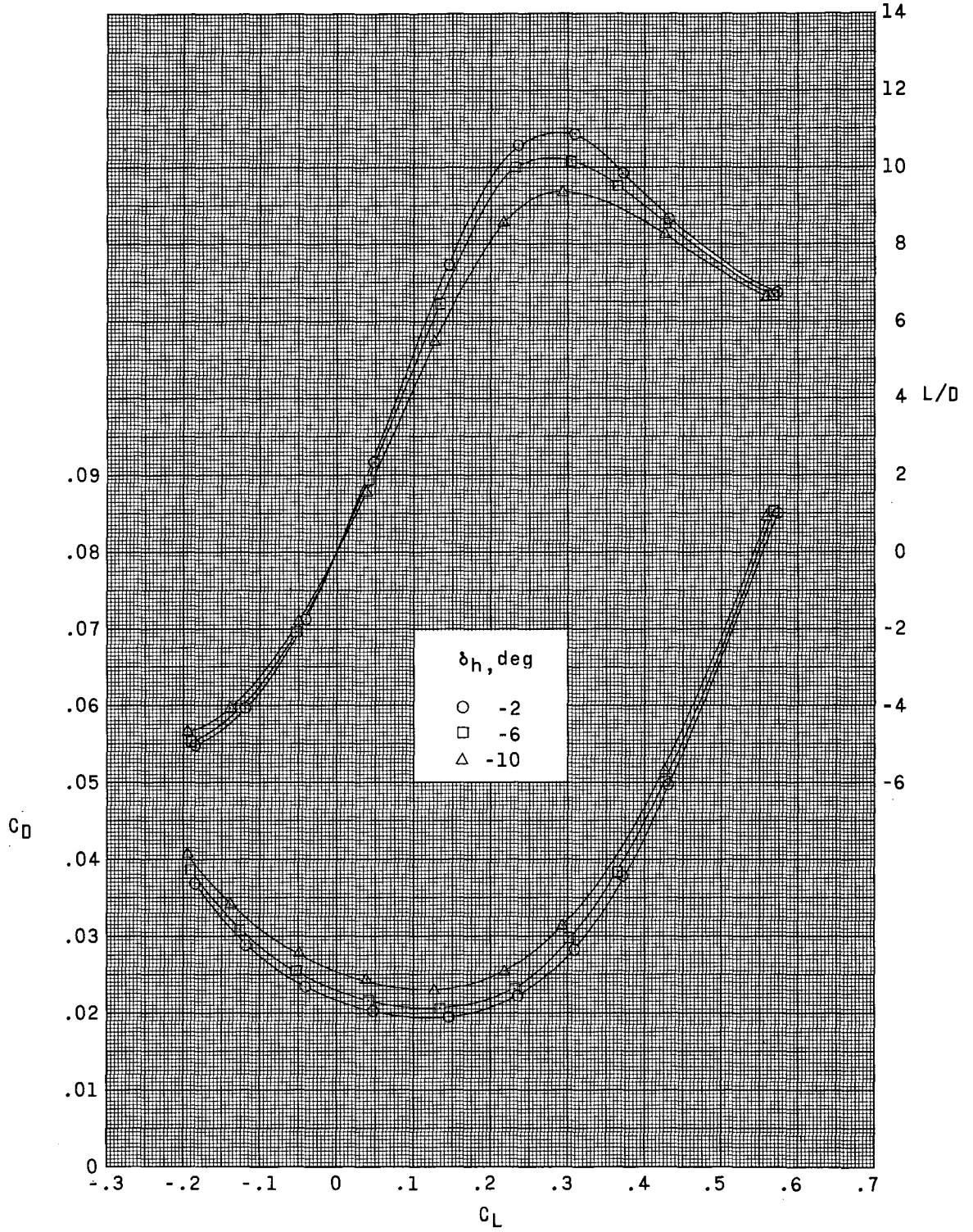

Figure 17.- Concluded.

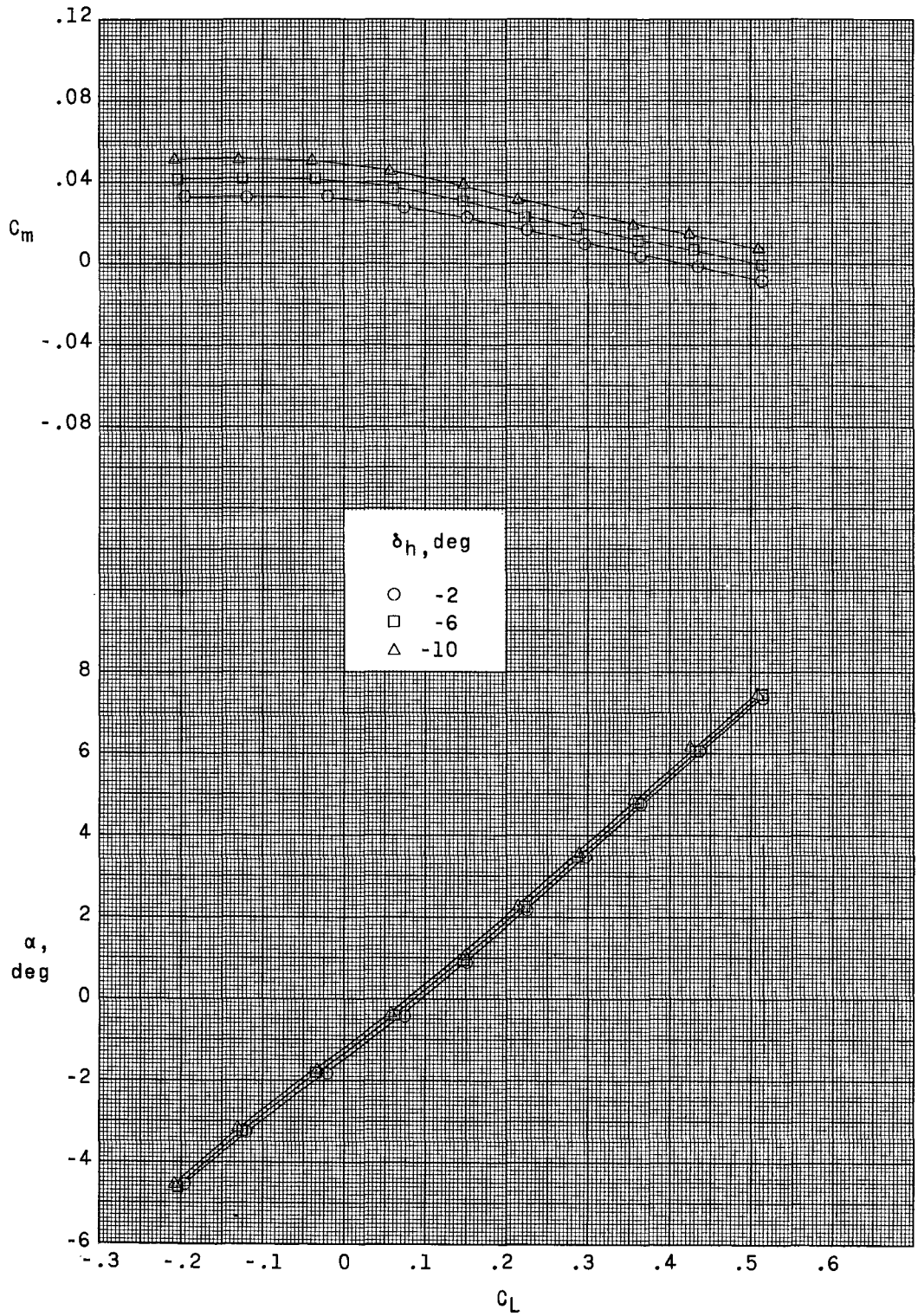

Figure 18.- Effect of horizontal-tail deflection on longitudinal aerodynamic characteristics at Mach number 0.90. $\Lambda = 35^{\circ}$.

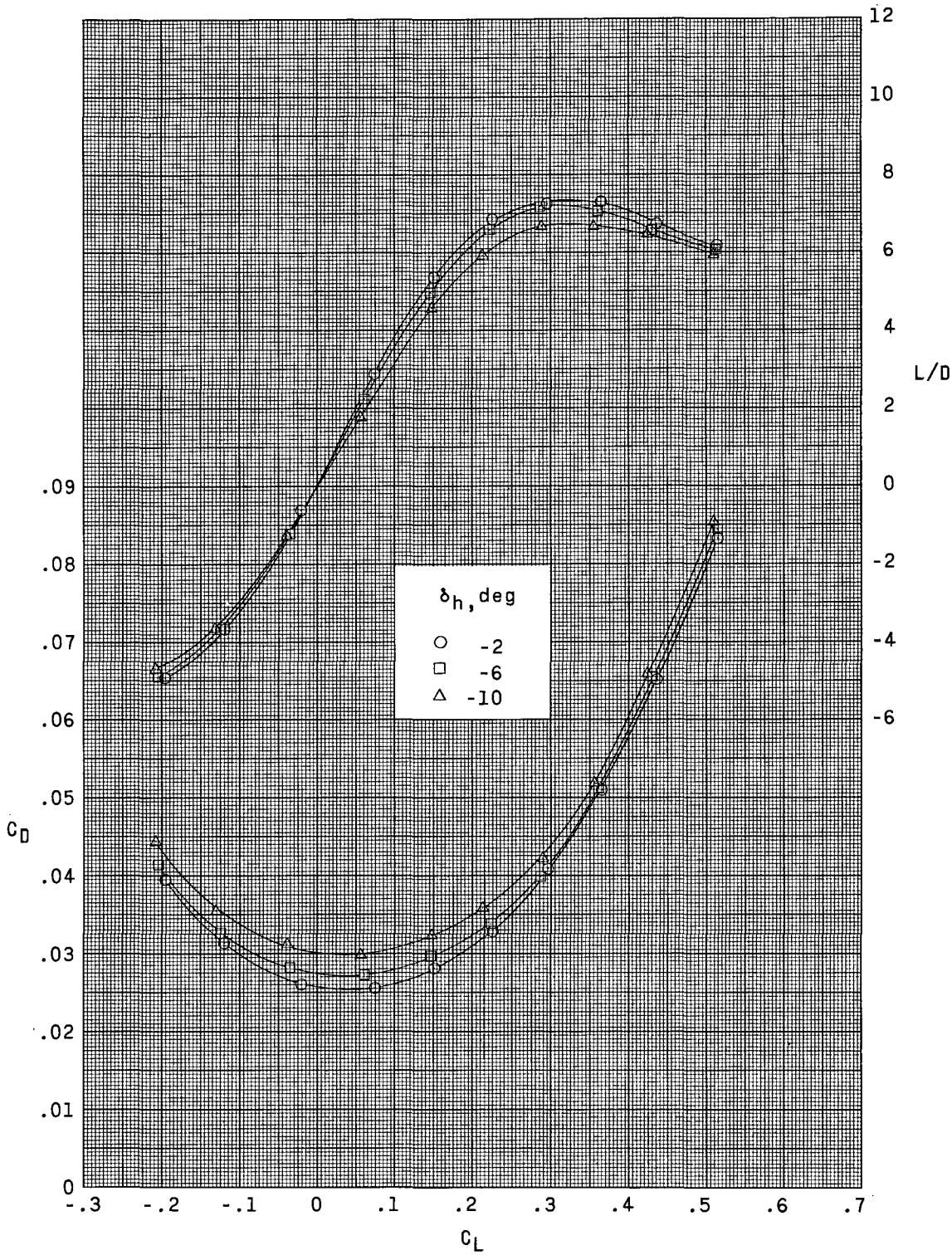

Figure 18.- Concluded.

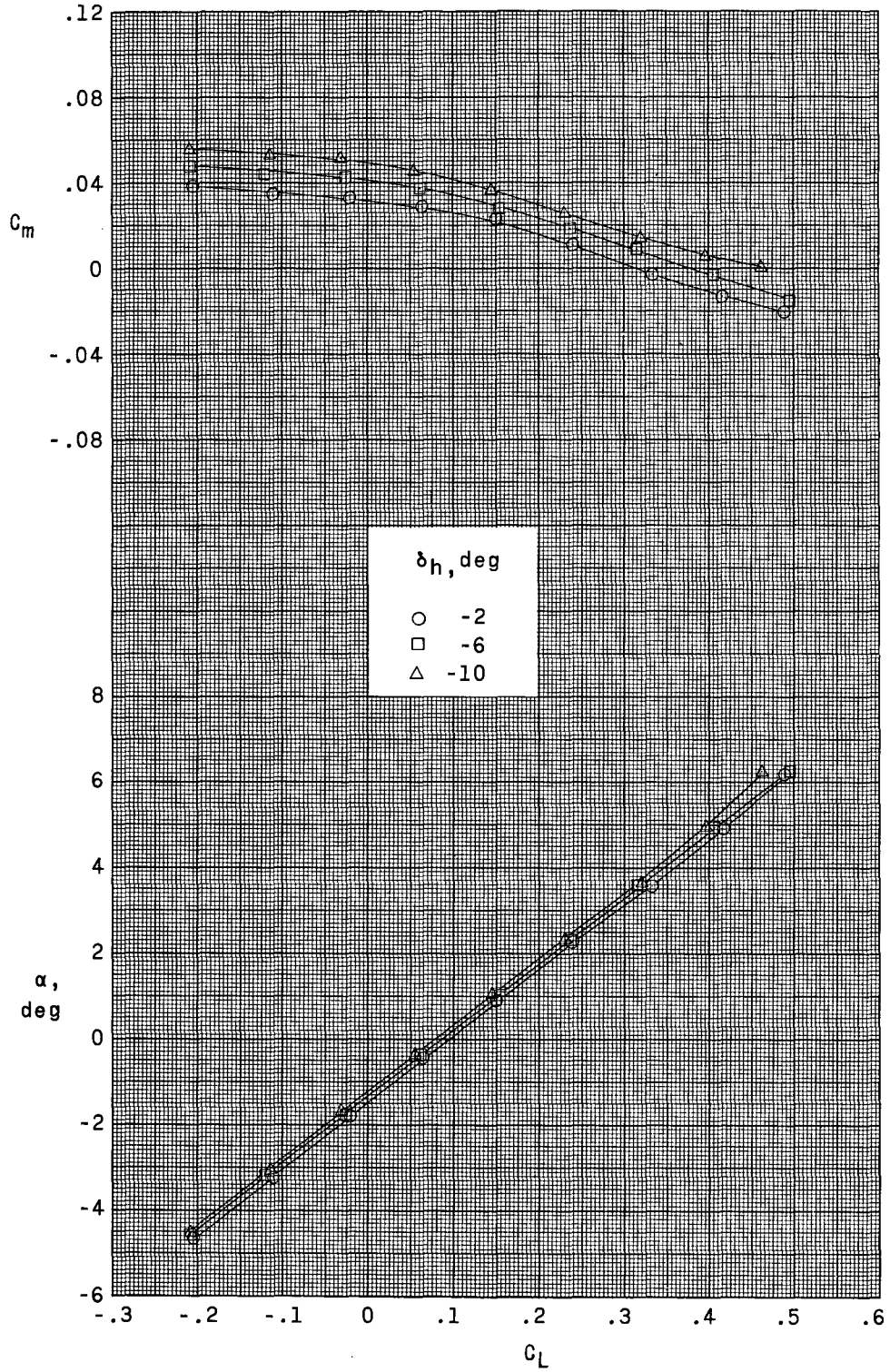

Figure 19.- Effect of horizontal-tail deflection on longitudinal aerodynamic characteristics at Mach number 0.94. $\Lambda = 35^\circ$.

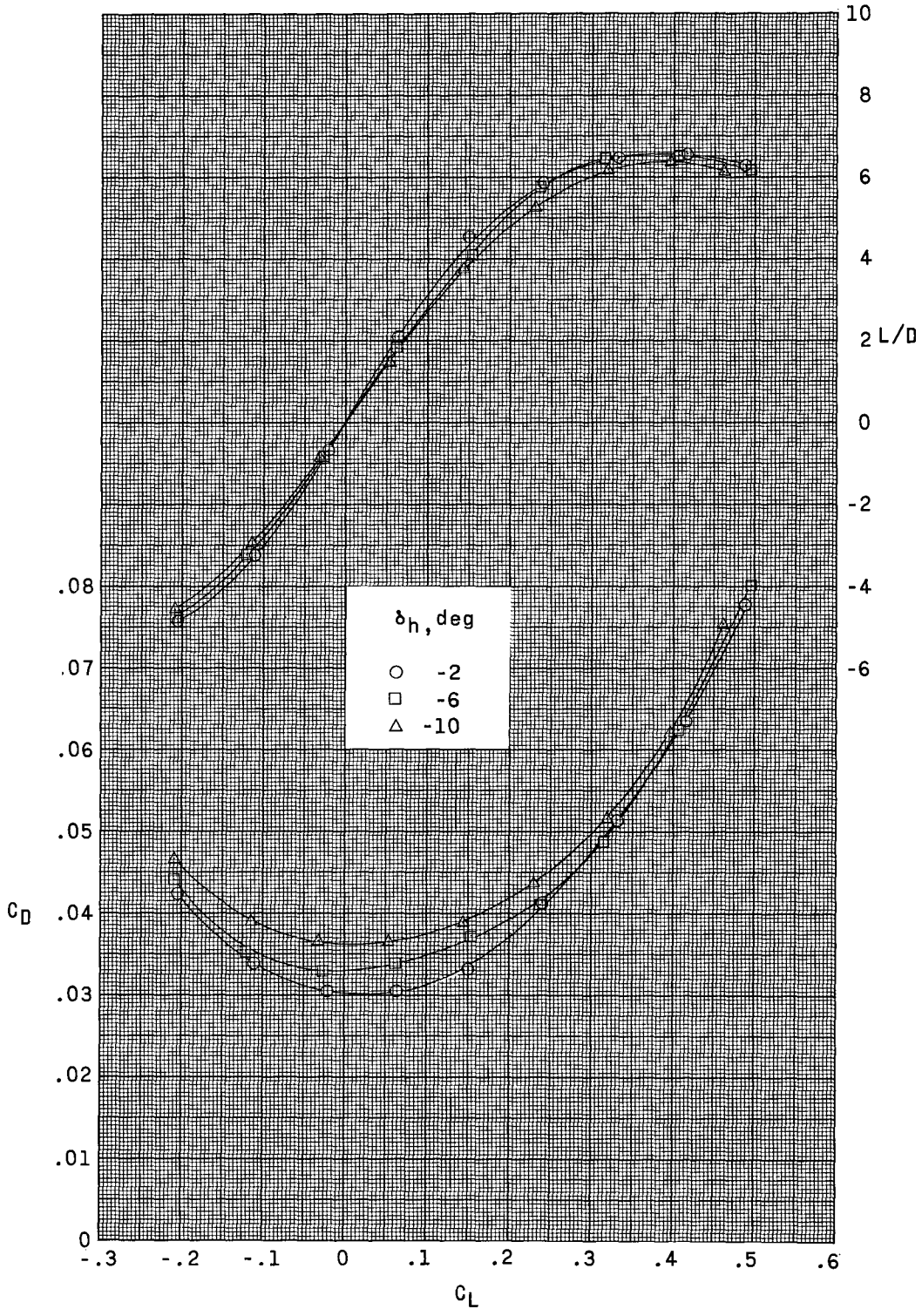

Figure 19.- Concluded.

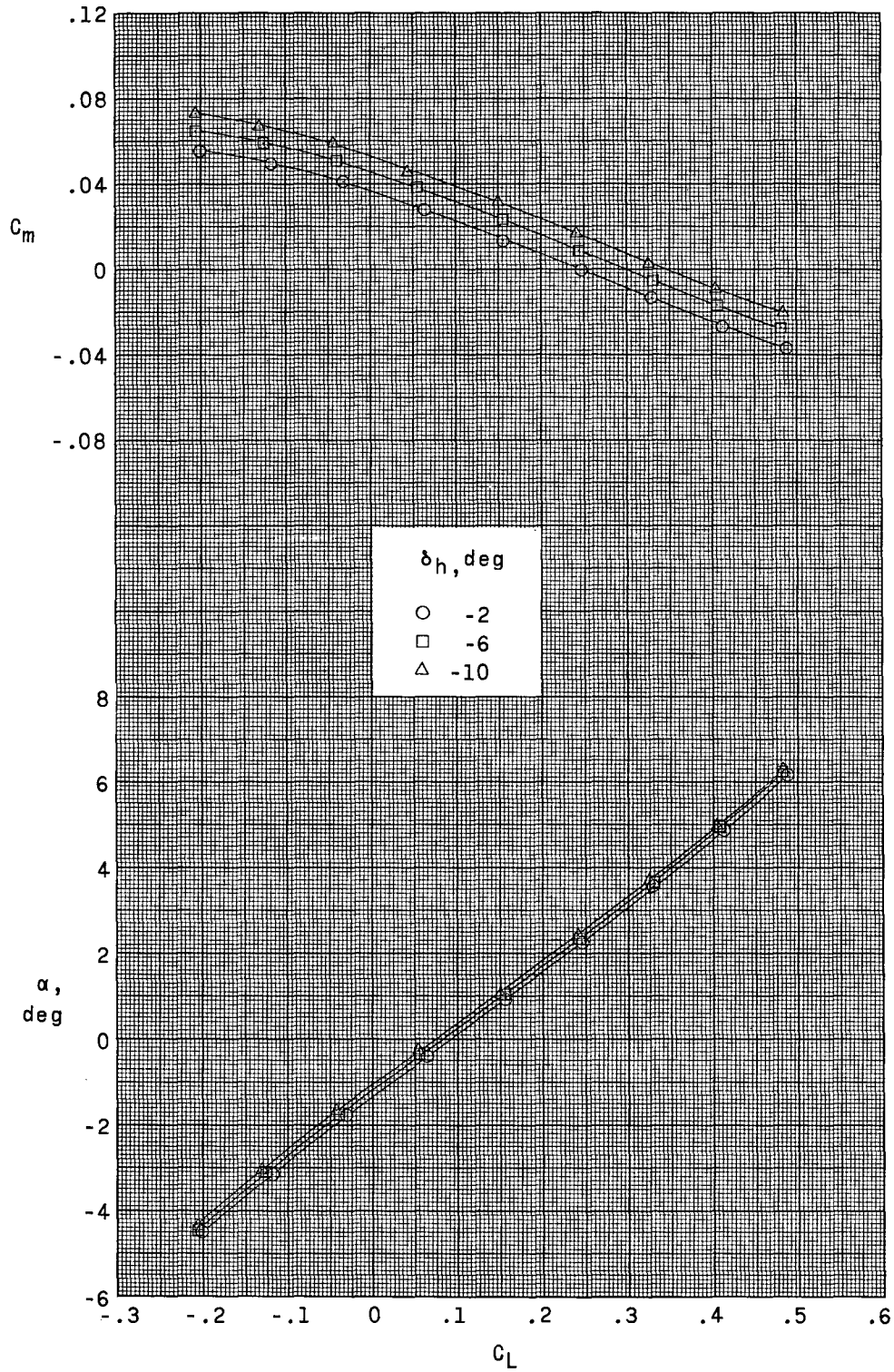

Figure 20.- Effect of horizontal-tail deflection on longitudinal aerodynamic characteristics at Mach number 1.03. $\Lambda = 35^\circ$.

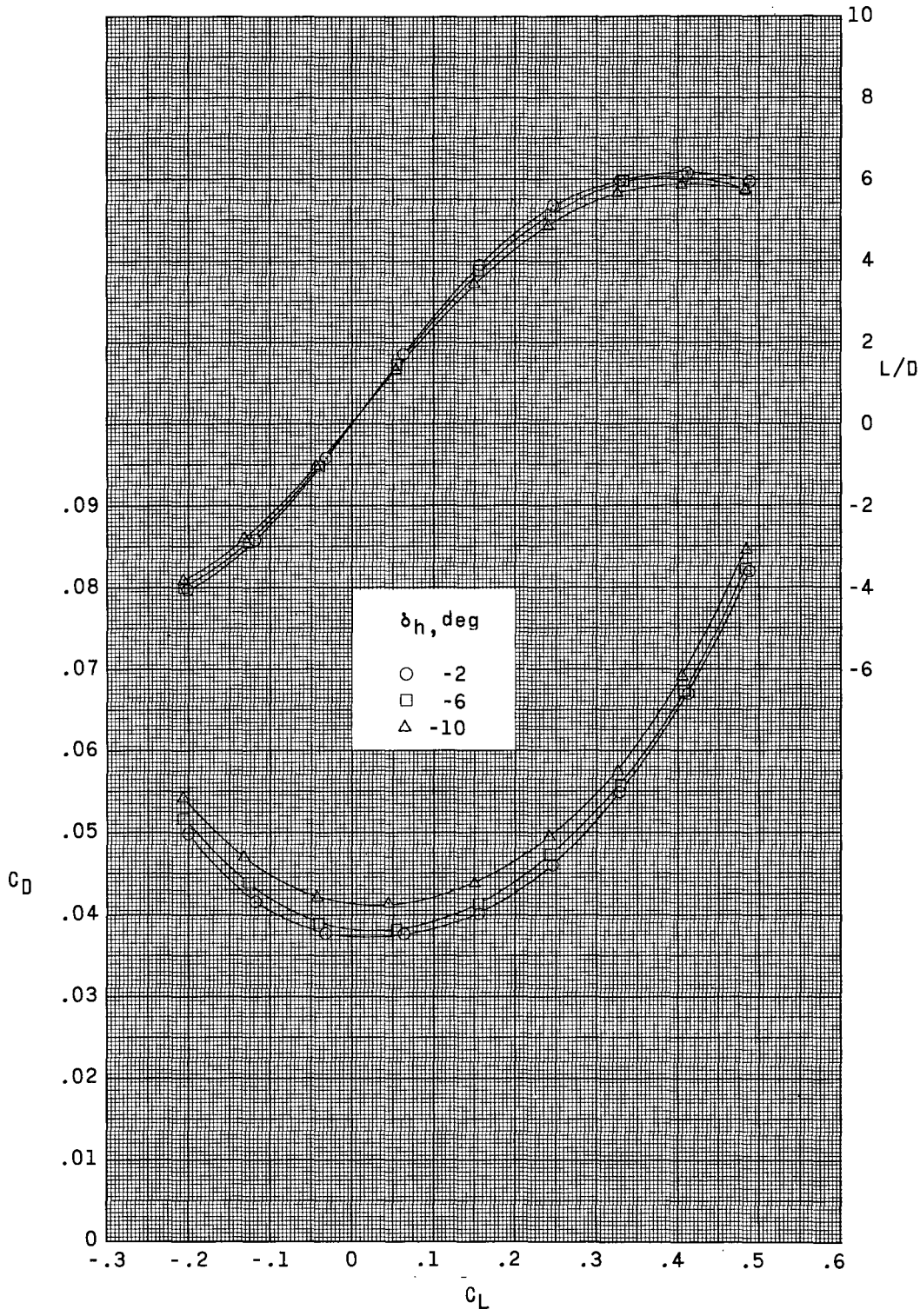

Figure 20.- Concluded.

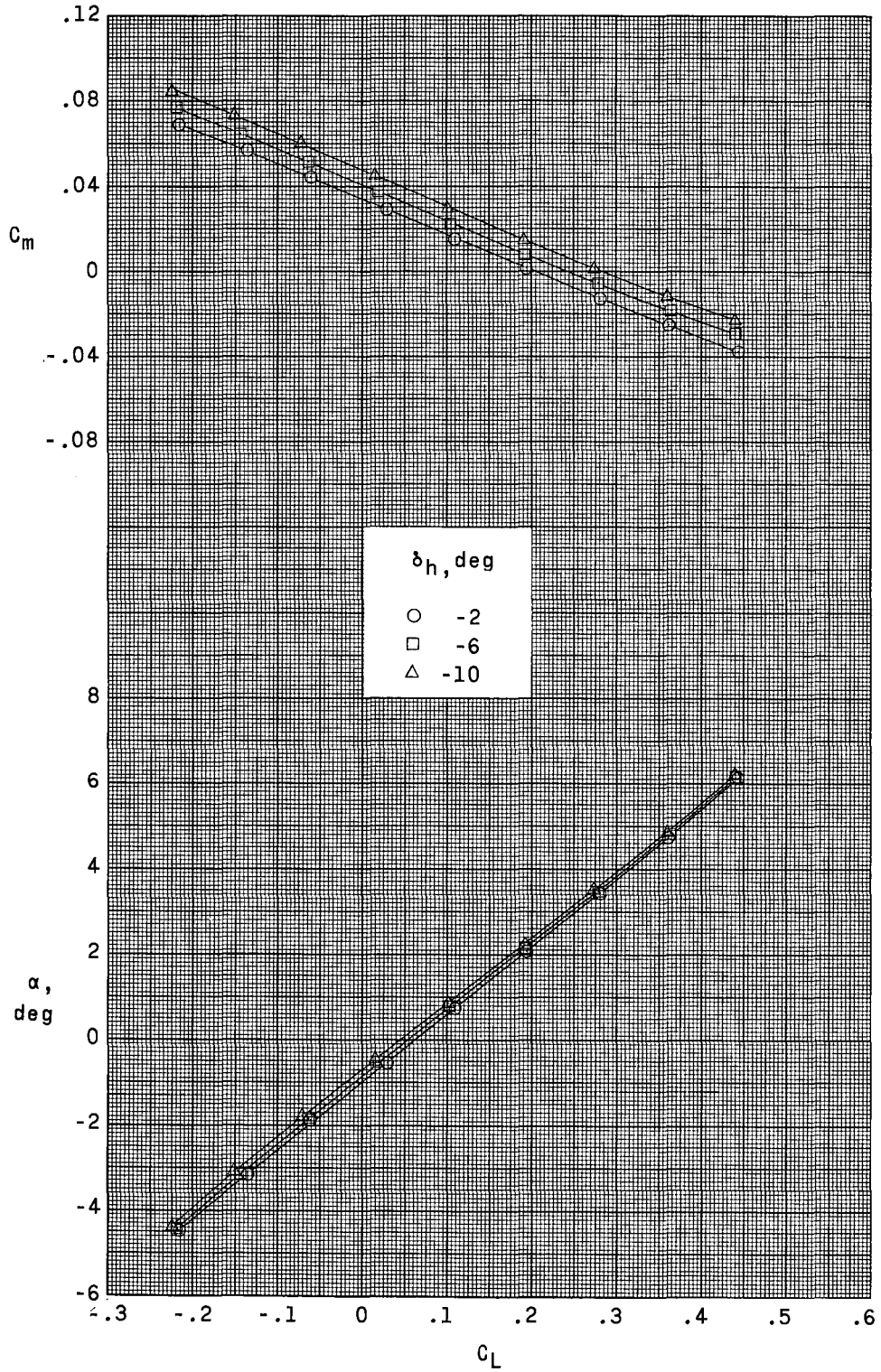

Figure 21.- Effect of horizontal-tail deflection on longitudinal aerodynamic characteristics at Mach number 1.20. $\Lambda = 35^\circ$.

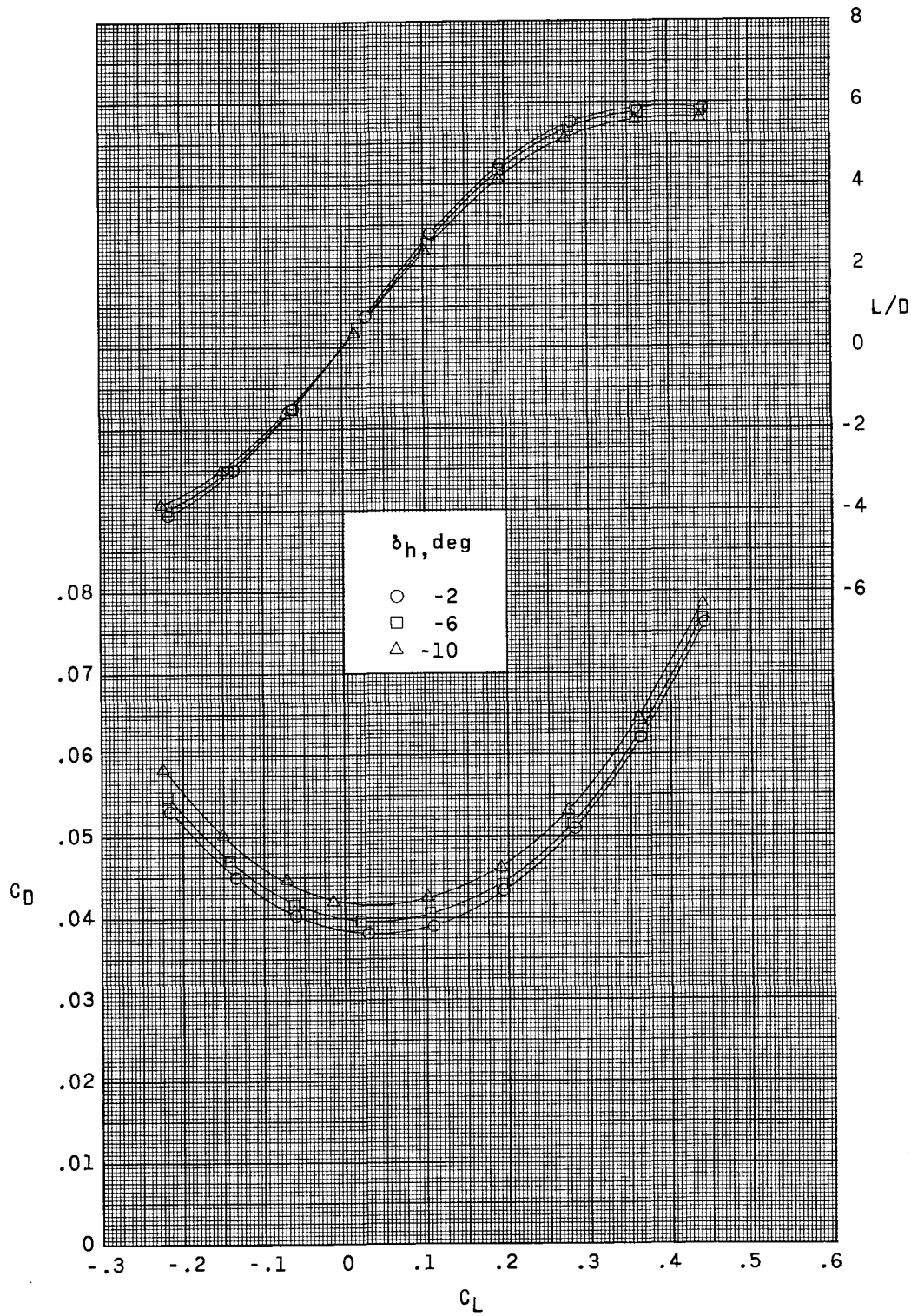

Figure 21.- Concluded.

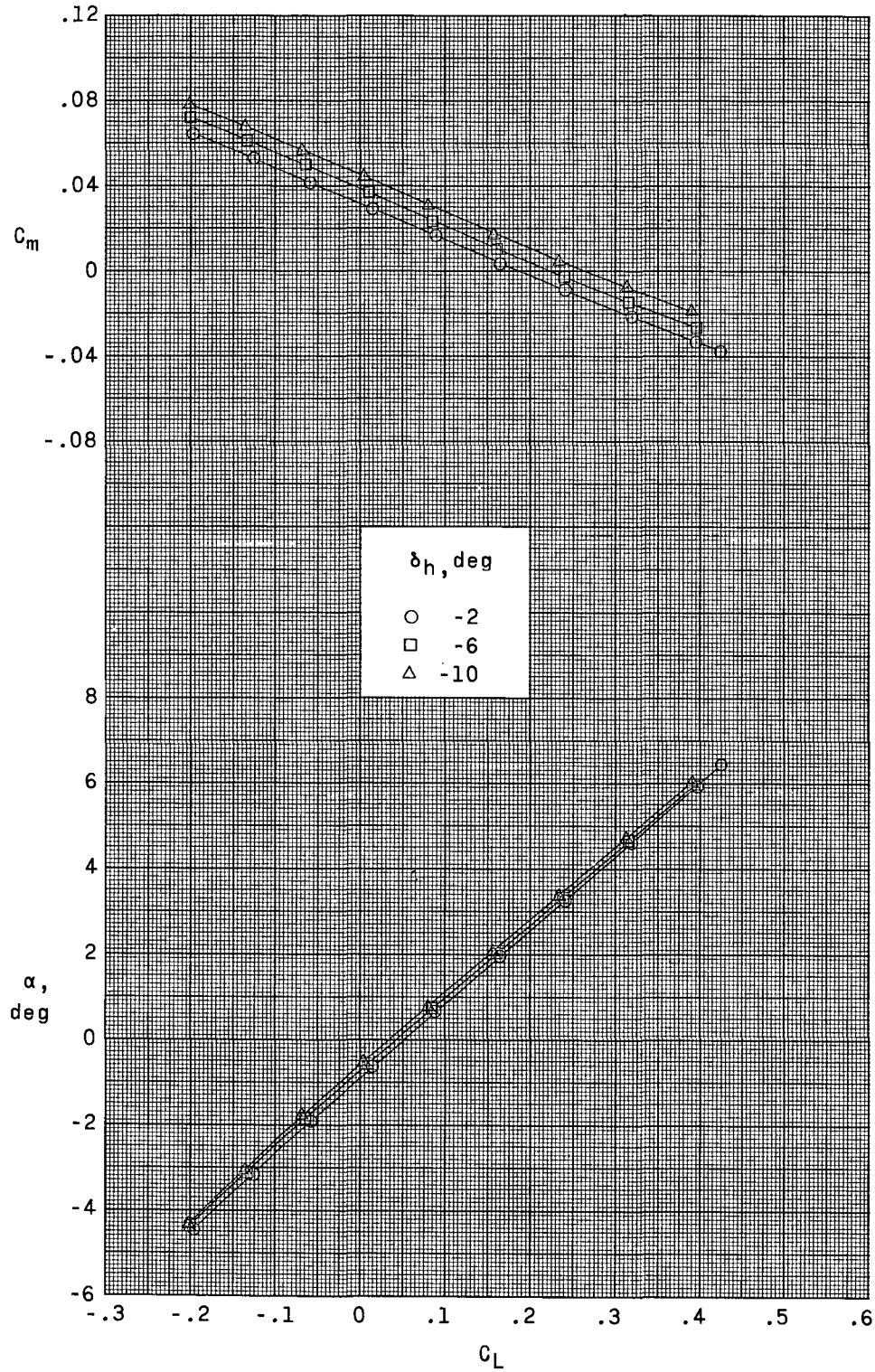

Figure 22.- Effect of horizontal-tail deflection on longitudinal aerodynamic characteristics at Mach number 1.30. $\Lambda = 35^{\circ}$.

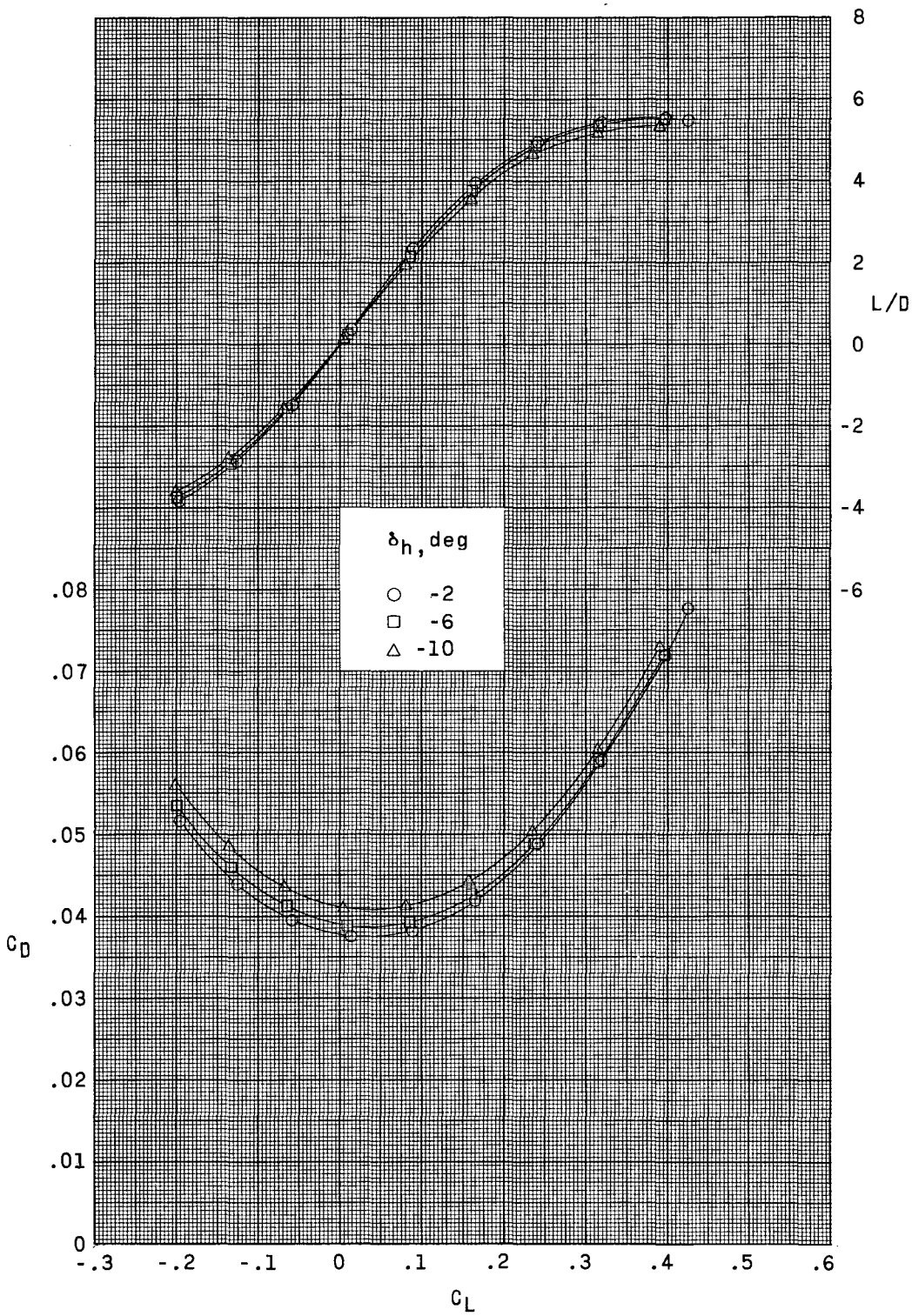

Figure 22.- Concluded.

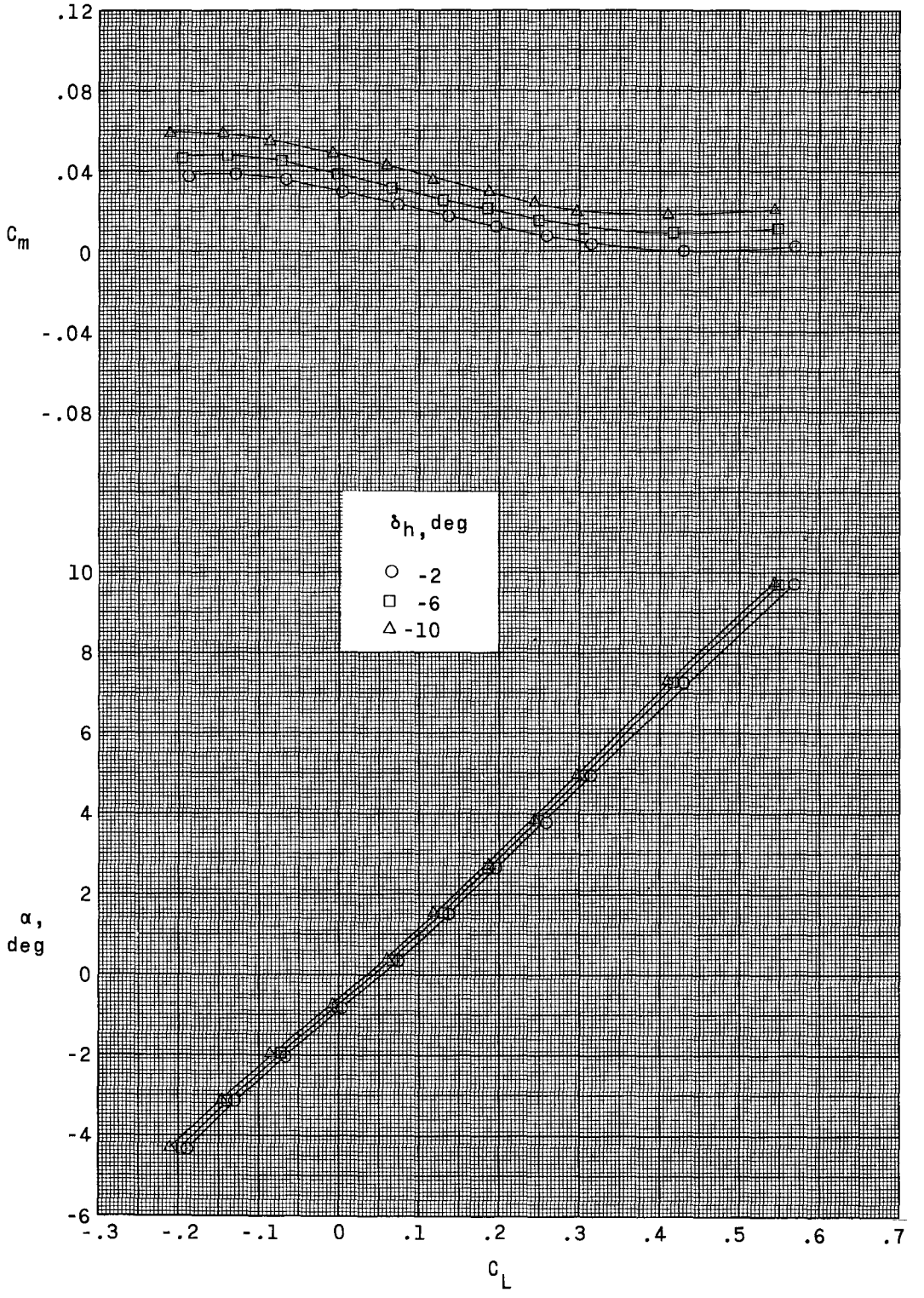

Figure 23.- Effect of horizontal-tail deflection on longitudinal aerodynamic characteristics at Mach number 0.50. $\Lambda = 45^\circ$.

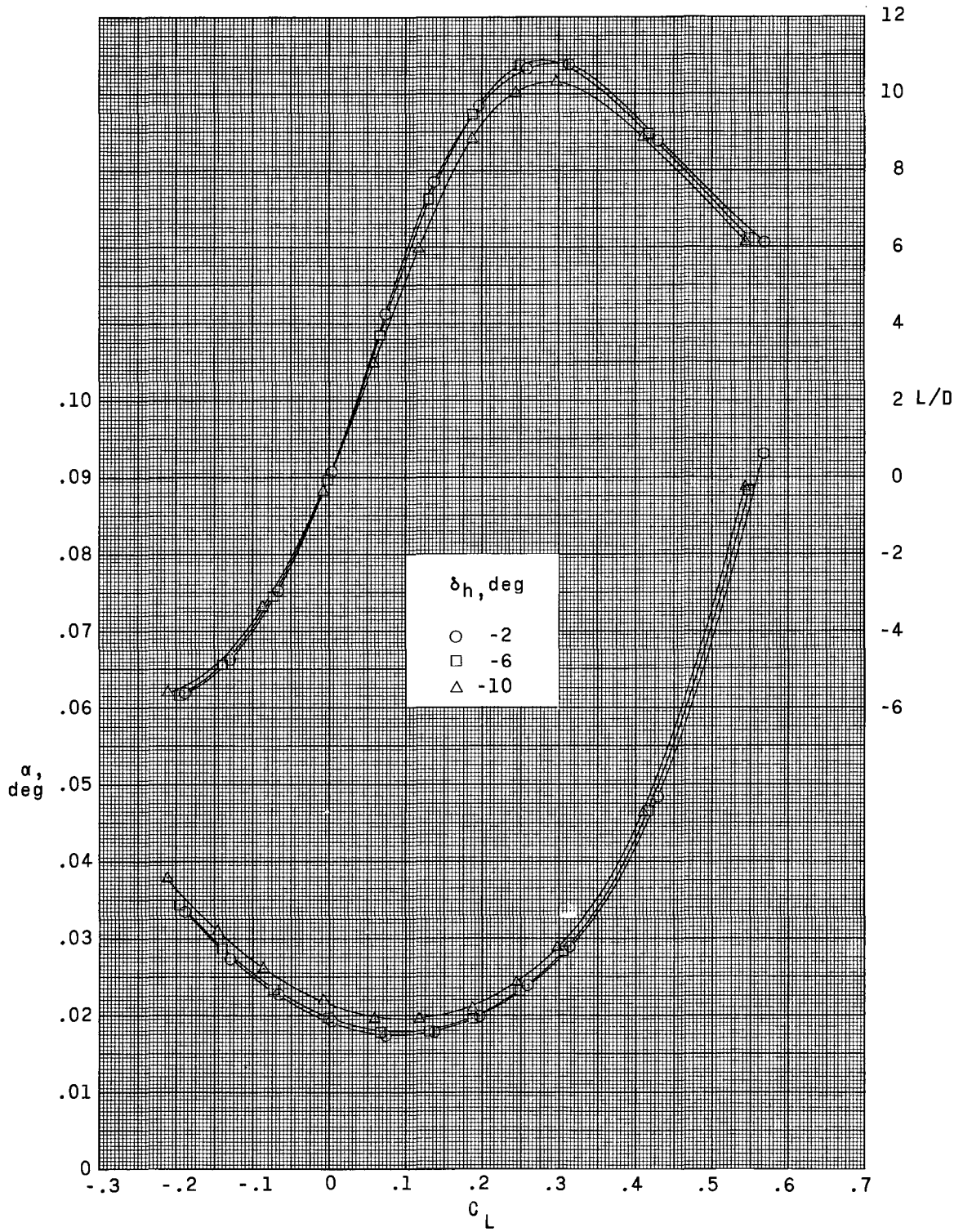

Figure 23.- Concluded.

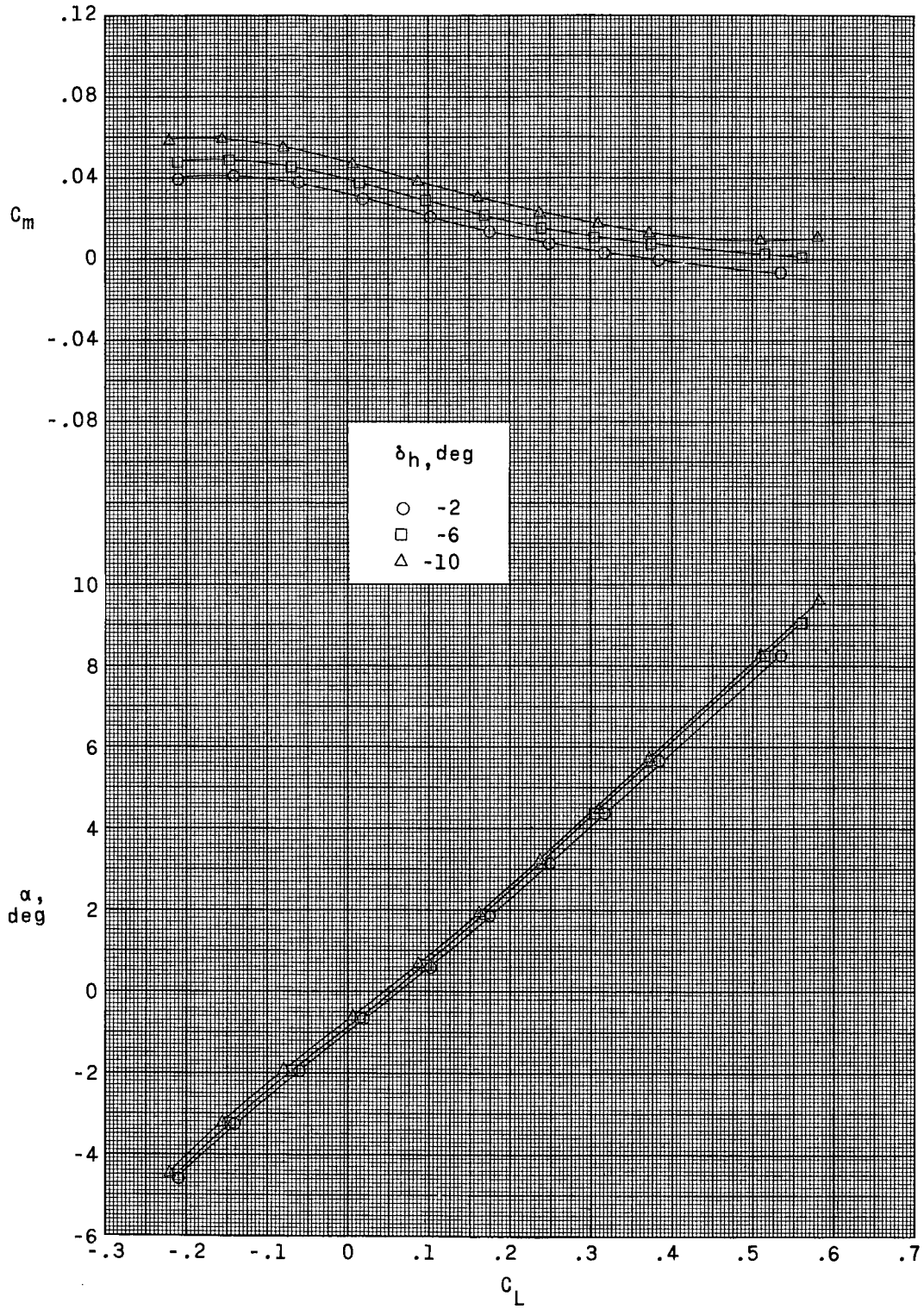

Figure 24.- Effect of horizontal-tail deflection on longitudinal aerodynamic characteristics at Mach number 0.80. $\Lambda = 45^\circ$.

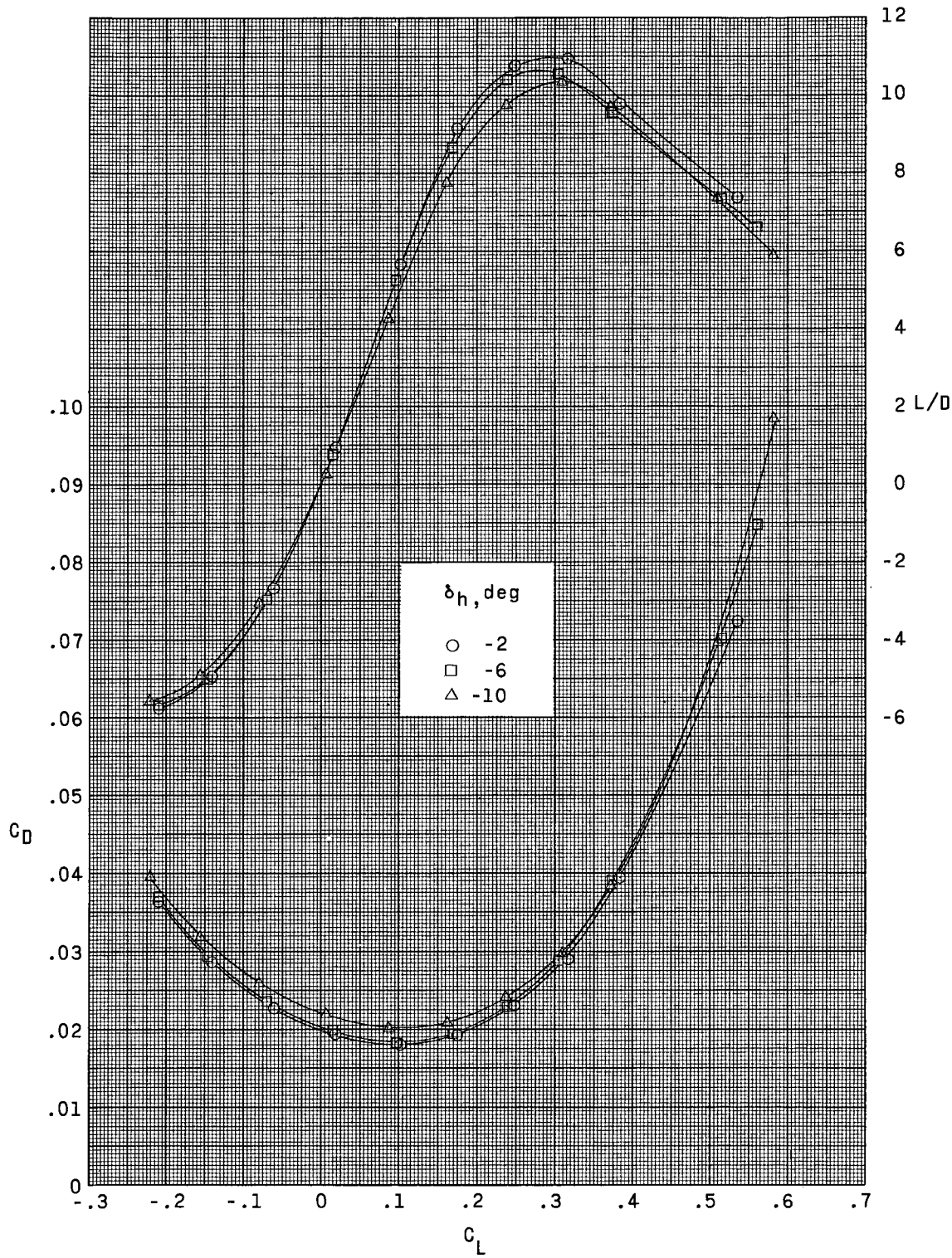

Figure 24.- Concluded.

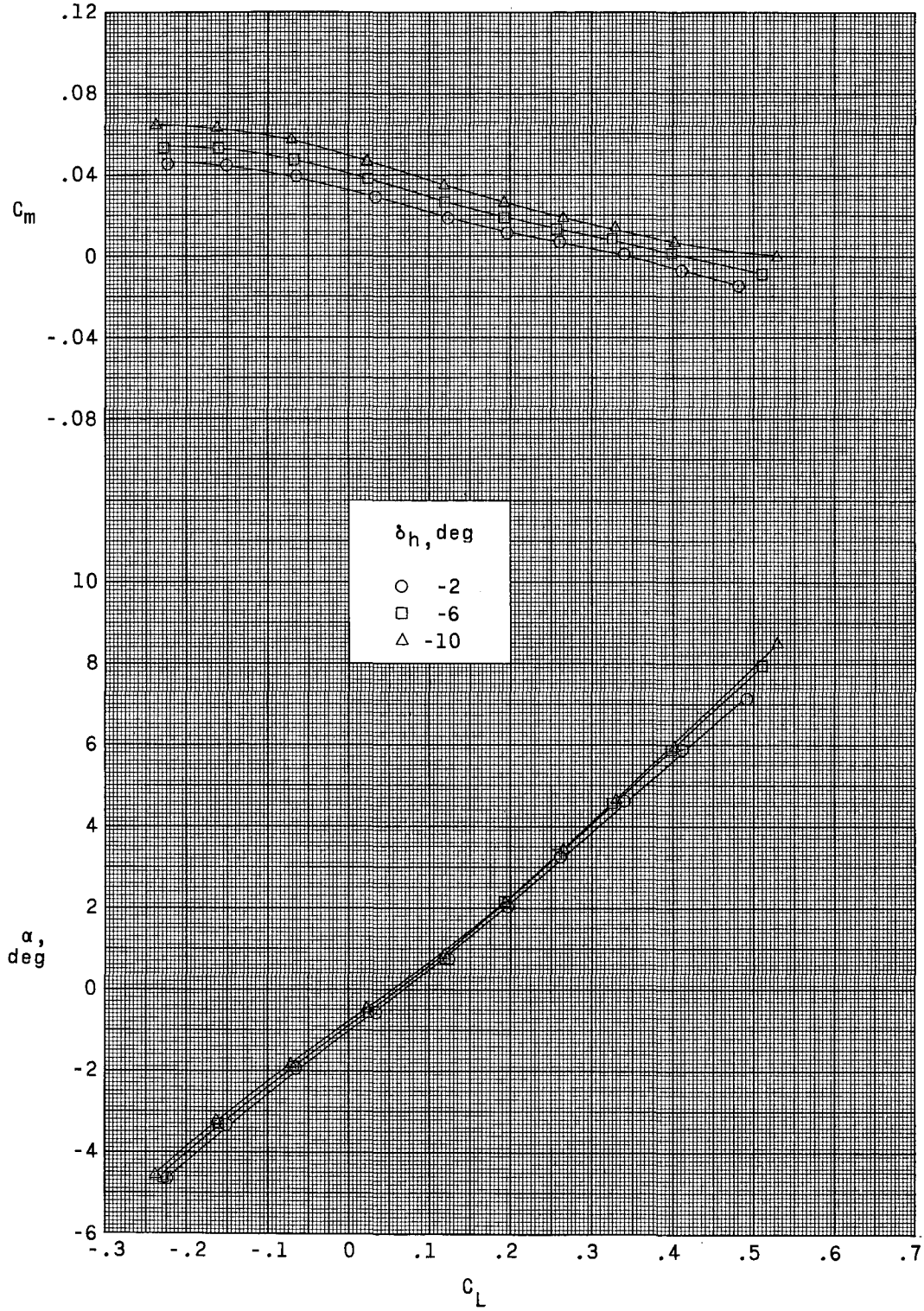

Figure 25.- Effect of horizontal-tail deflection on longitudinal aerodynamic characteristics at Mach number 0.90. $\Lambda = 45^\circ$.

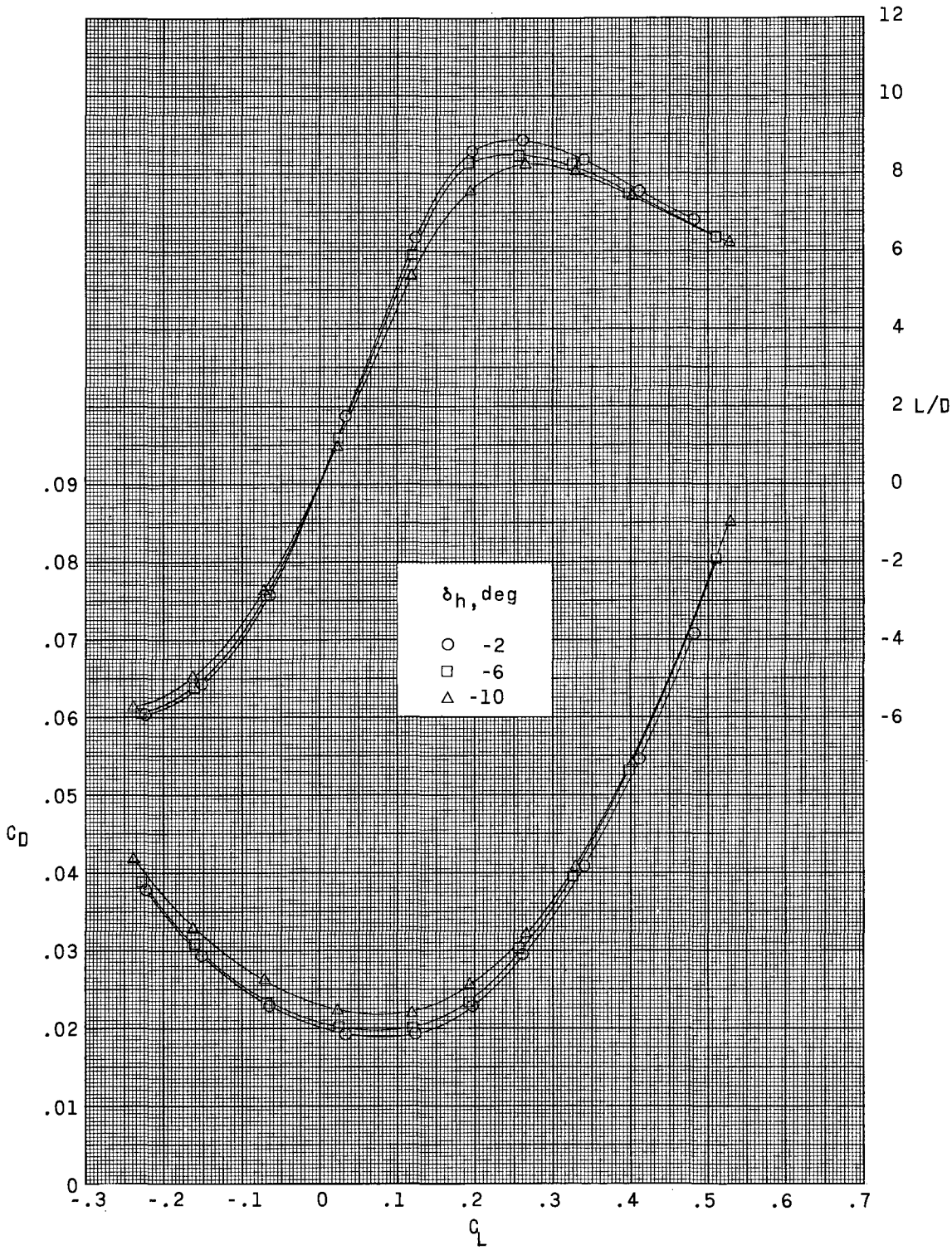

Figure 25.- Concluded.

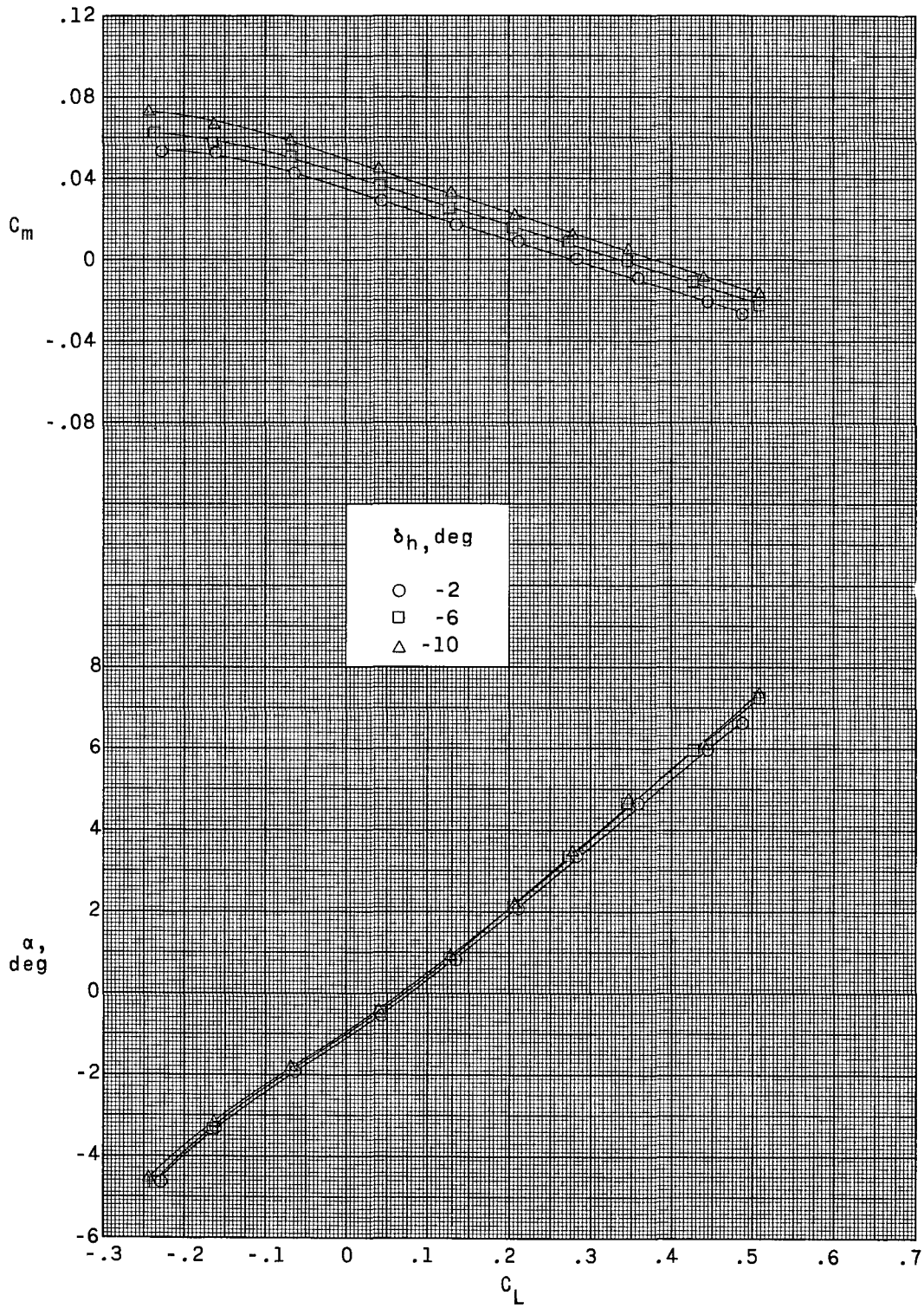

Figure 26.- Effect of horizontal-tail deflection on longitudinal aerodynamic characteristics at Mach number 0.94. $\Lambda = 45^\circ$.

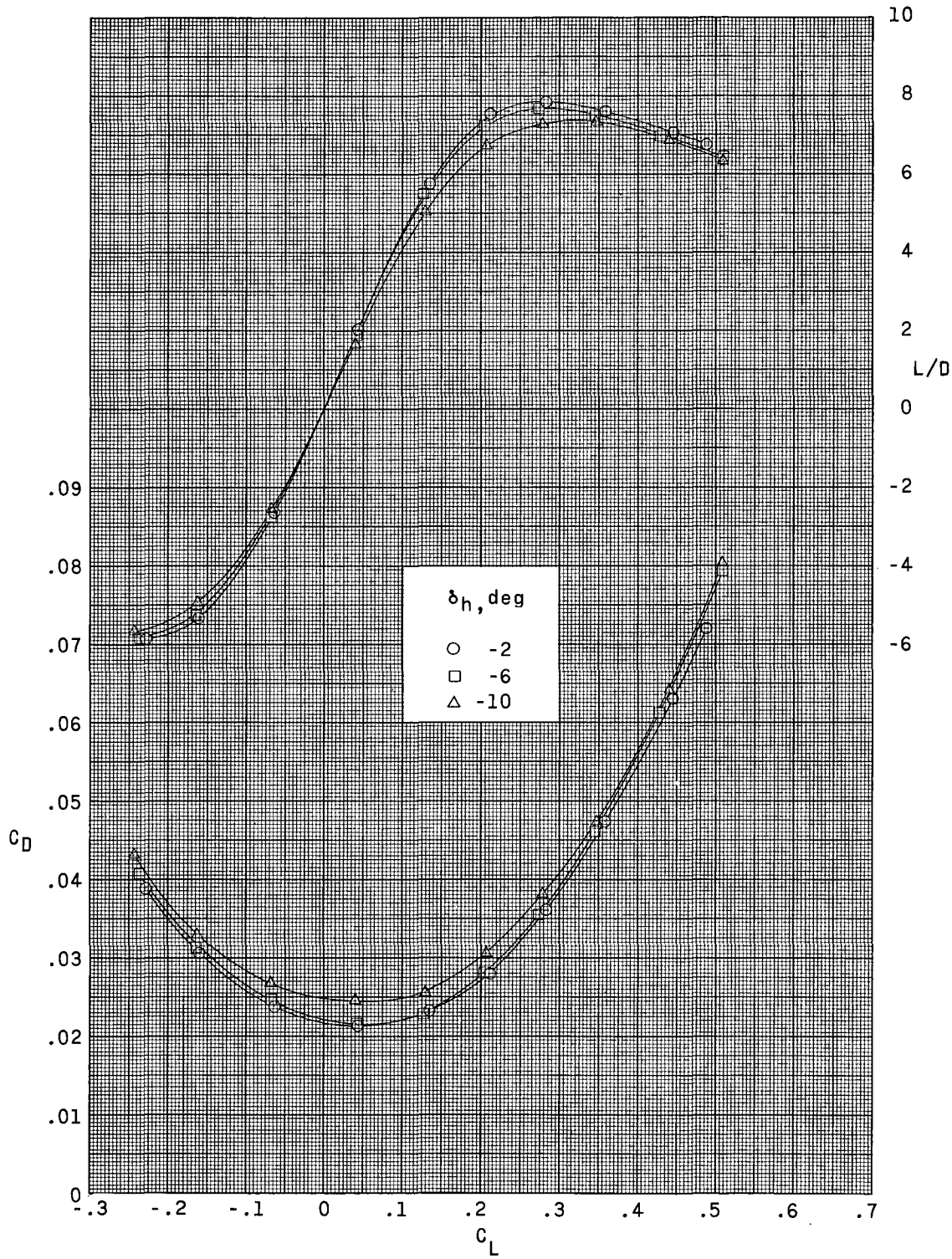

Figure 26.- Concluded.

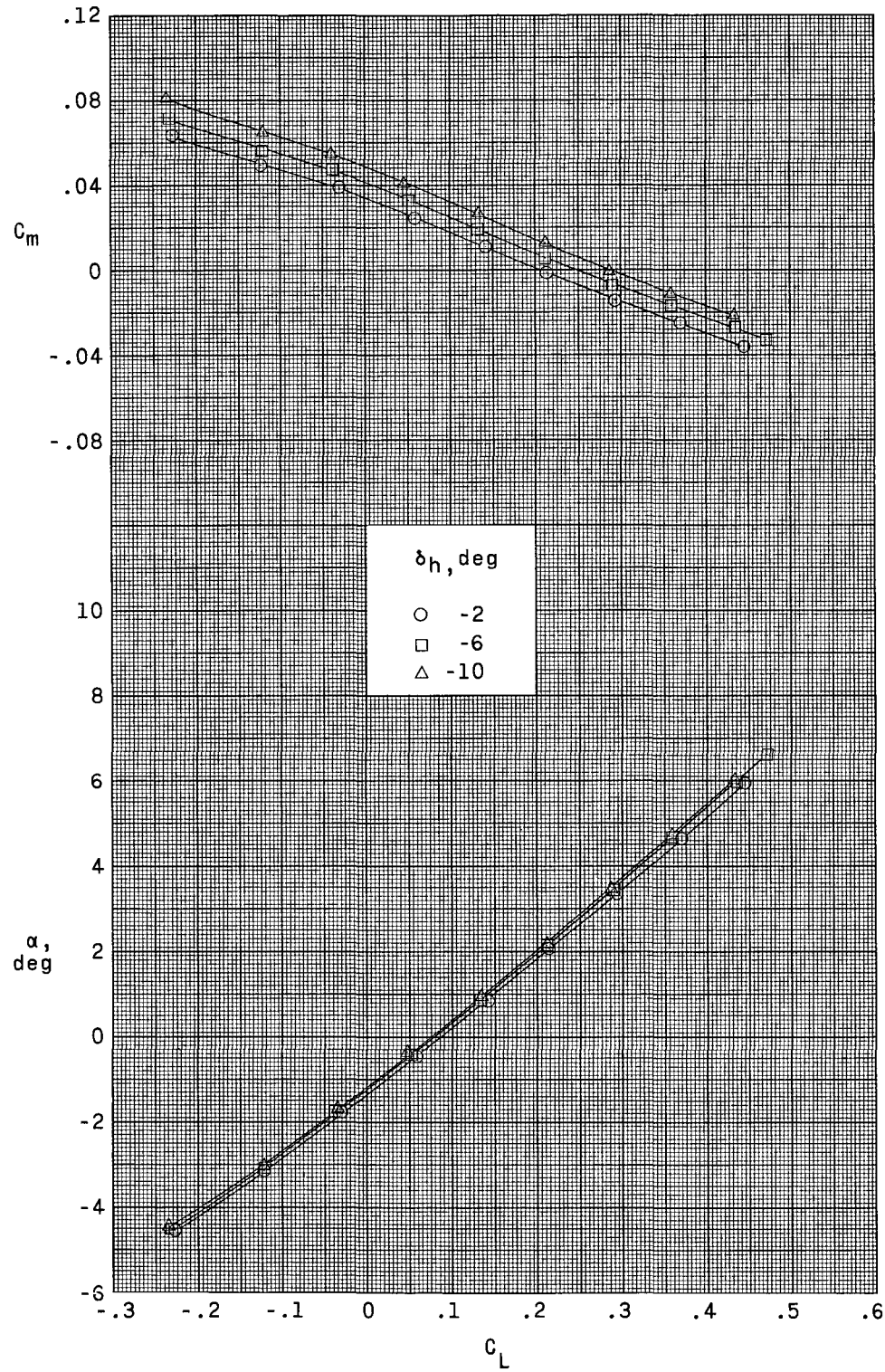

Figure 27.- Effect of horizontal-tail deflection on longitudinal aerodynamic characteristics at Mach number 1.03. $\Lambda = 45^\circ$.

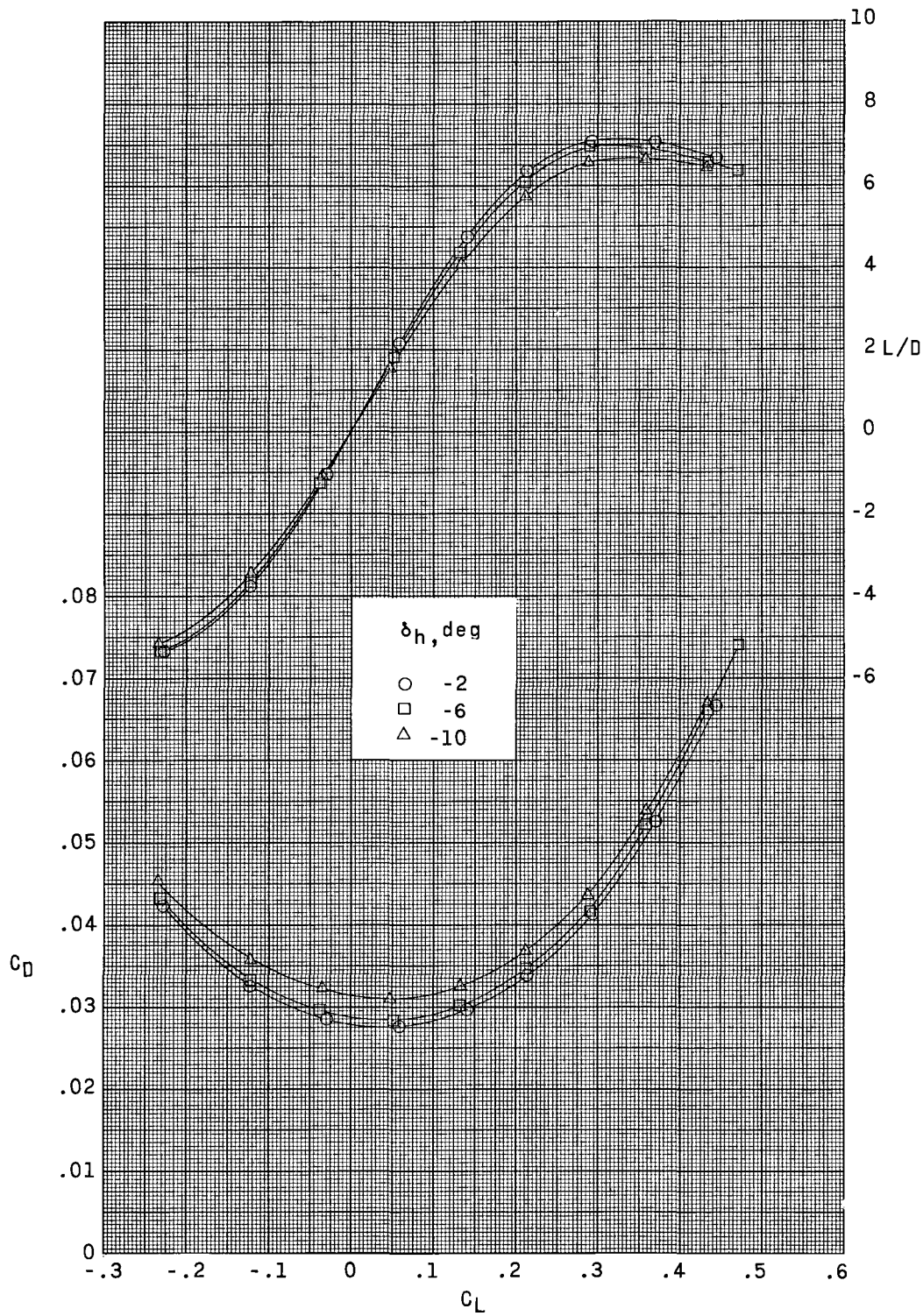

Figure 27.- Concluded.

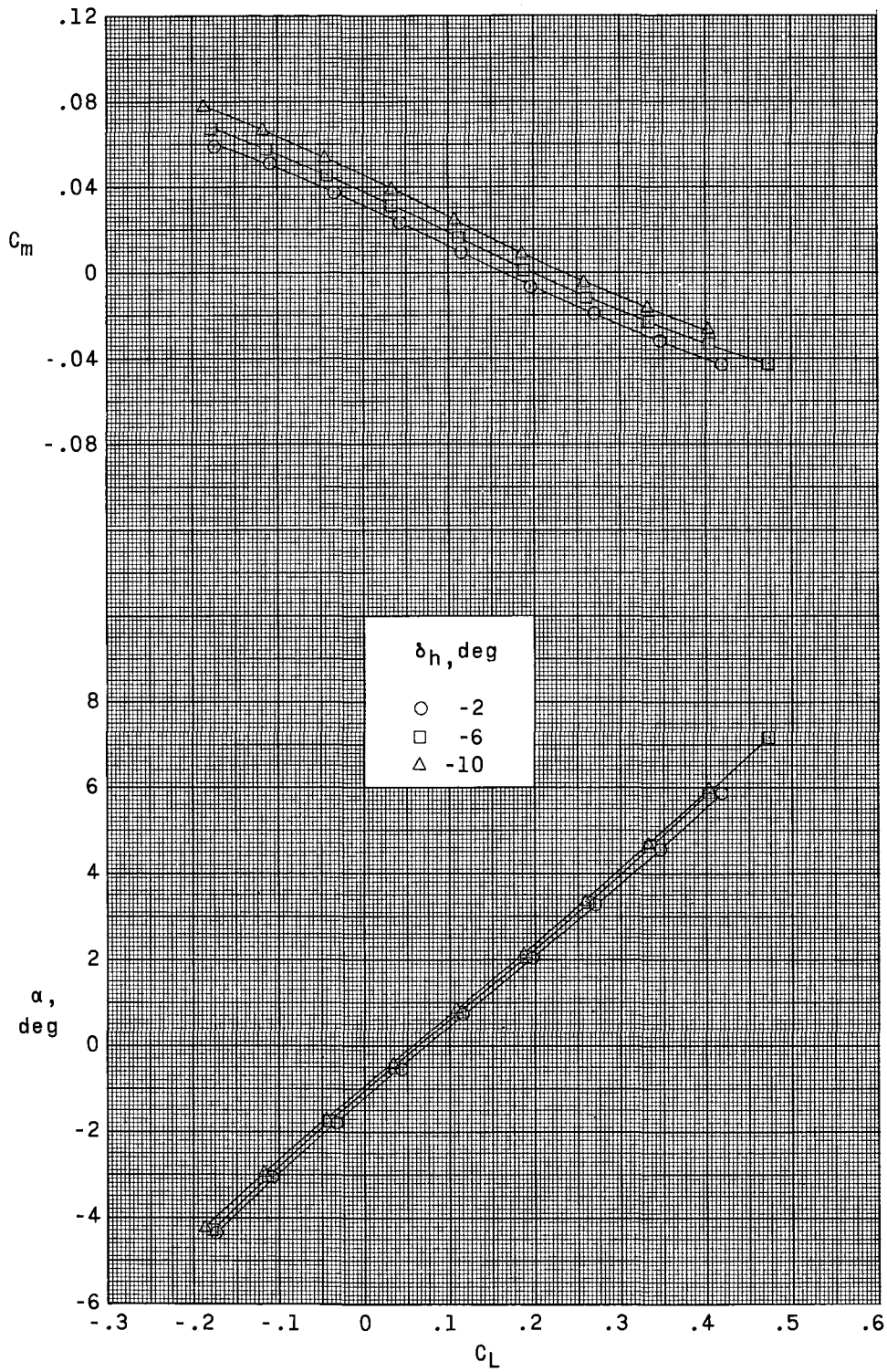

Figure 28.- Effect of horizontal-tail deflection on longitudinal aerodynamic characteristics at Mach number 1.20. $\Lambda = 45^\circ$.

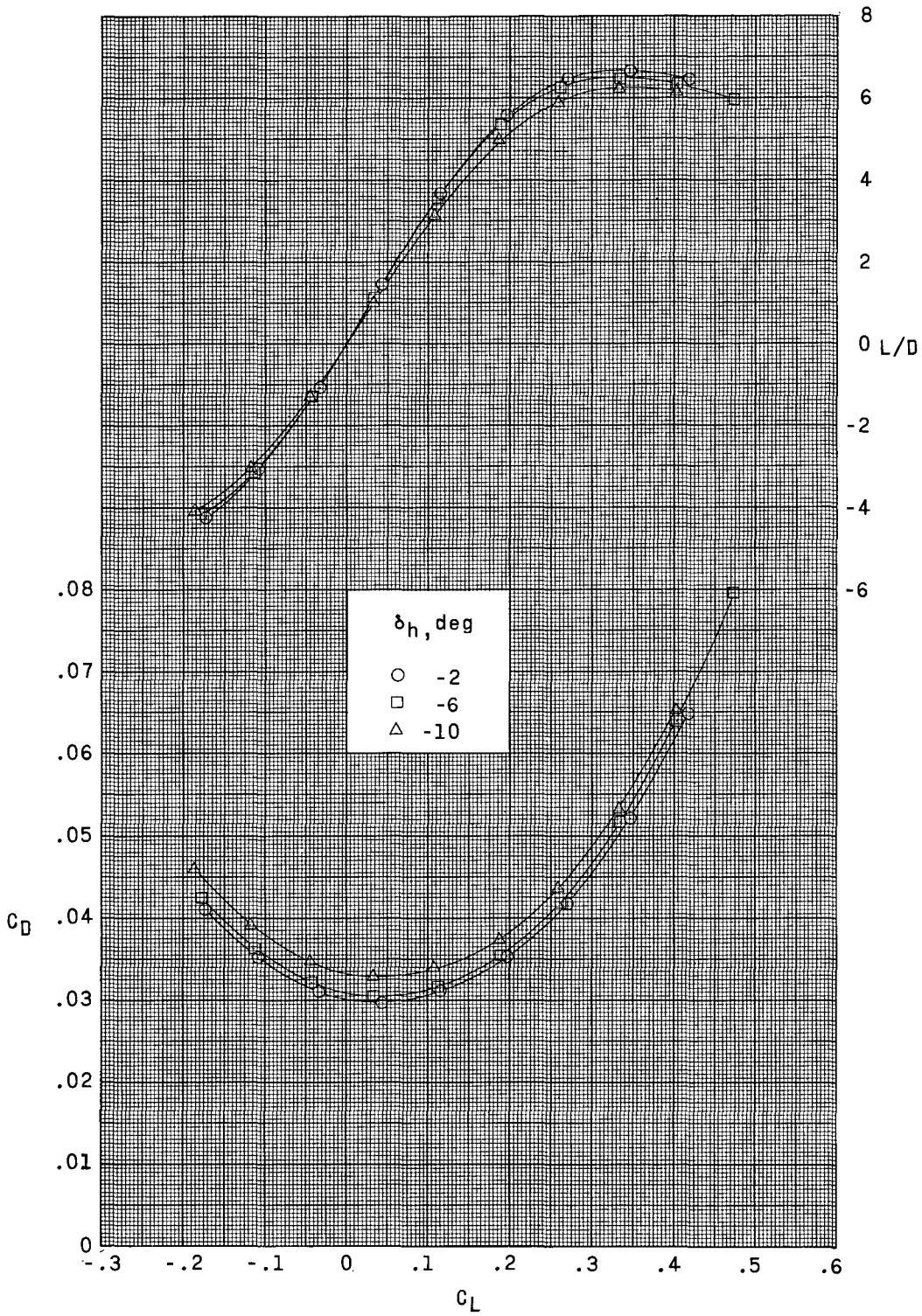

Figure 28.- Concluded.

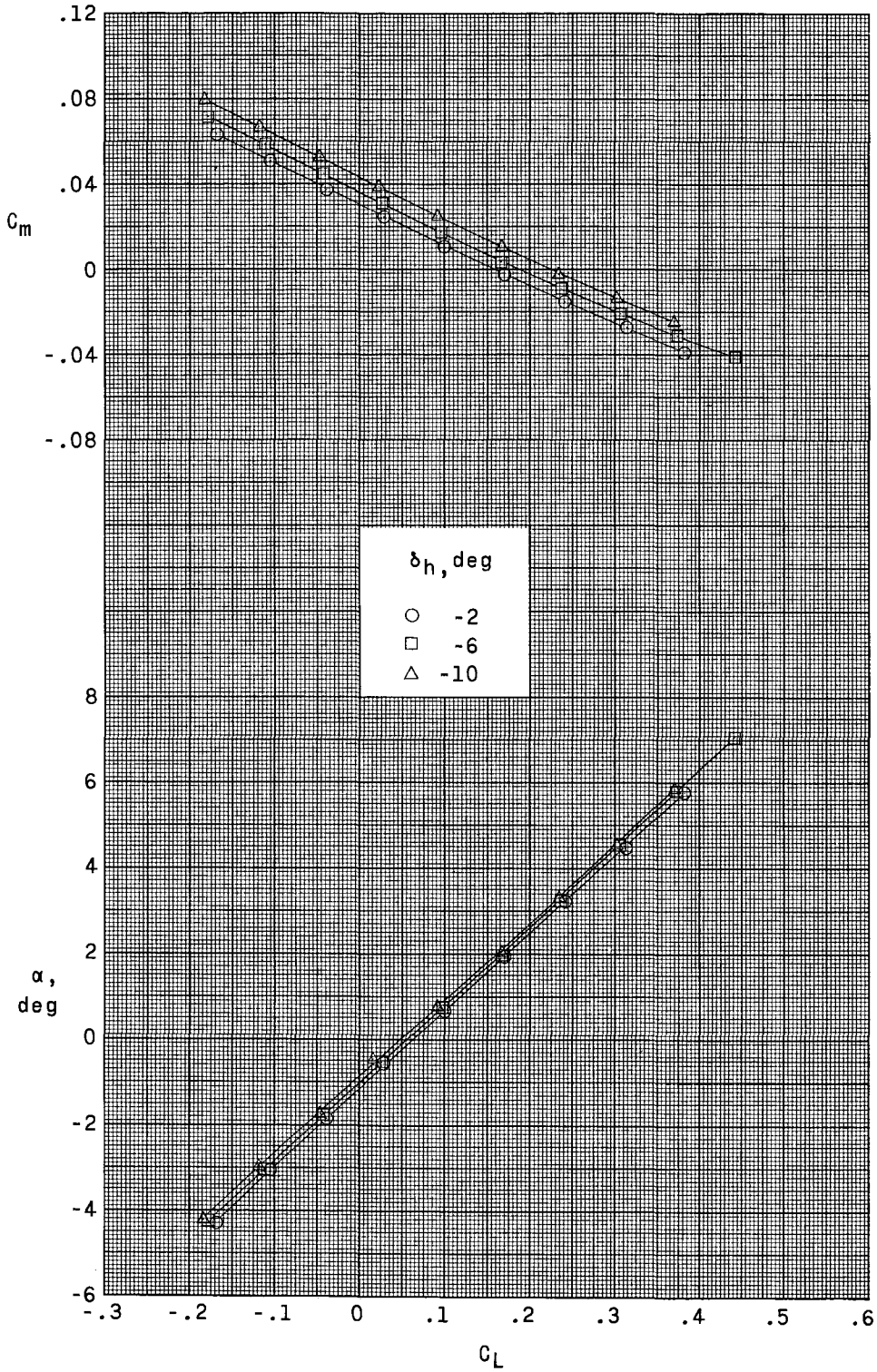

Figure 29.- Effect of horizontal-tail deflection on longitudinal aerodynamic characteristics at Mach number 1.30. $\Lambda = 45^\circ$.

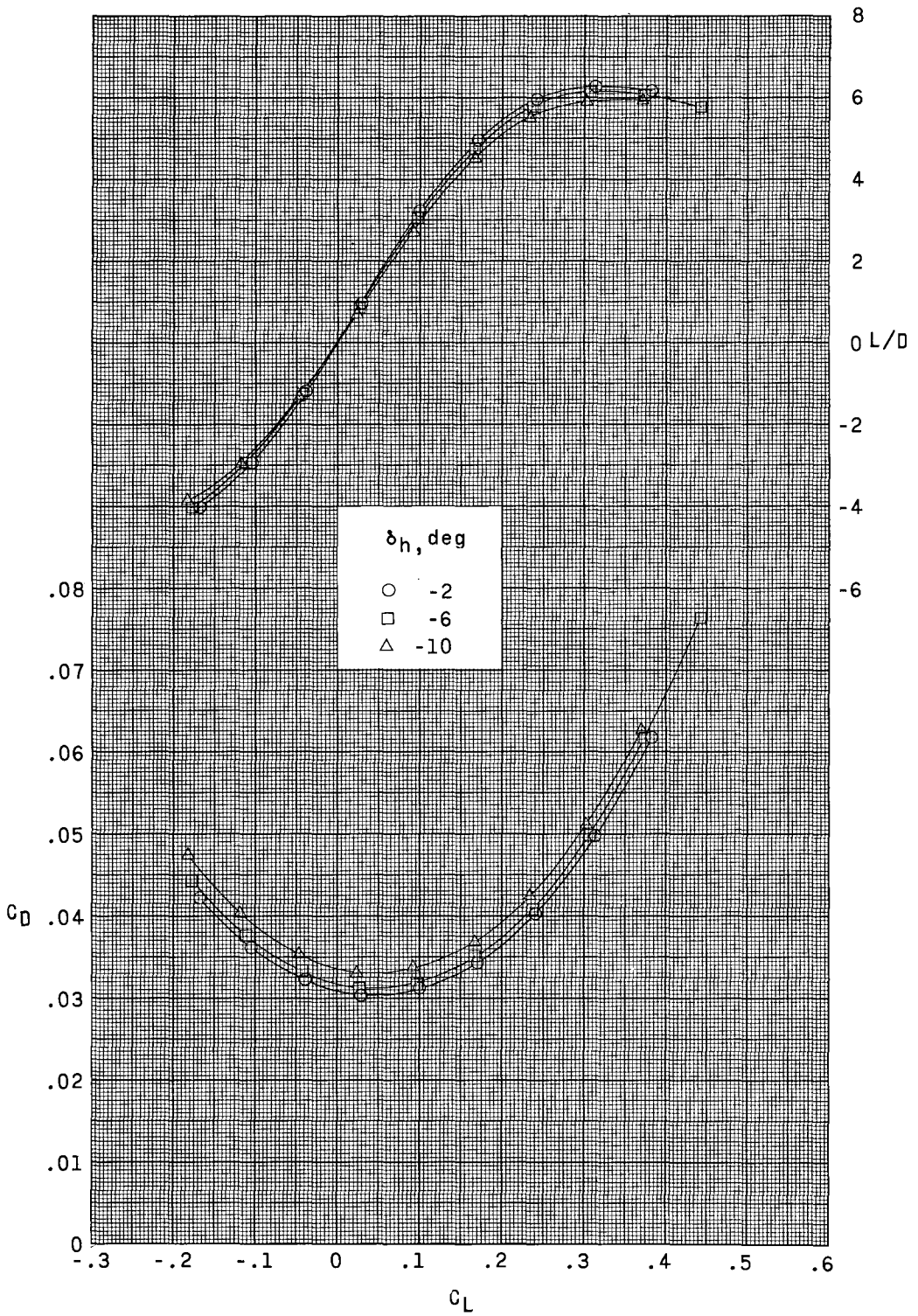

Figure 29.- Concluded.

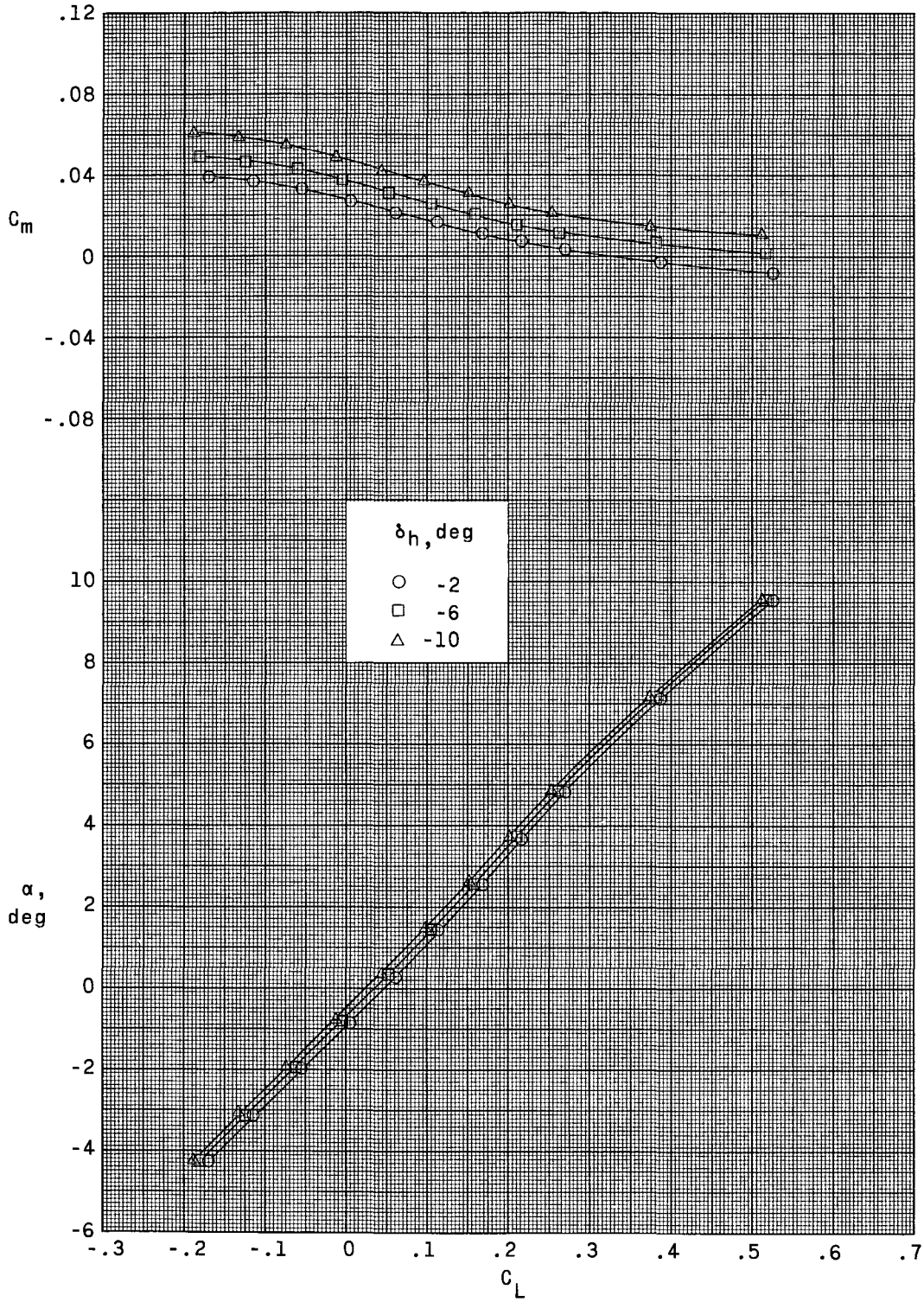

Figure 30.- Effect of horizontal-tail deflection on longitudinal aerodynamic characteristics at Mach number 0.50. $\Lambda = 55^\circ$.

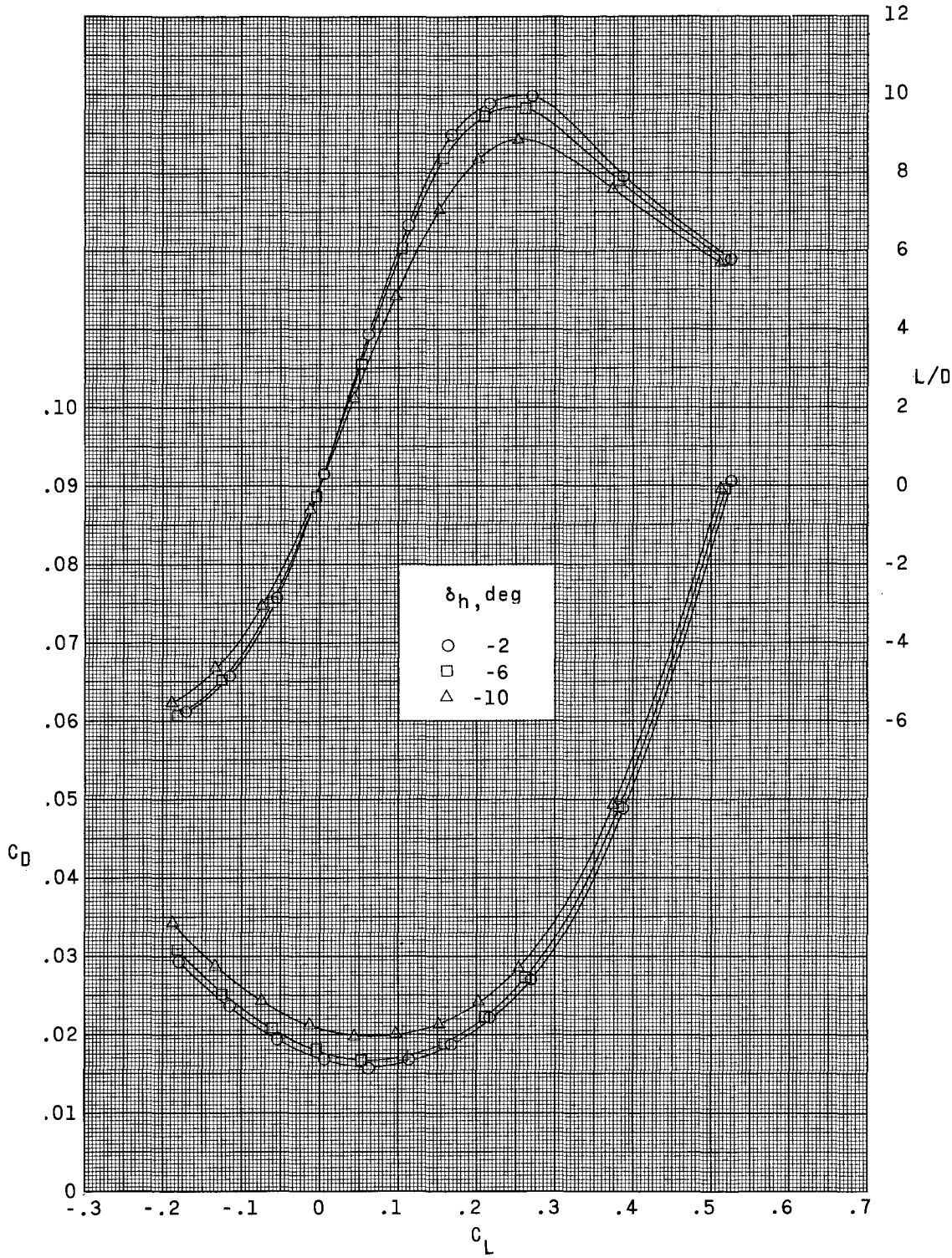

Figure 30.- Concluded.

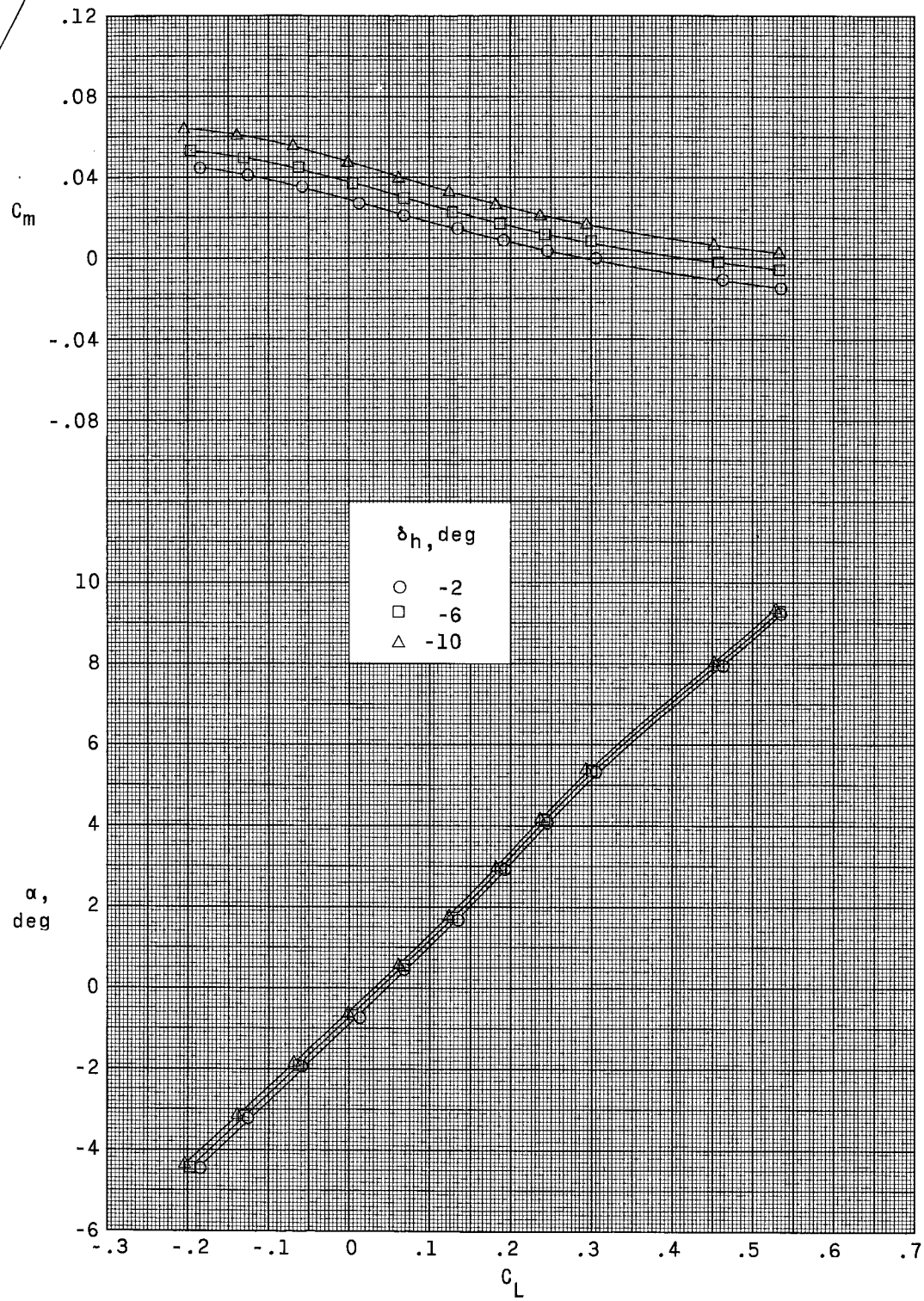

Figure 31.- Effect of horizontal-tail deflection on longitudinal aerodynamic characteristics at Mach number 0.80. $\Lambda = 55^\circ$.

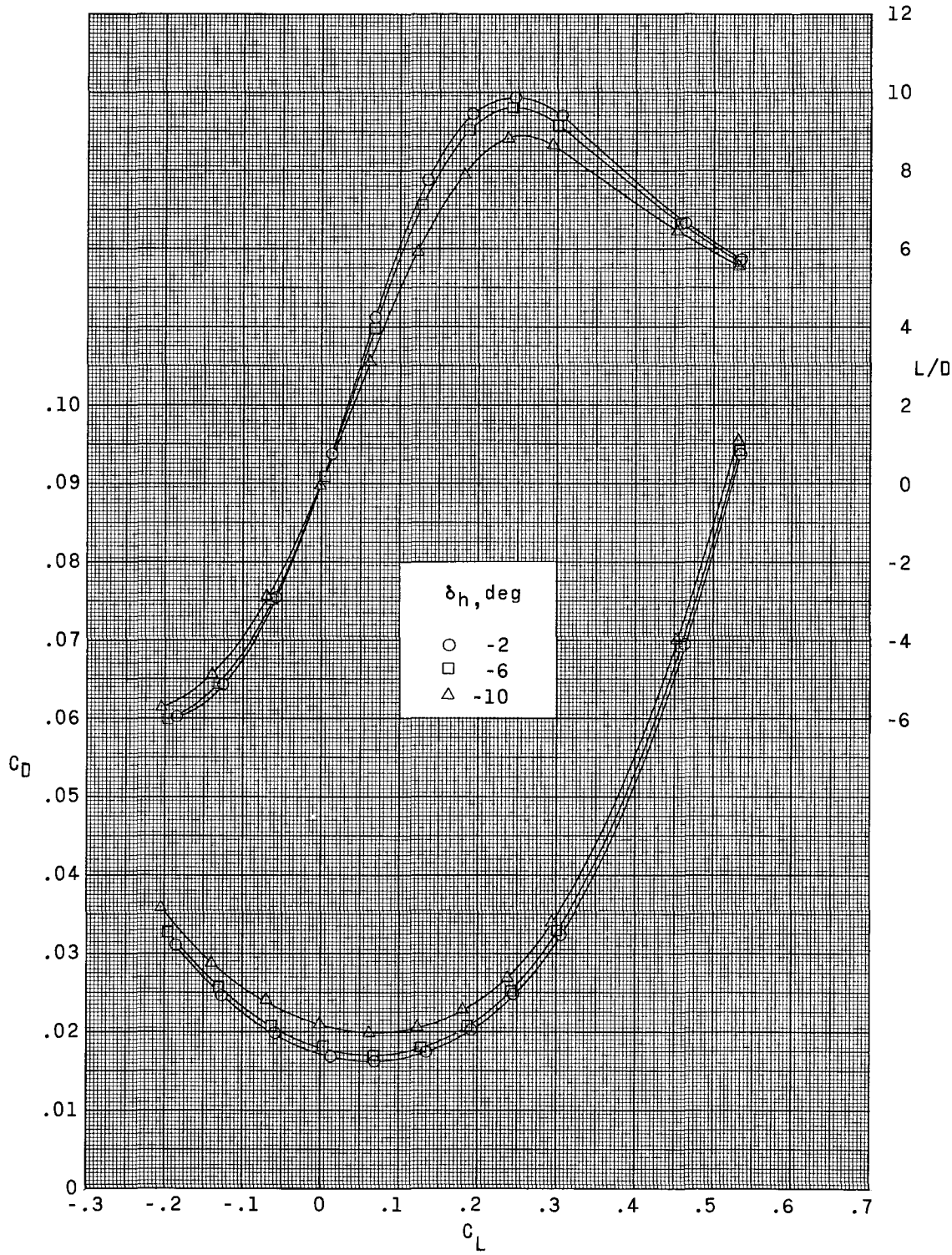

Figure 31.- Concluded.

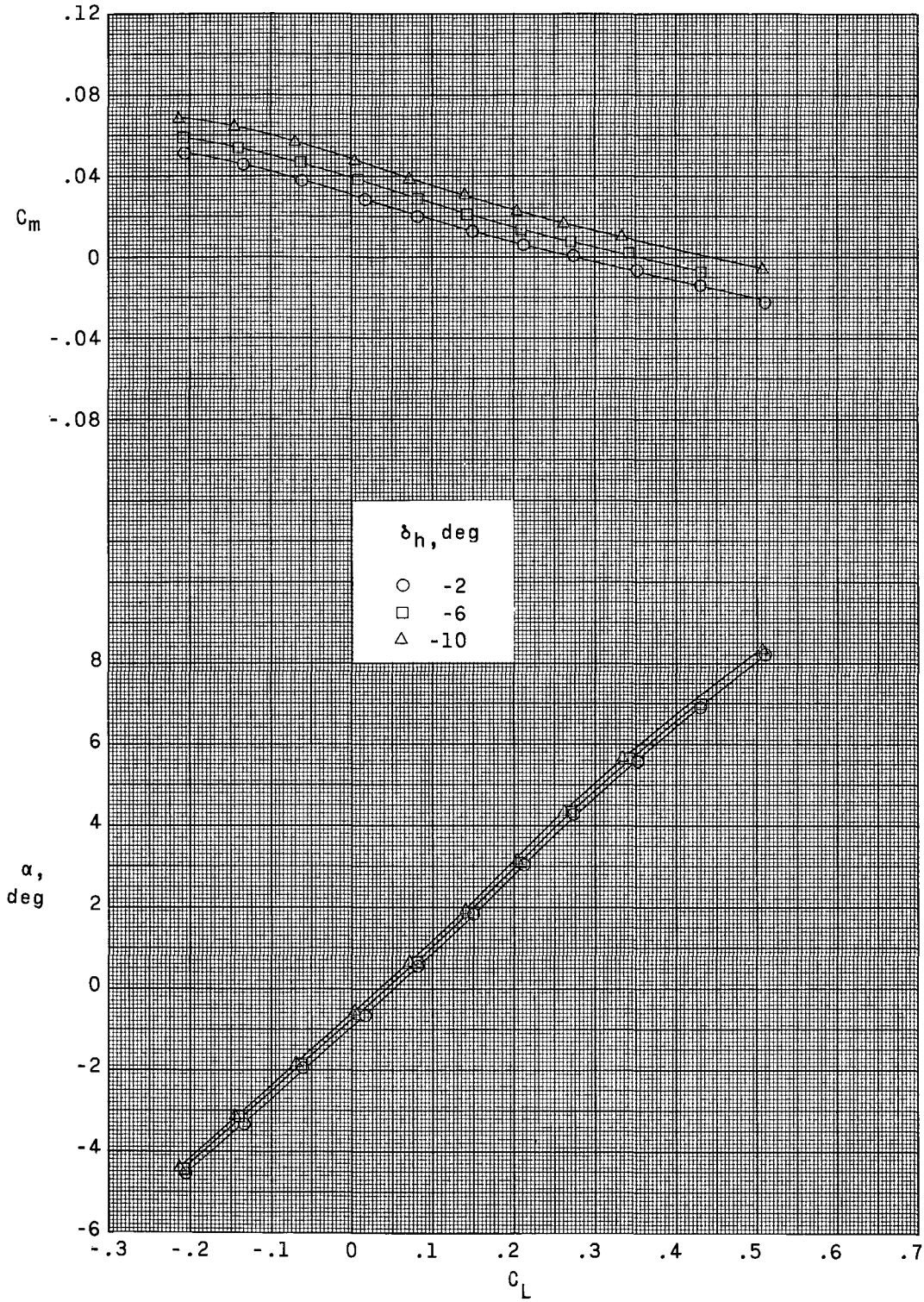

Figure 32.- Effect of horizontal-tail deflection on longitudinal aerodynamic characteristics at Mach number 0.90. $\Lambda = 55^\circ$.

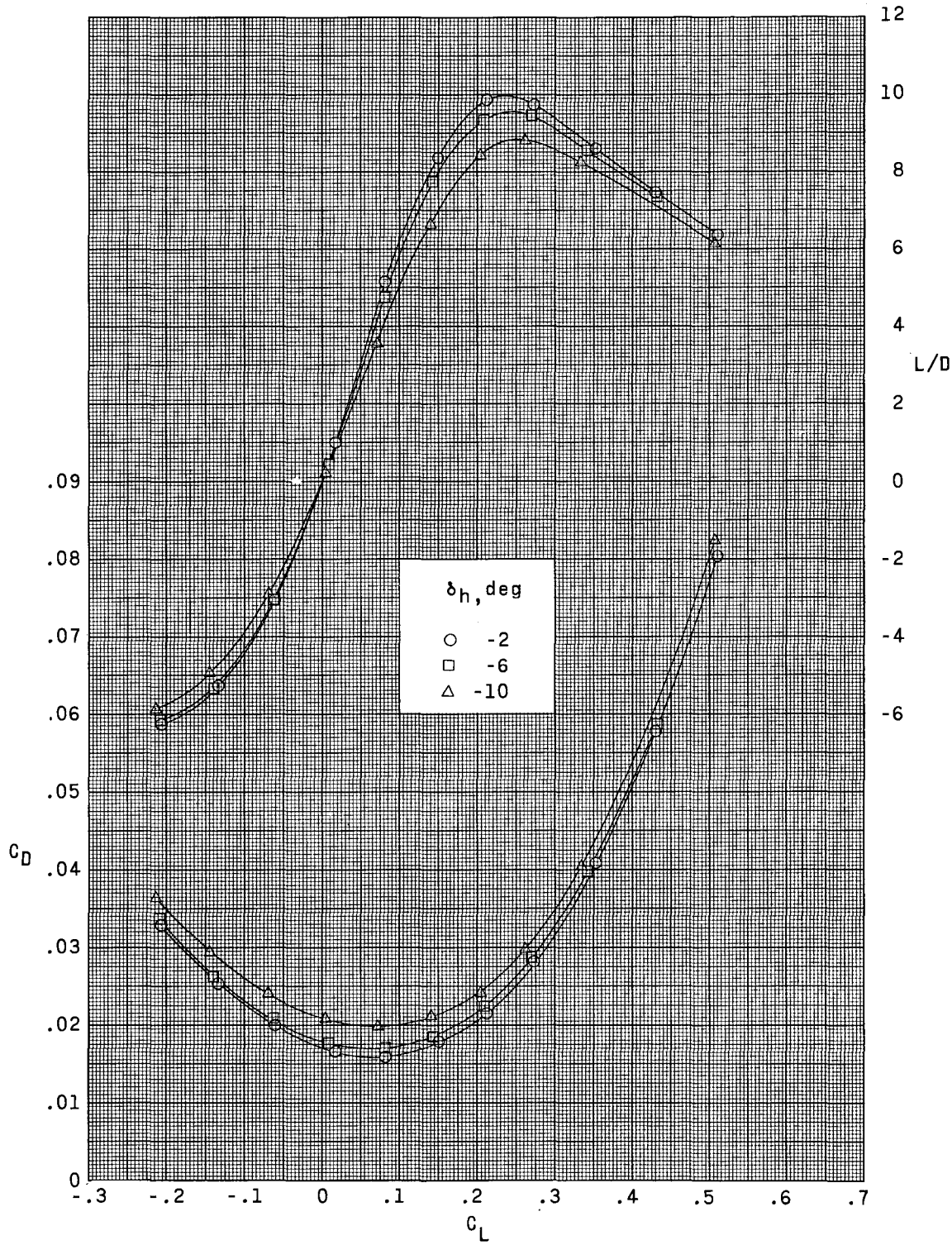

Figure 32.- Concluded.

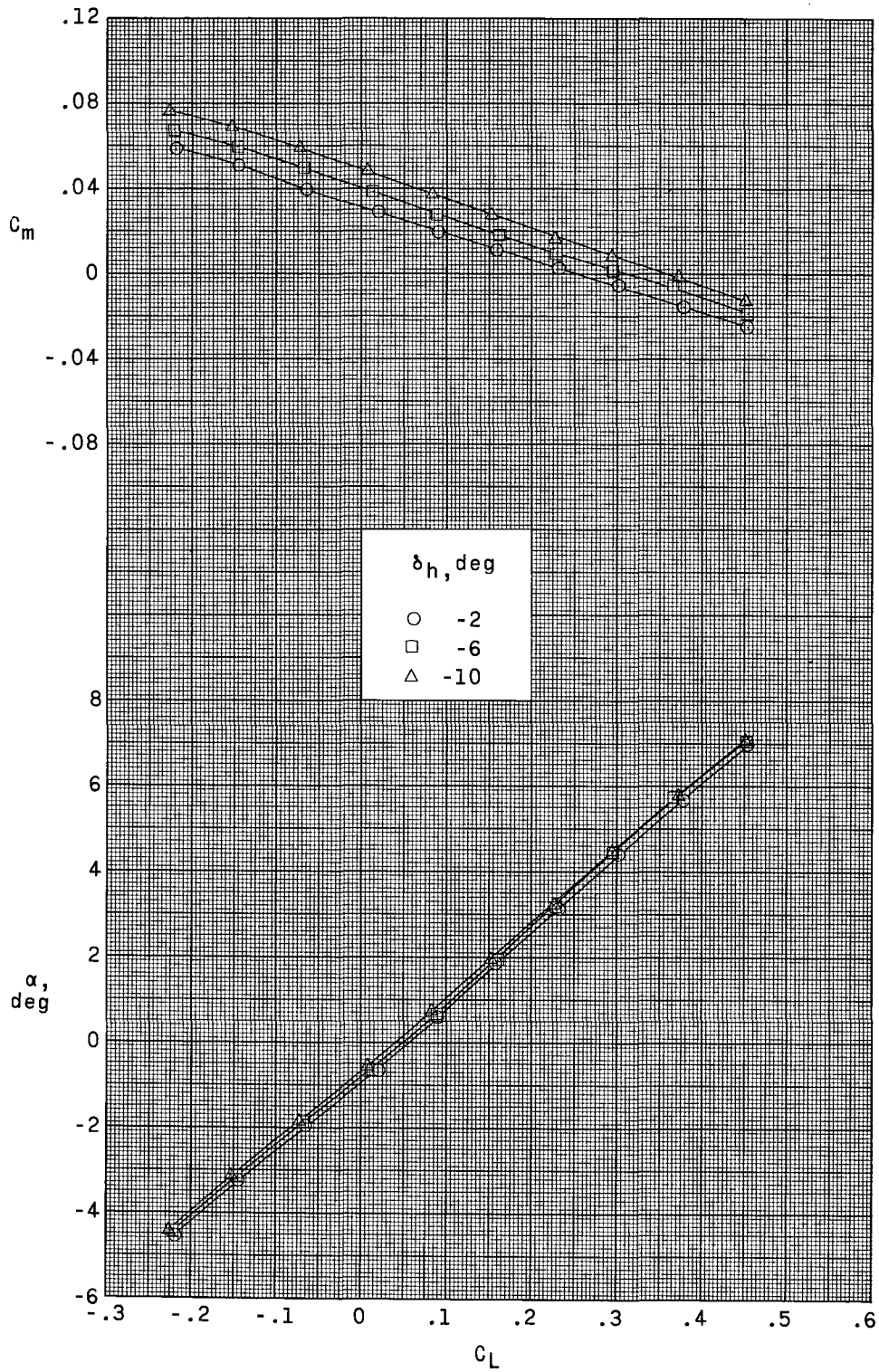

Figure 33.- Effect of horizontal-tail deflection on longitudinal aerodynamic characteristics at Mach number 0.94. $\Lambda = 55°$.

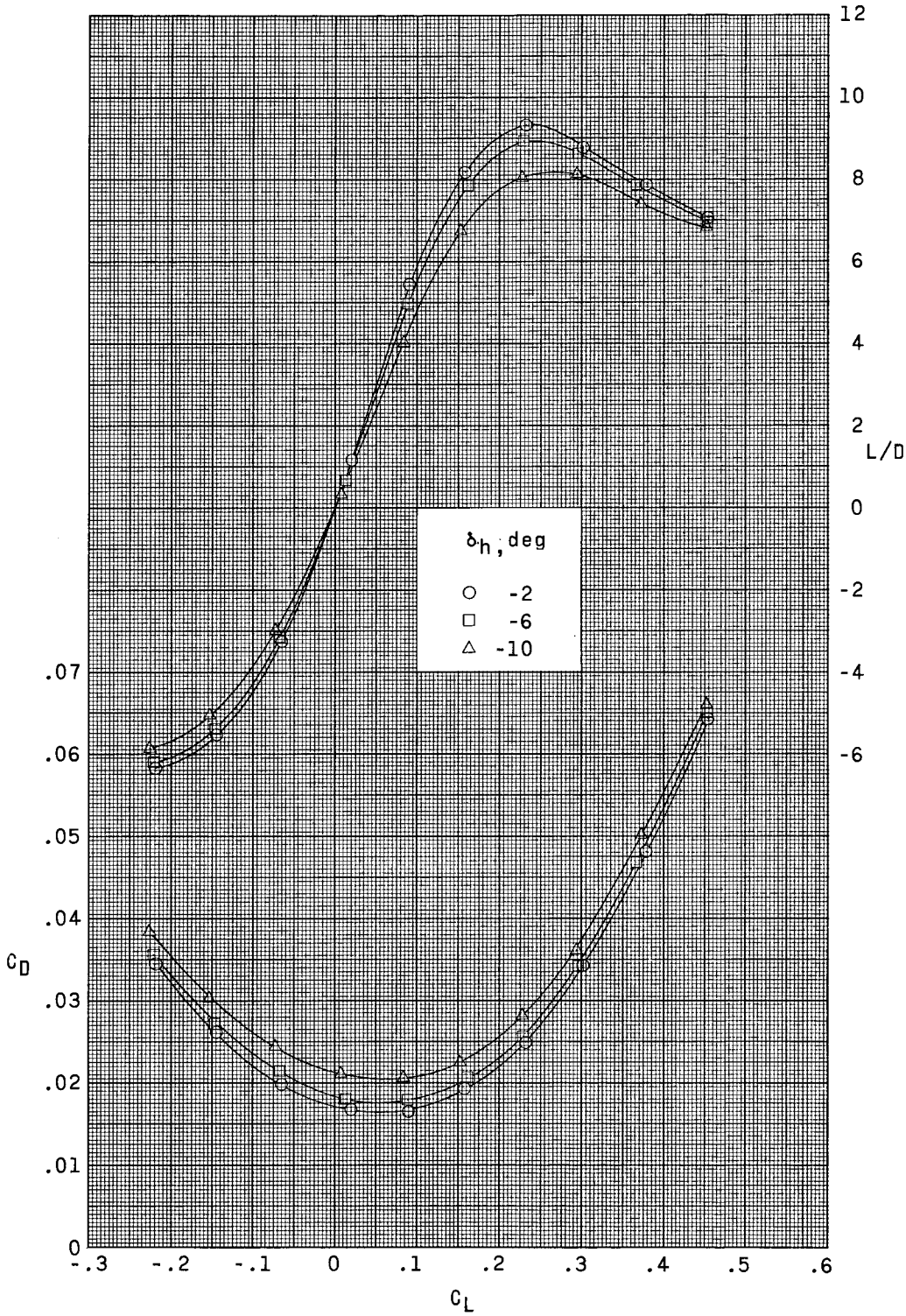

Figure 33.- Concluded.

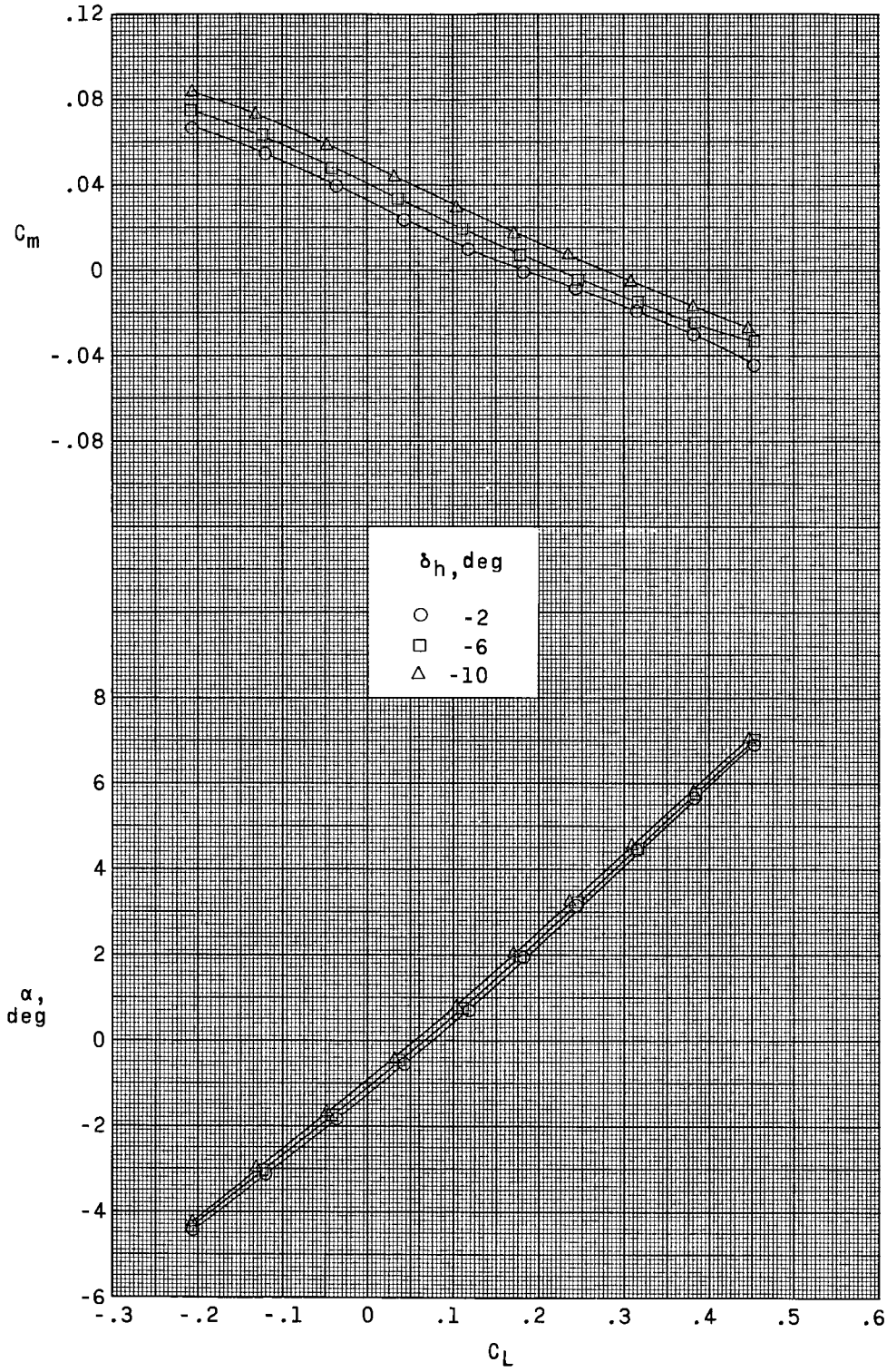

Figure 34.- Effect of horizontal-tail deflection on longitudinal aerodynamic characteristics at Mach number 1.03. $\Lambda = 55^\circ$.

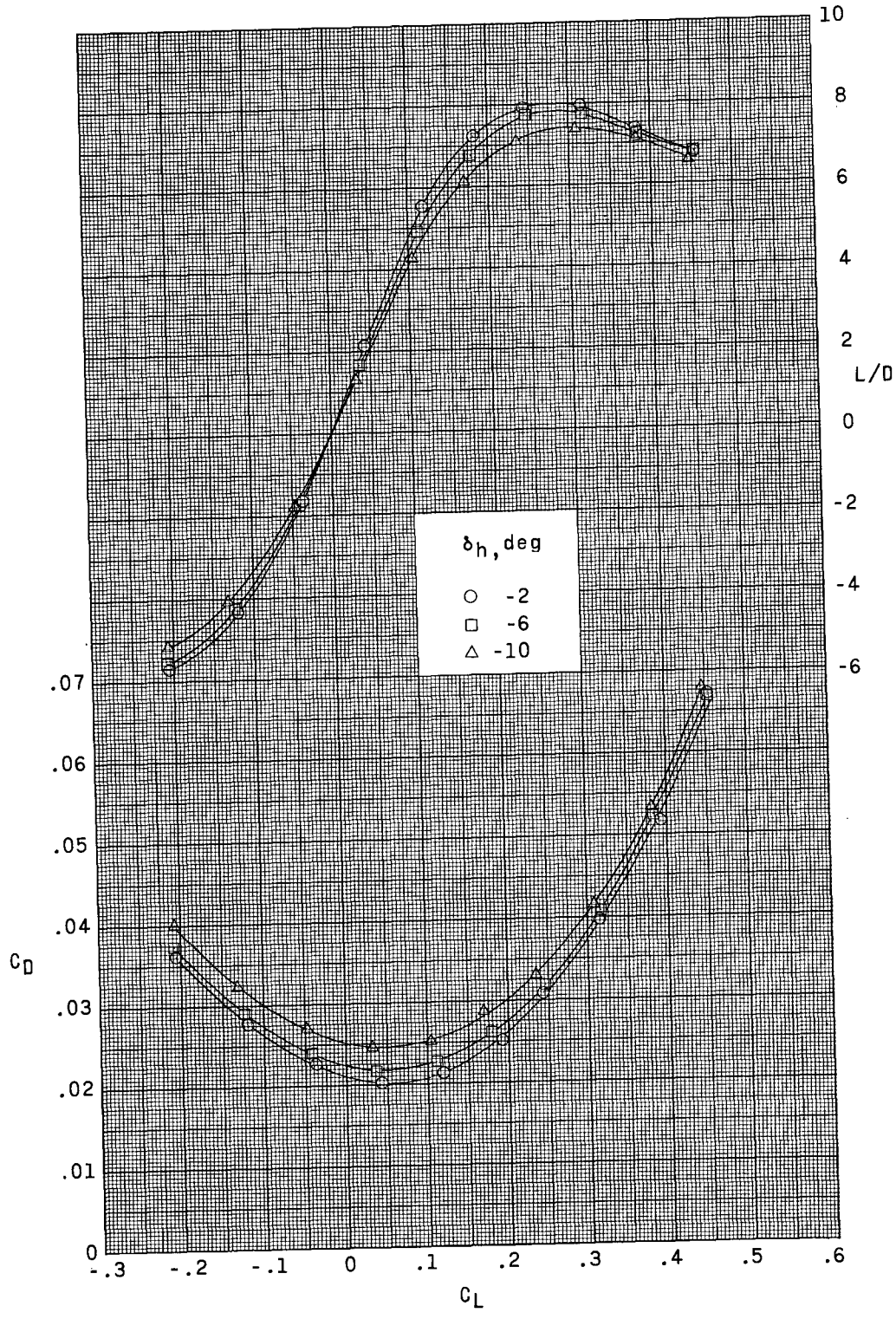

Figure 34.- Concluded.

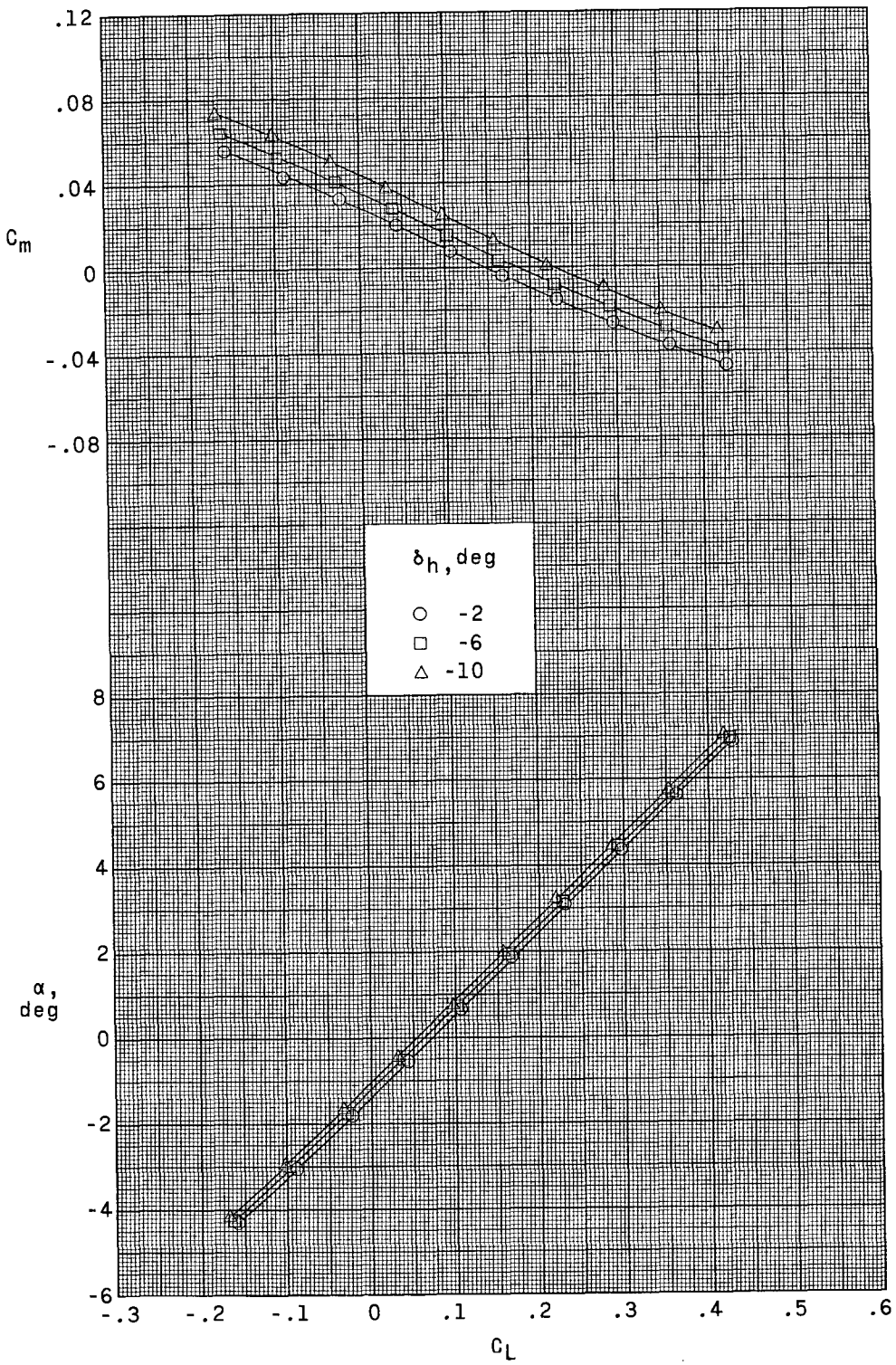

Figure 35.- Effect of horizontal-tail deflection on longitudinal aerodynamic characteristics at Mach number 1.20. $\Lambda = 55^\circ$.

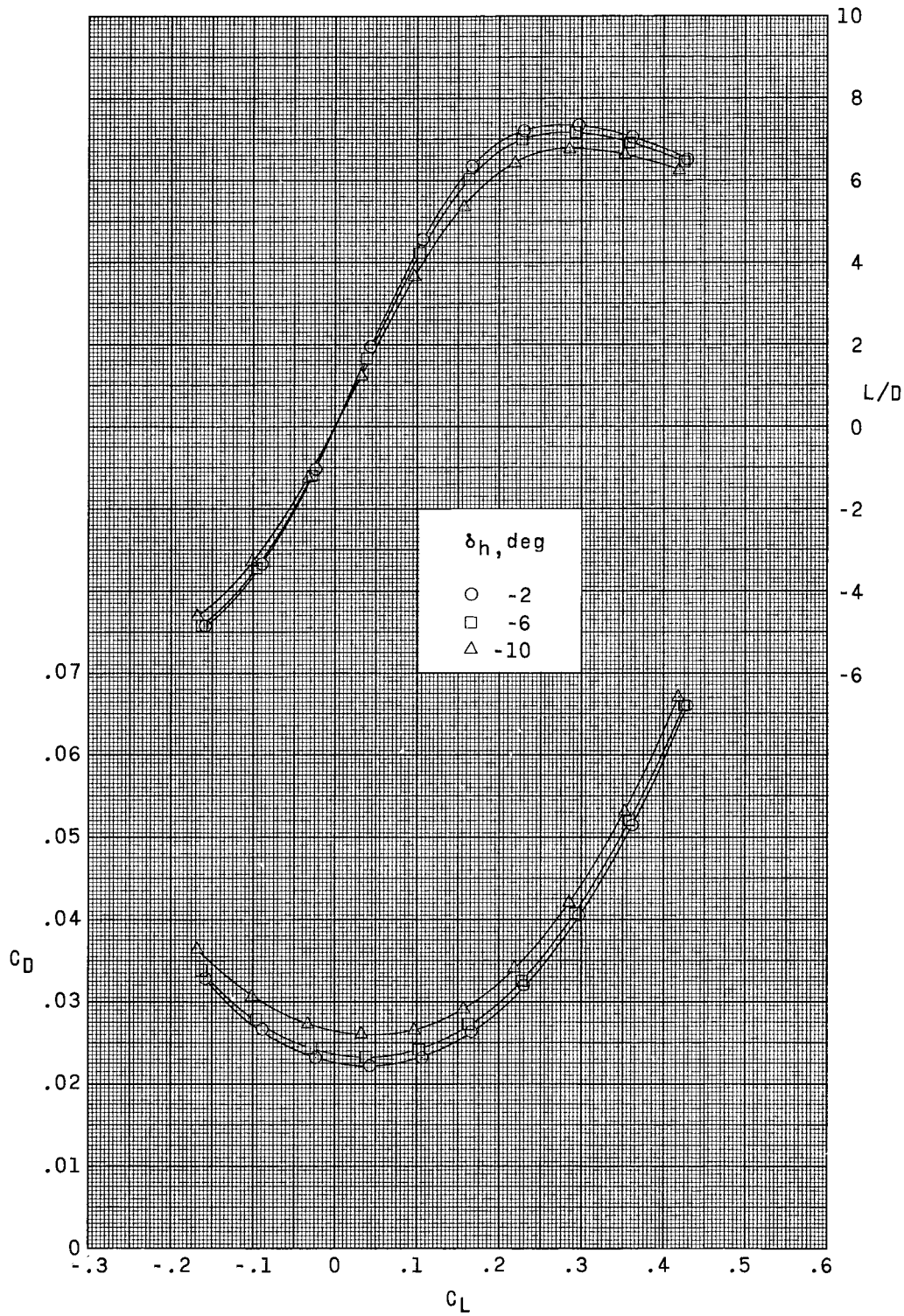

Figure 35.- Concluded.

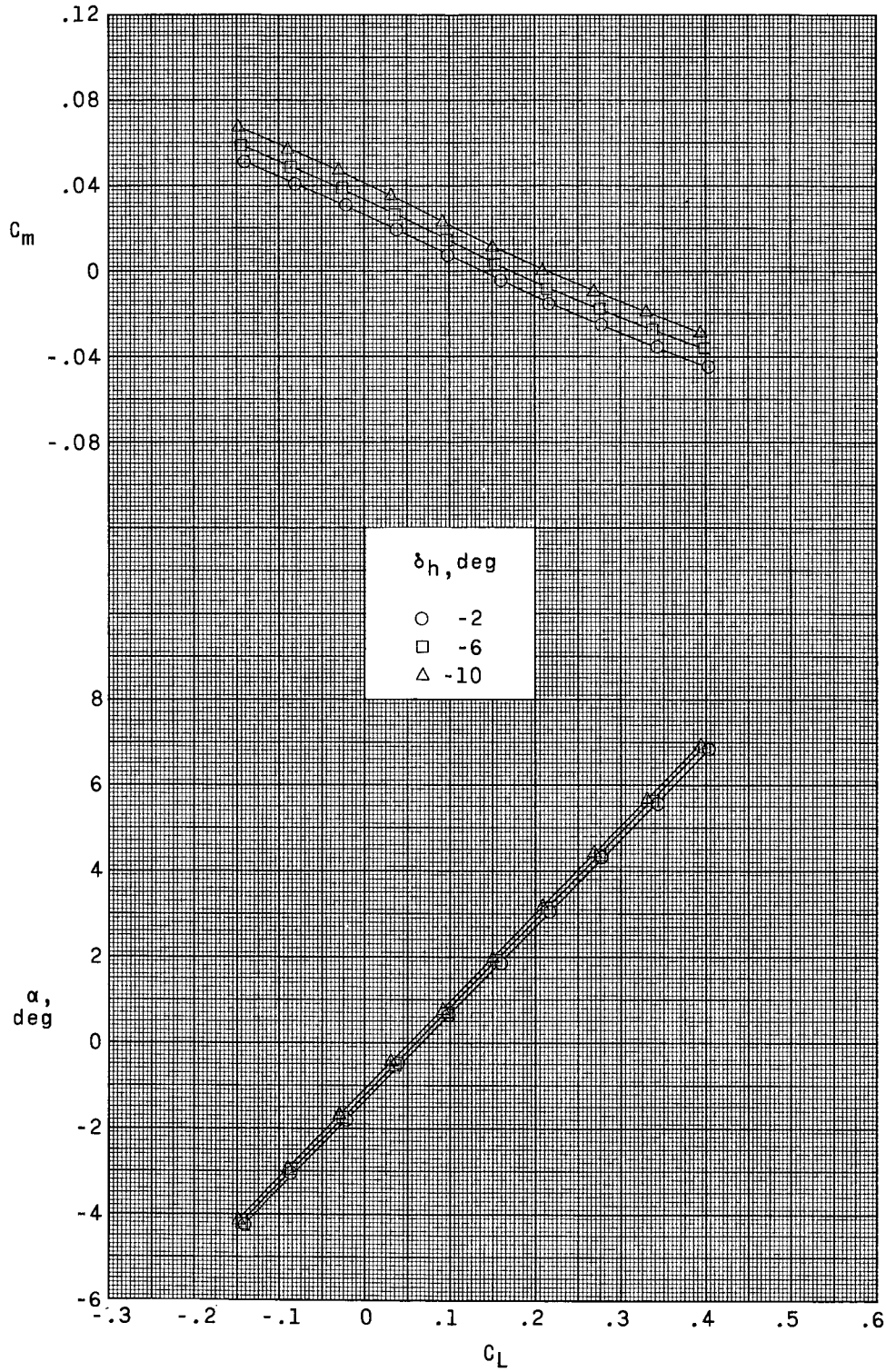

Figure 36.- Effect of horizontal-tail deflection on longitudinal aerodynamic characteristics at Mach number 1.30. $\Lambda = 55^\circ$.

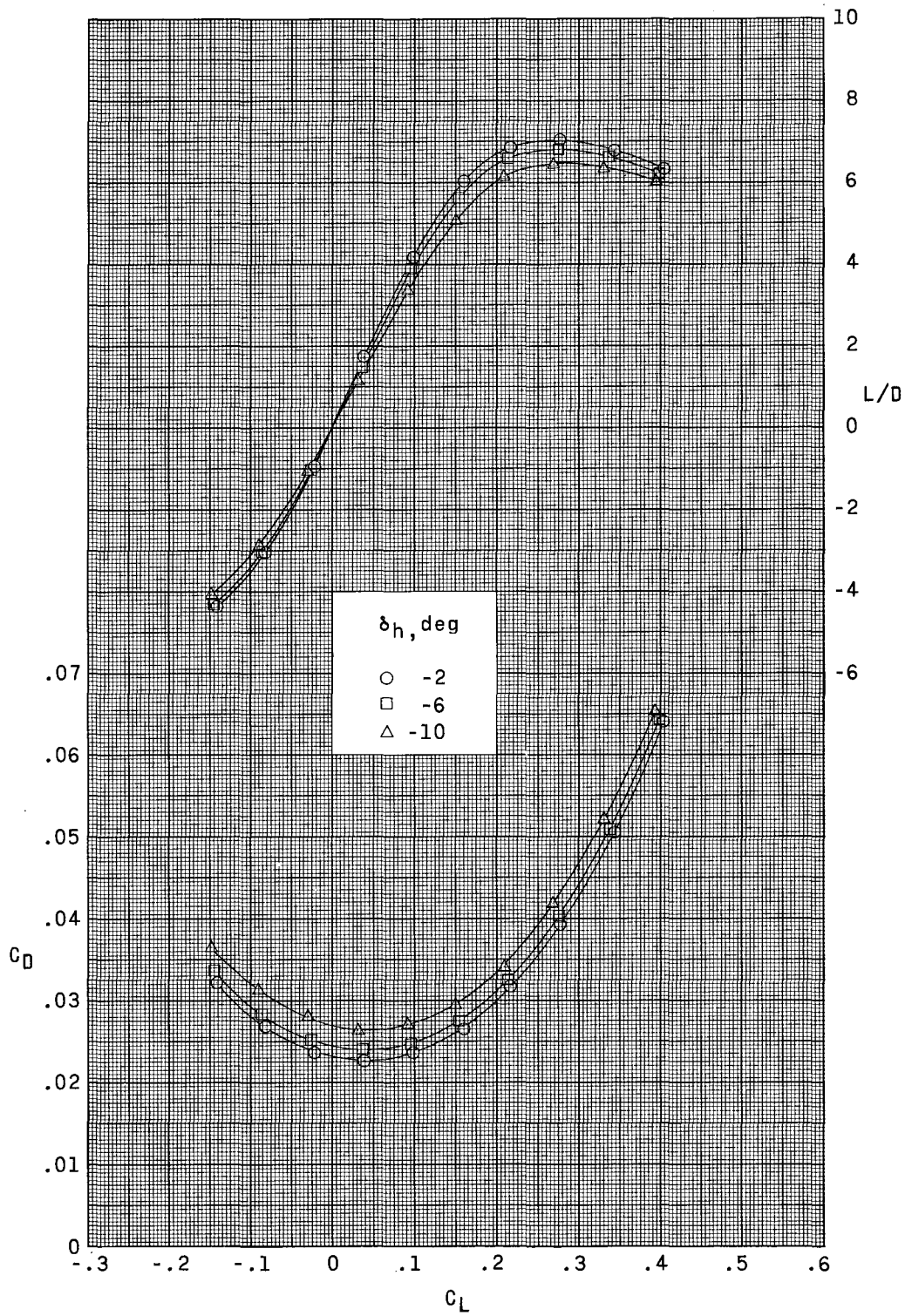

Figure 36.- Concluded.

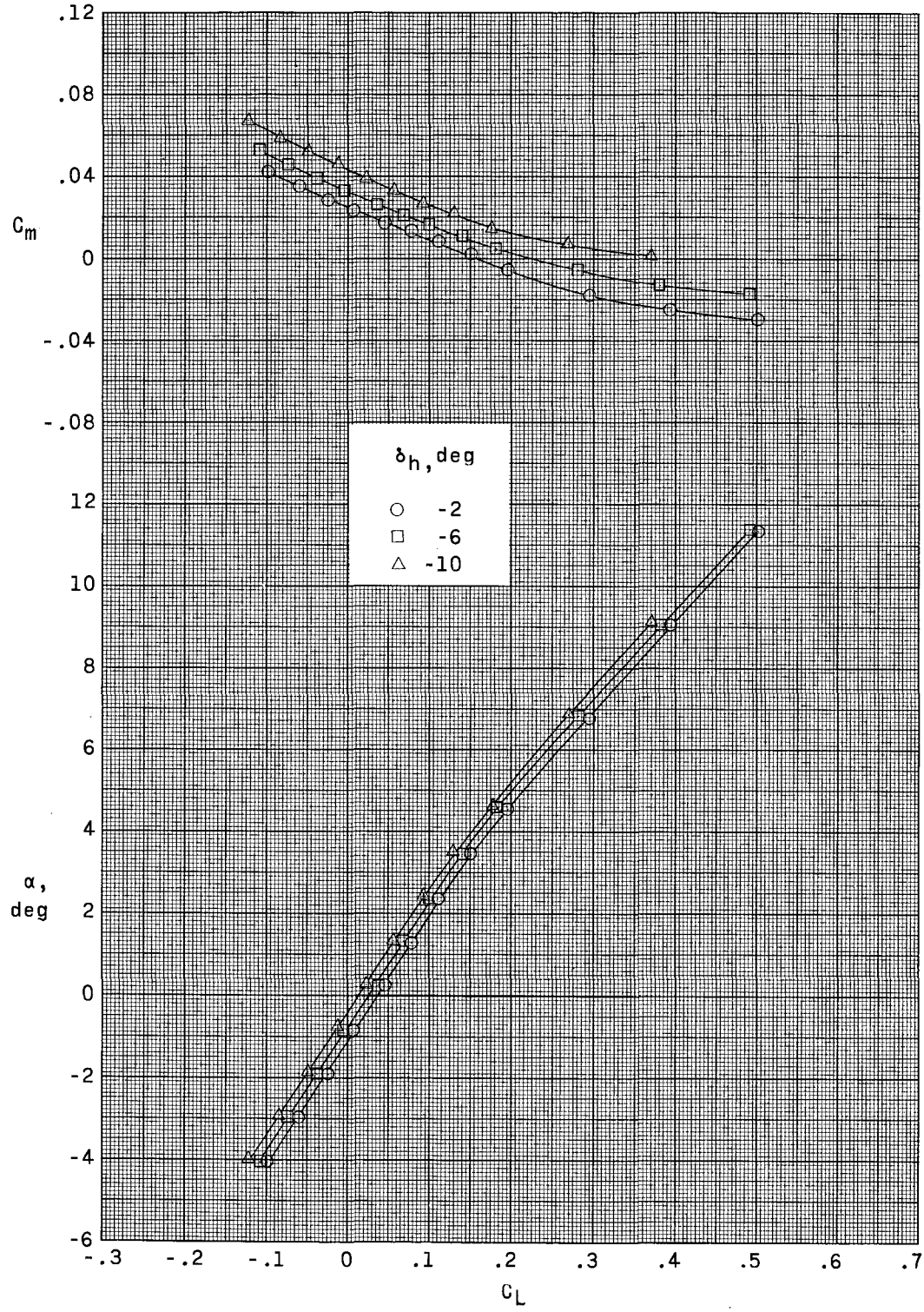

Figure 37.- Effect of horizontal-tail deflection on longitudinal aerodynamic characteristics at Mach number 0.50. $\Lambda = 75^{\circ}$.

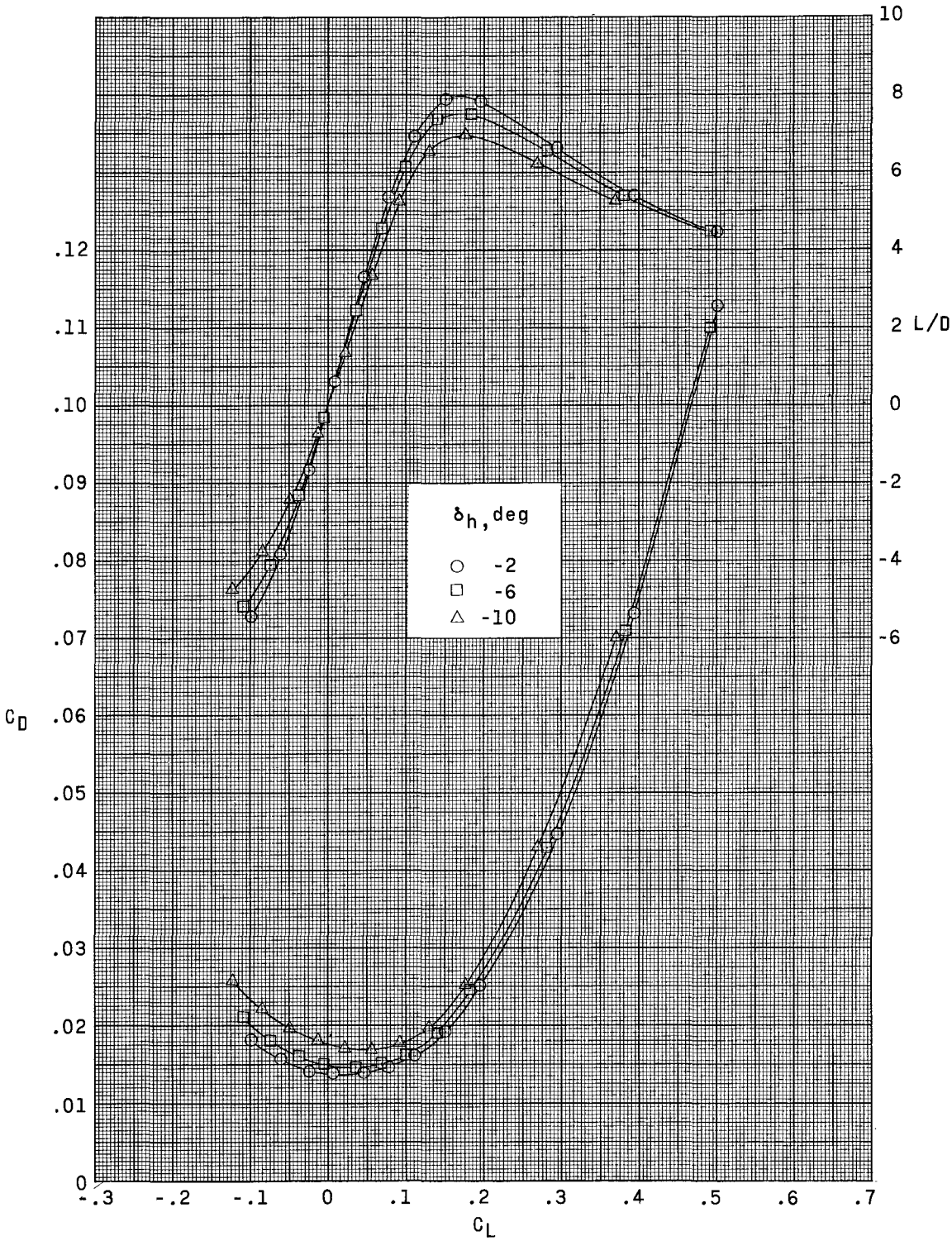

Figure 37.- Concluded.

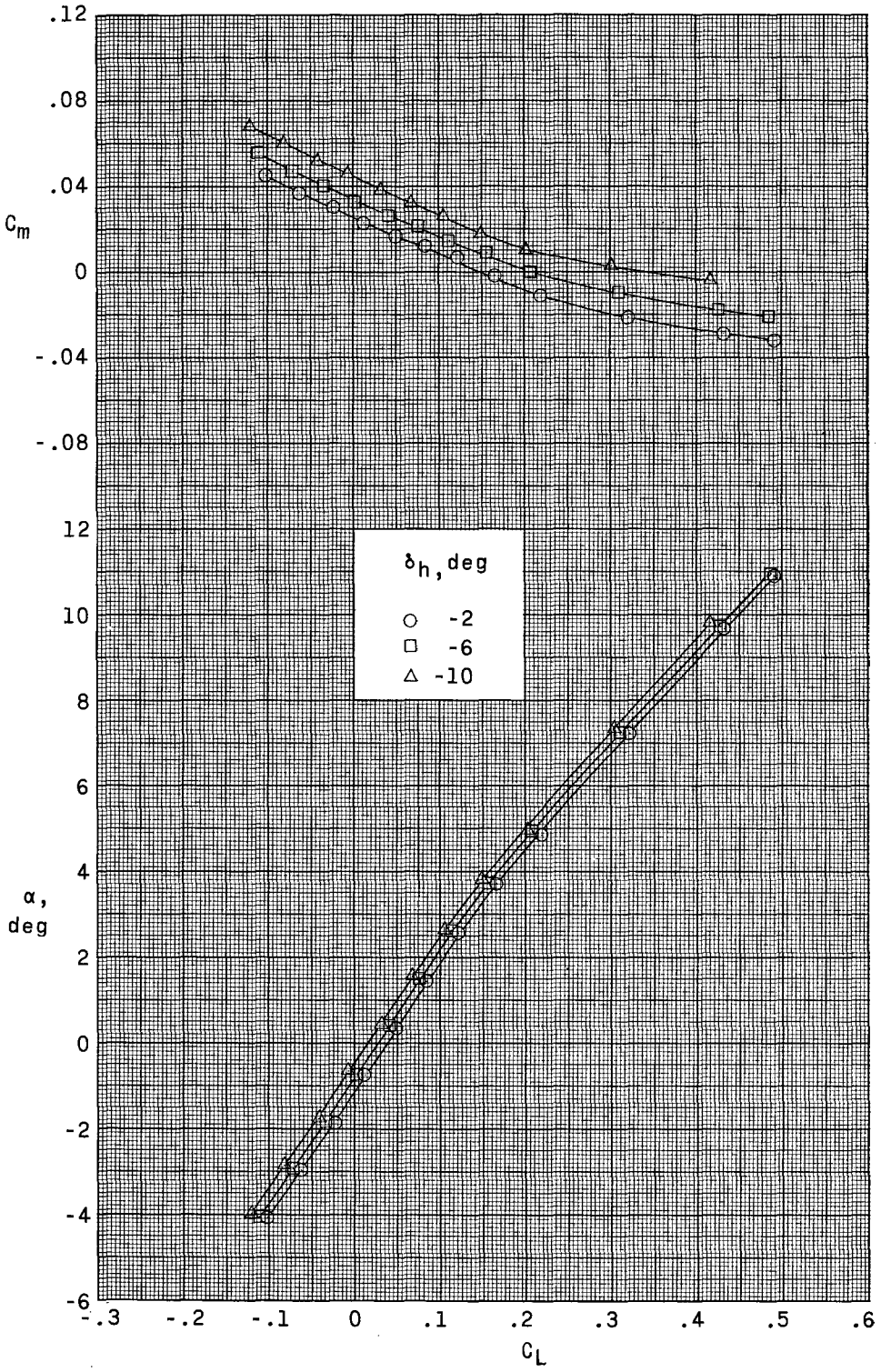

Figure 38.- Effect of horizontal-tail deflection on longitudinal aerodynamic characteristics at Mach number 0.80. $\Lambda = 75^\circ$.

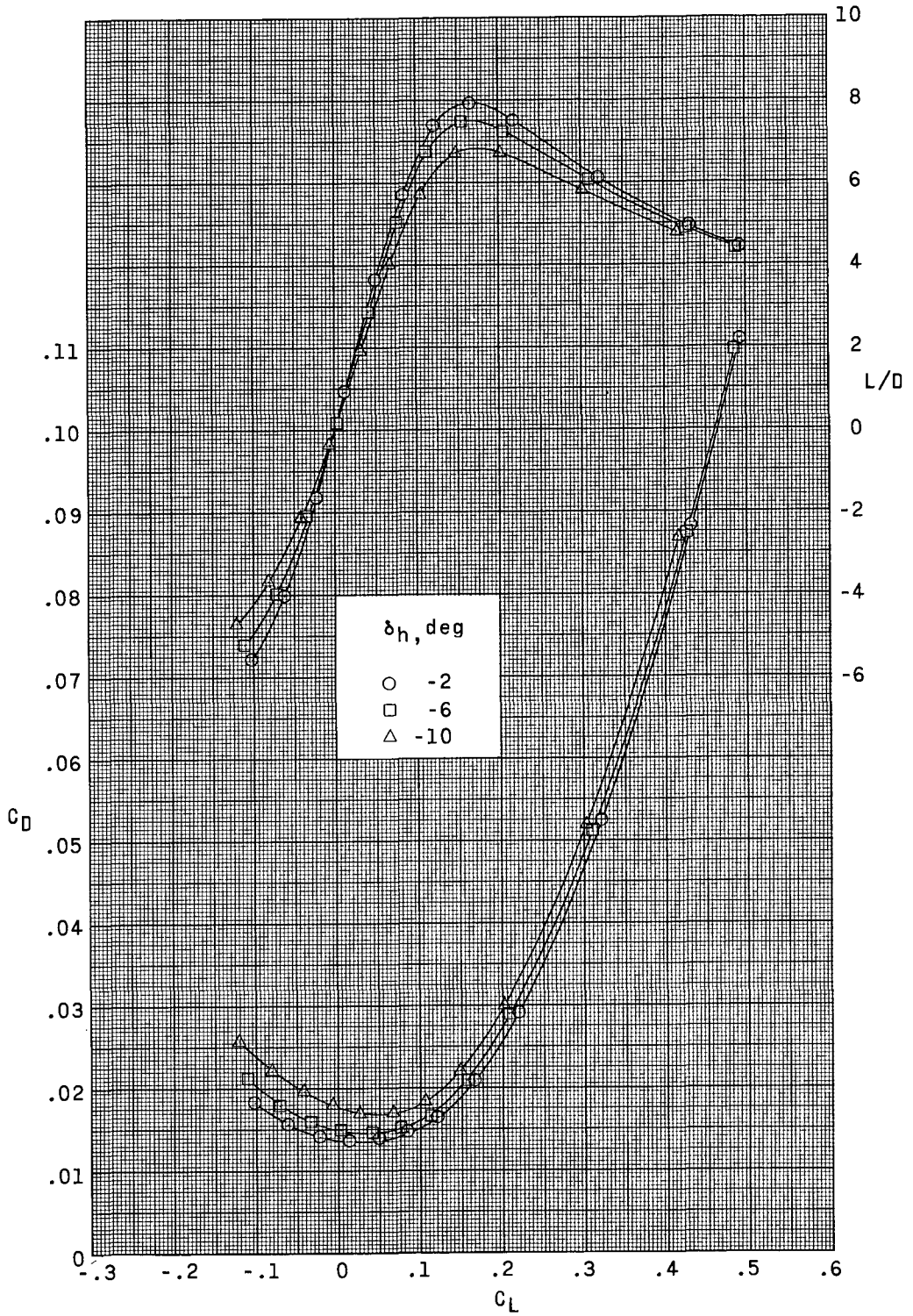

Figure 38.- Concluded.

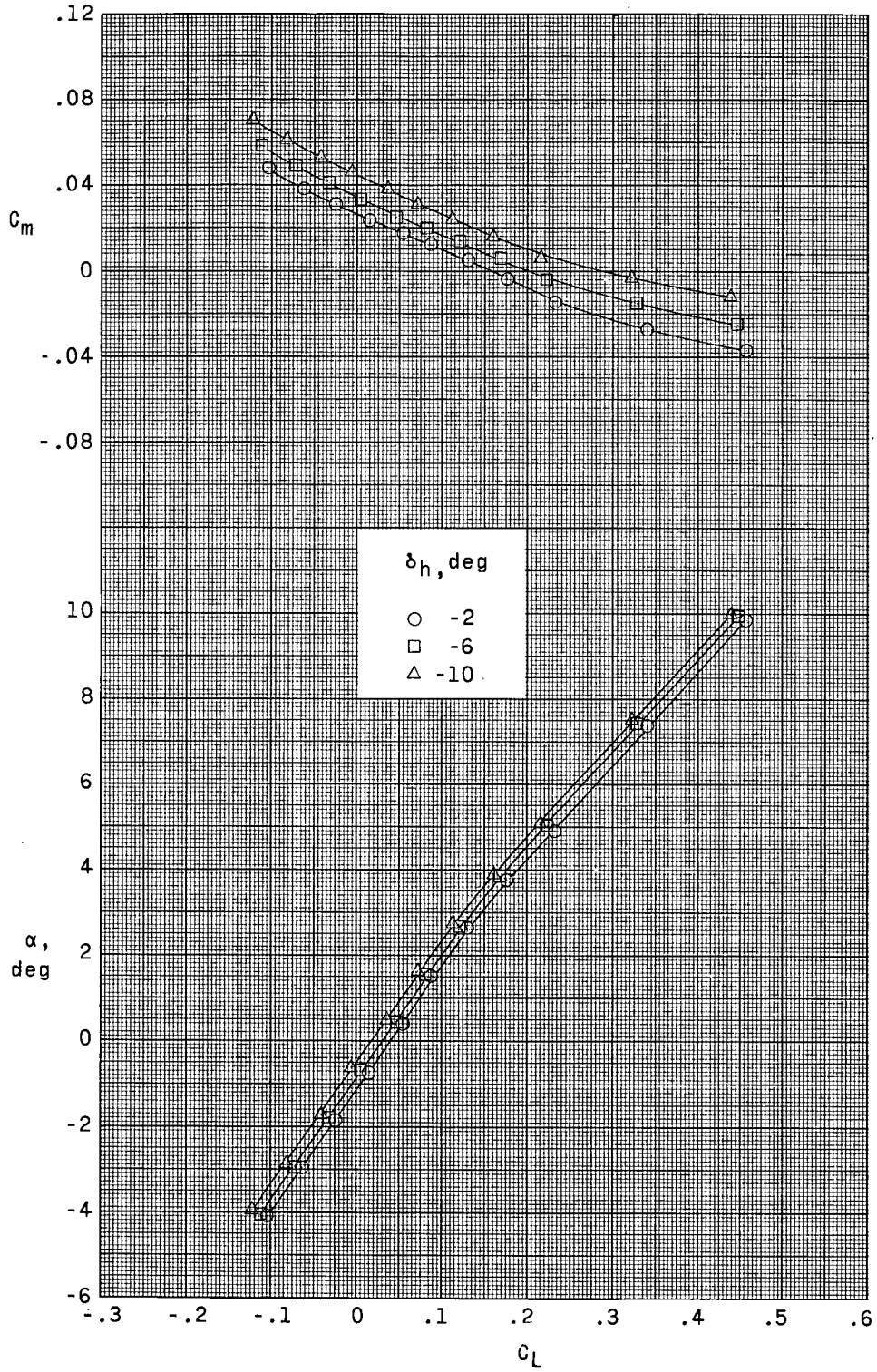

Figure 39.- Effect of horizontal-tail deflection on longitudinal aerodynamic characteristics at Mach number 0.90. $\Lambda = 75^{\circ}$.

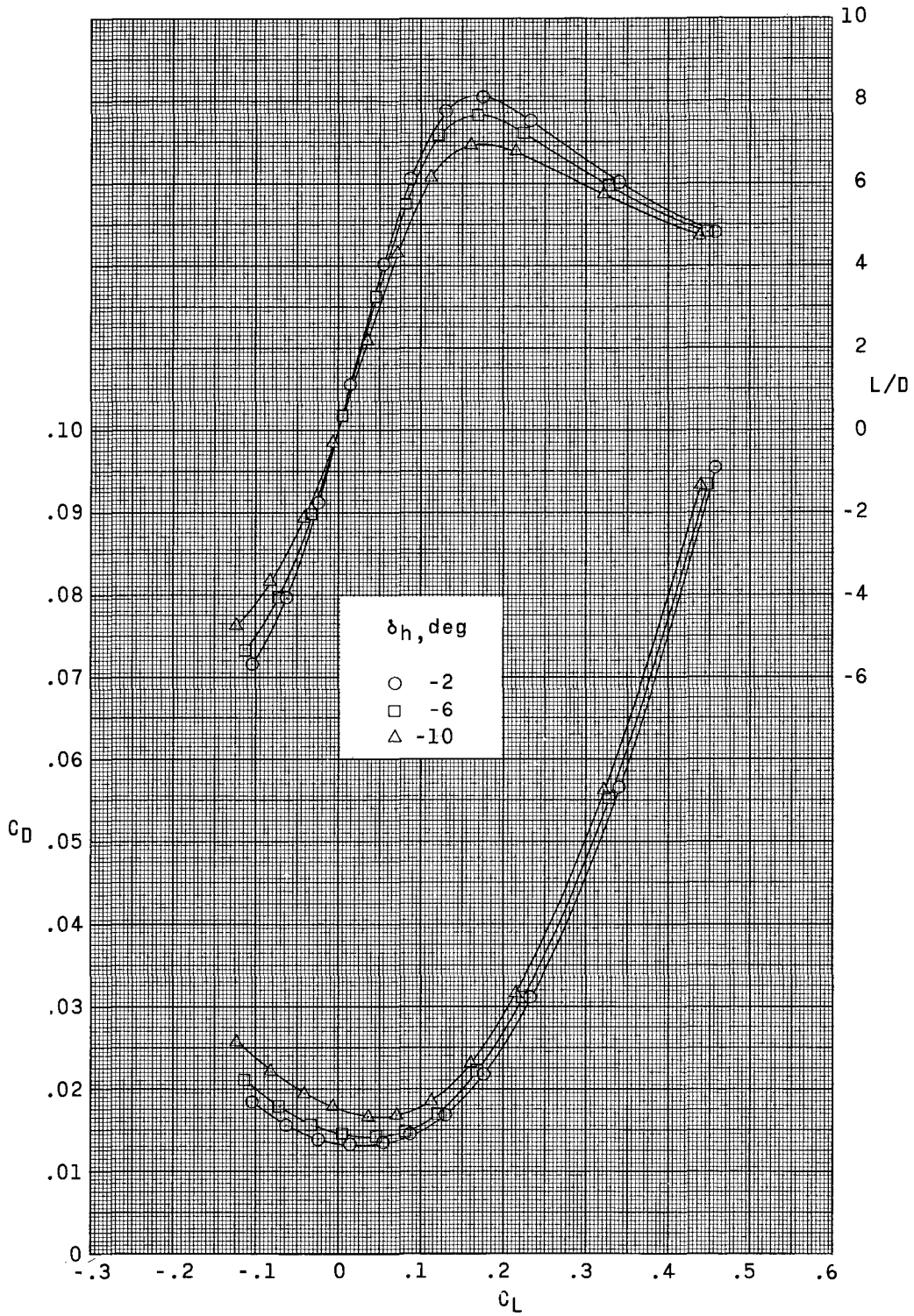

Figure 39.- Concluded.

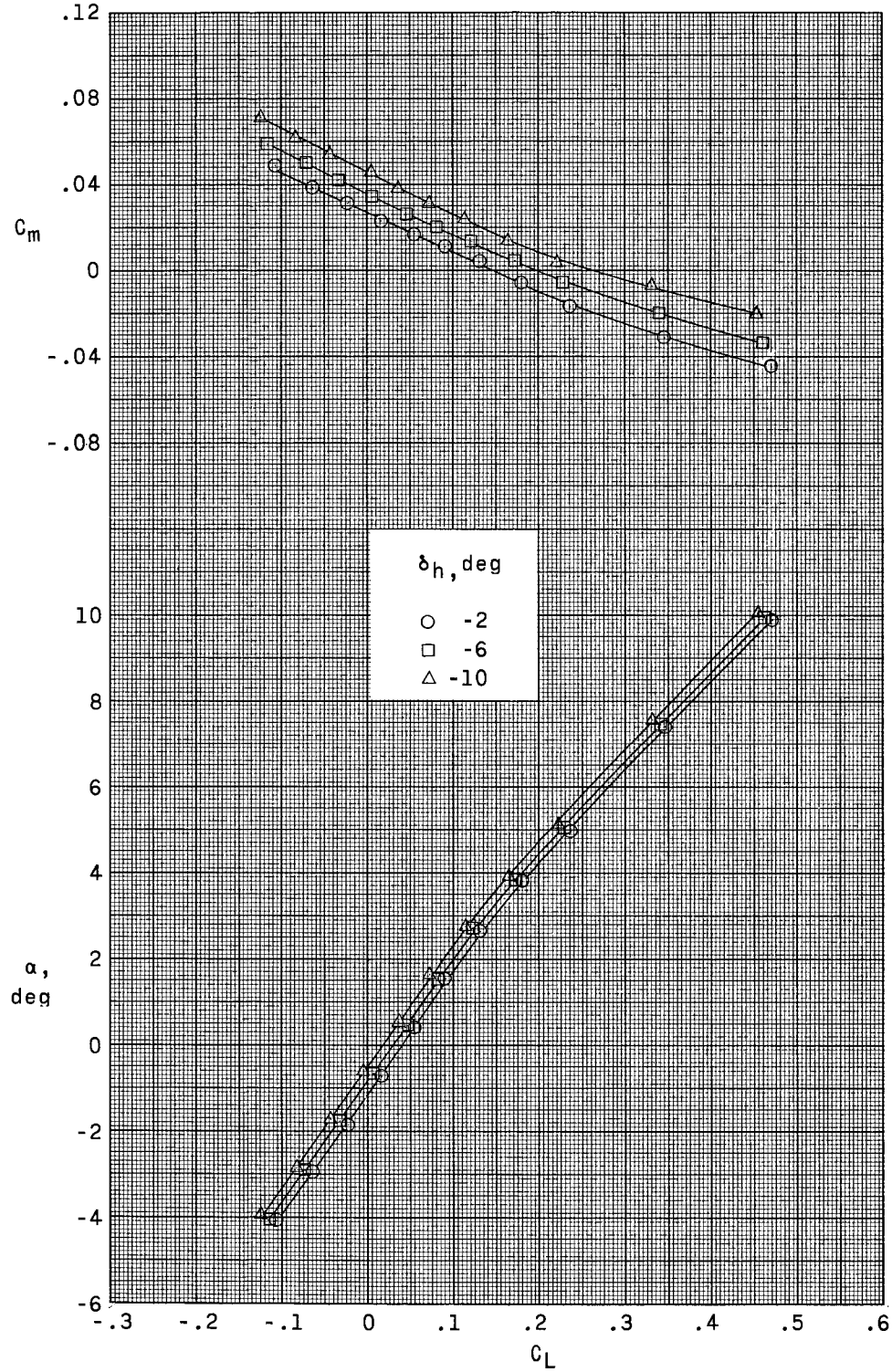

Figure 40.- Effect of horizontal-tail deflection on longitudinal aerodynamic characteristics at Mach number 0.94. $\Lambda = 75^{\circ}$.

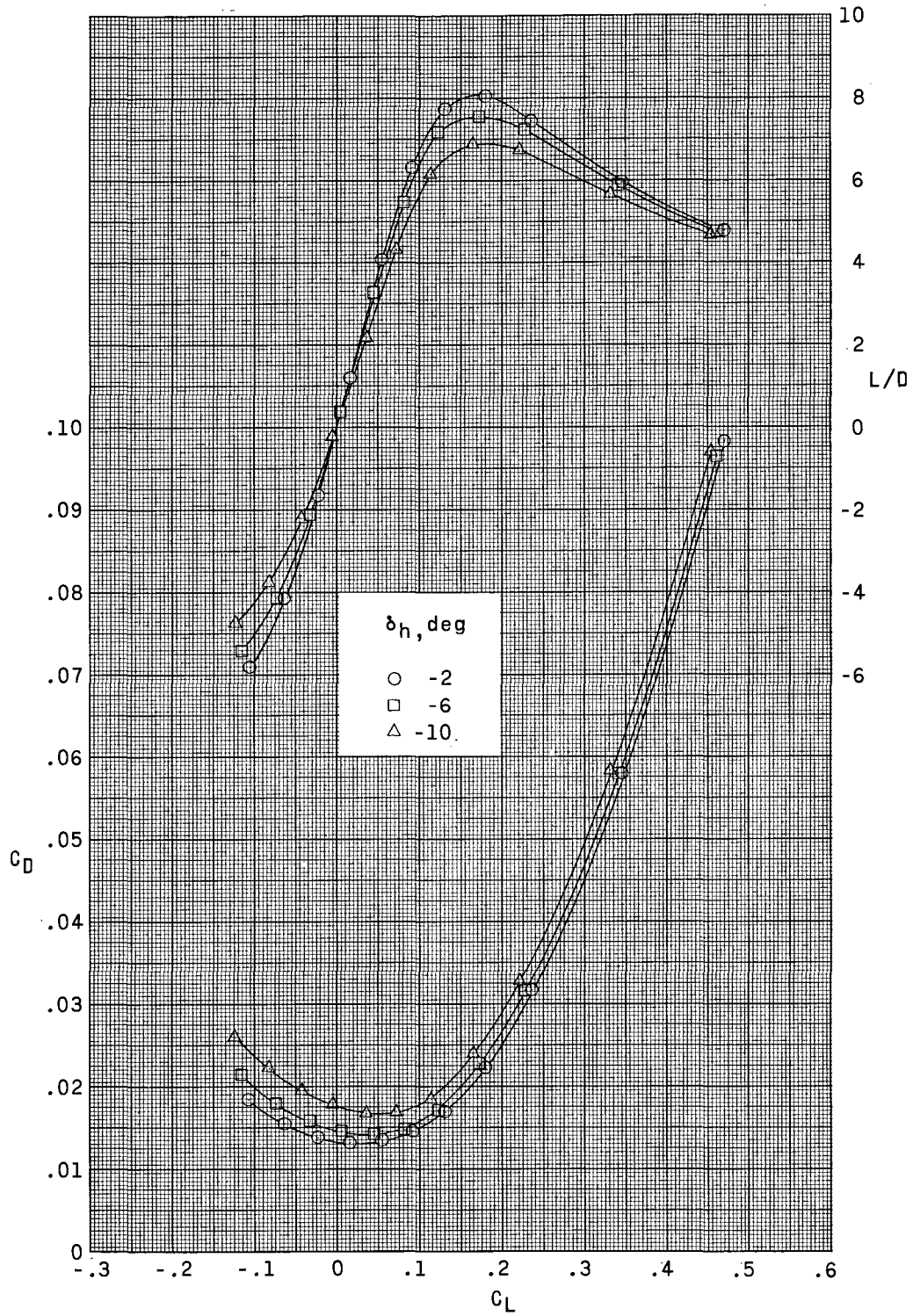

Figure 40.- Concluded.

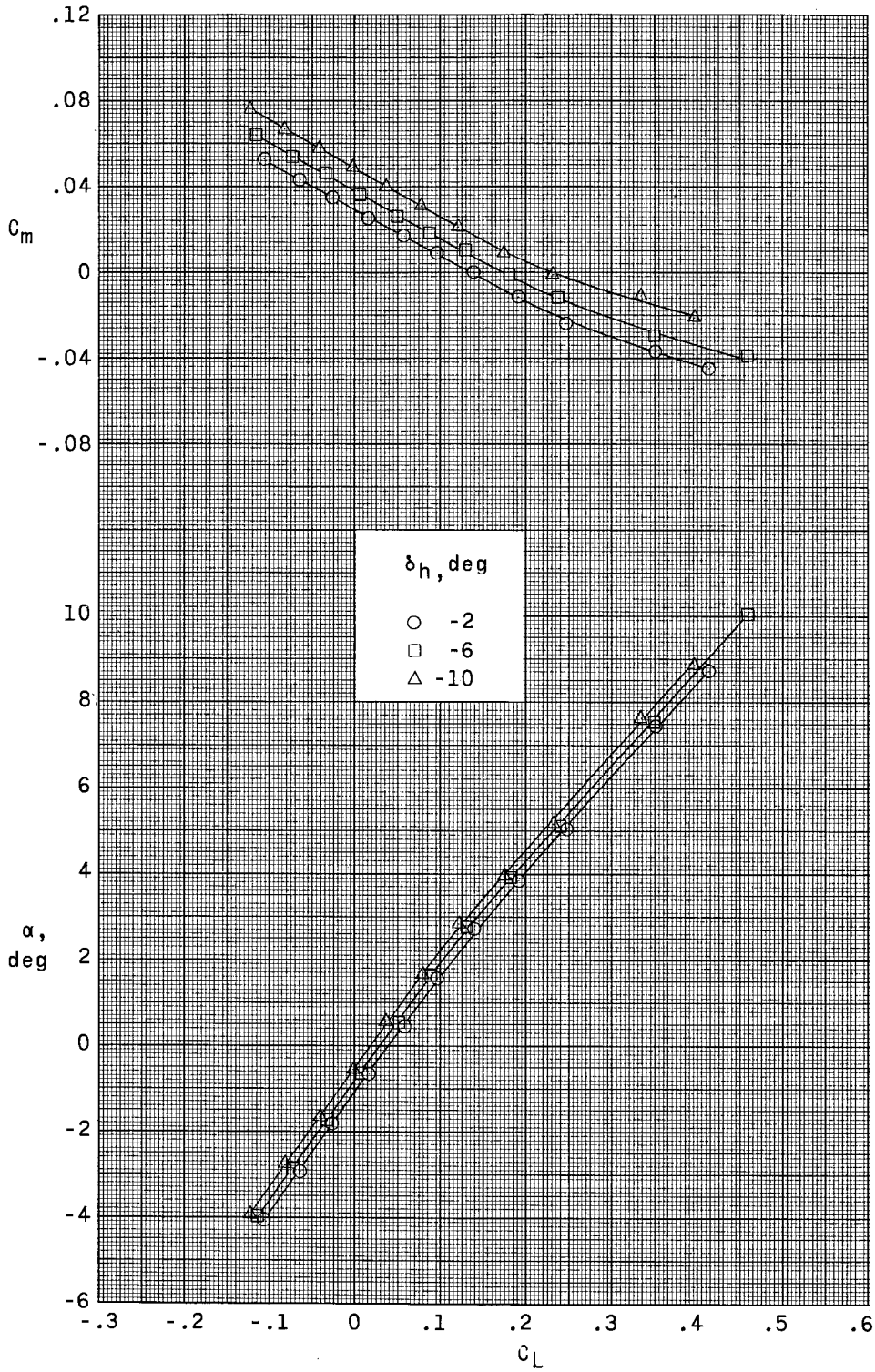

Figure 41.- Effect of horizontal-tail deflection on longitudinal aerodynamic characteristics at Mach number 1.03. $\Lambda = 75^{\circ}$.

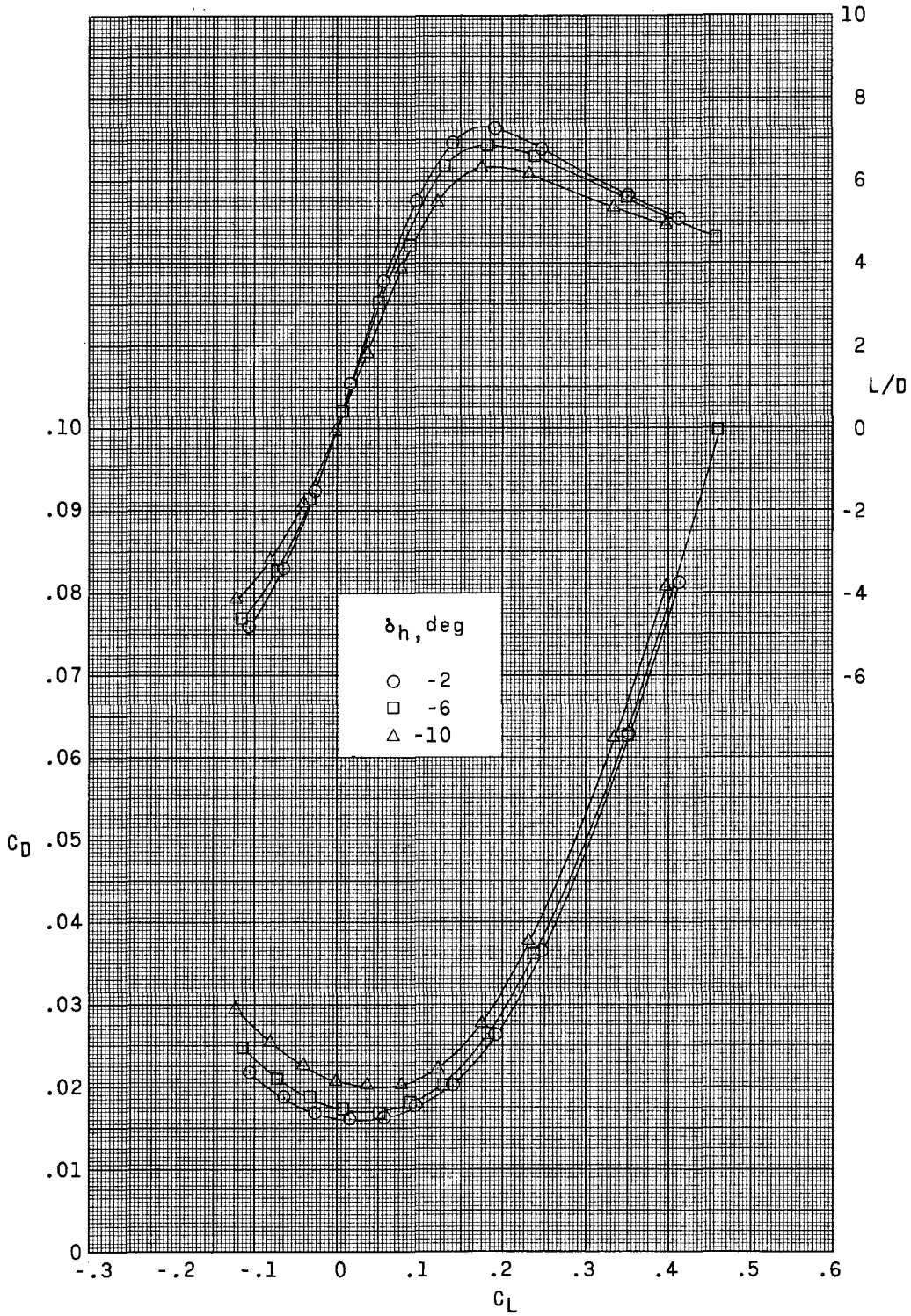

Figure 41.- Concluded.

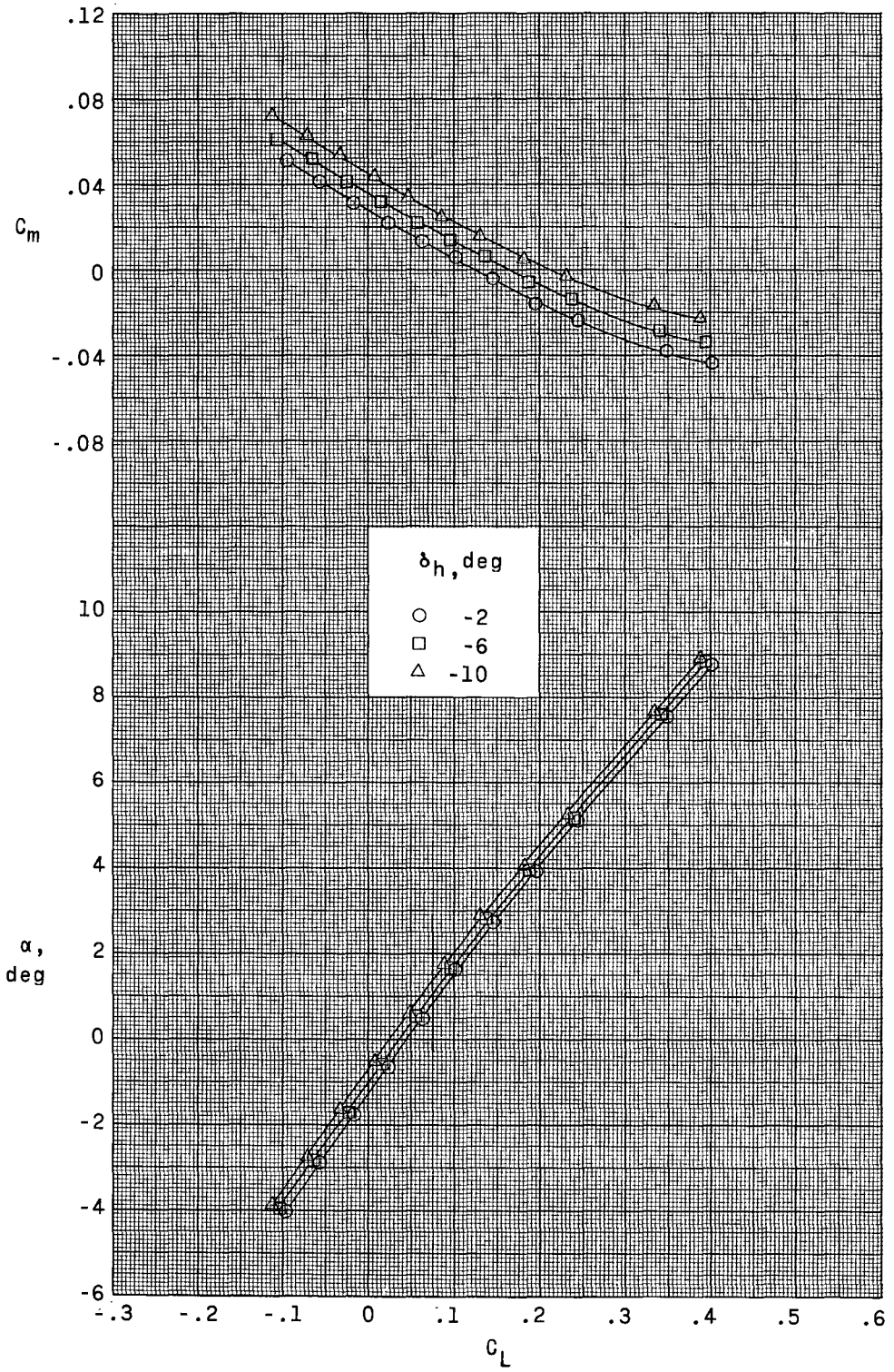

Figure 42.- Effect of horizontal-tail deflection on longitudinal aerodynamic characteristics at Mach number 1.20. $\Lambda = 75^{\circ}$.

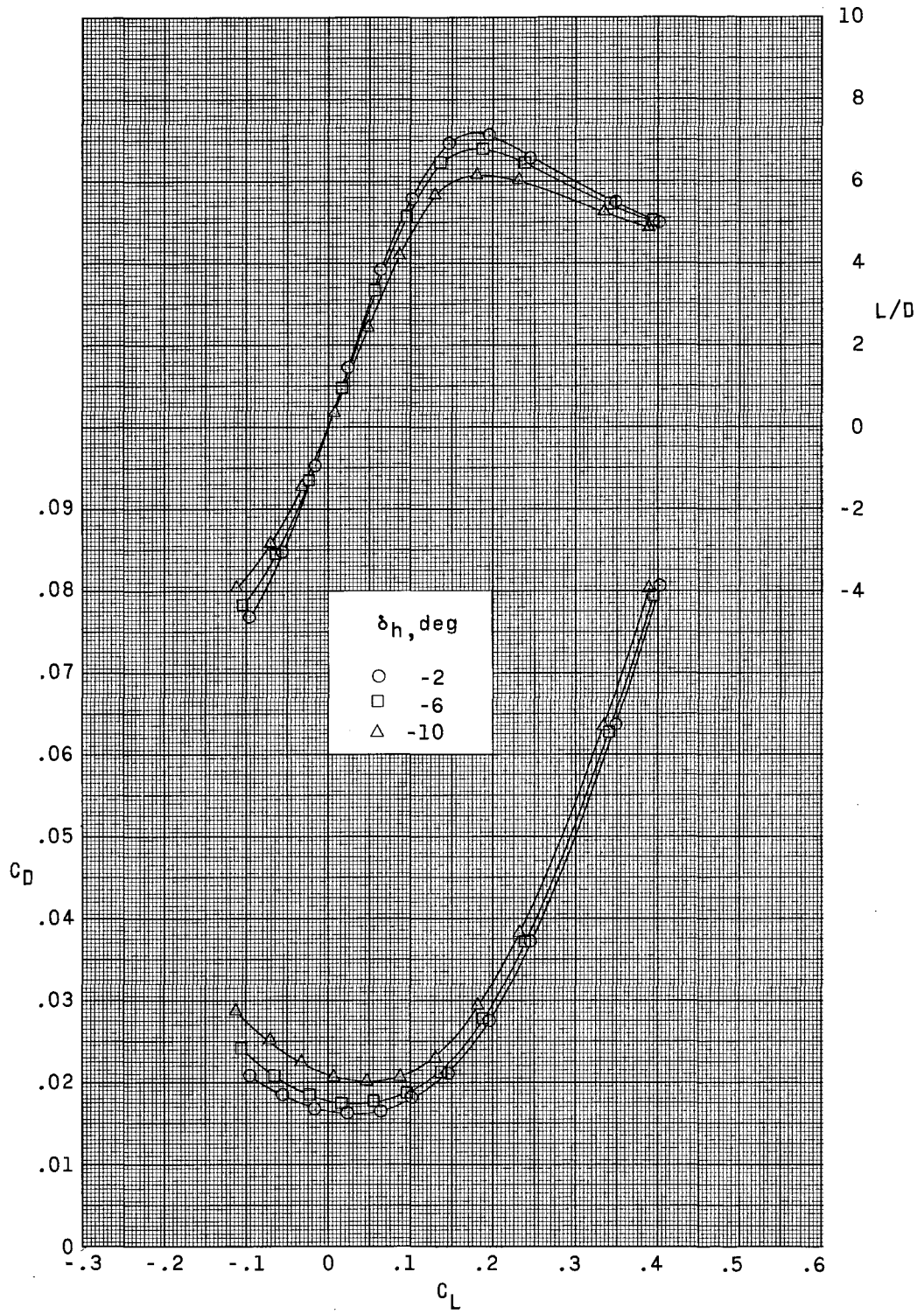

Figure 42.- Concluded.

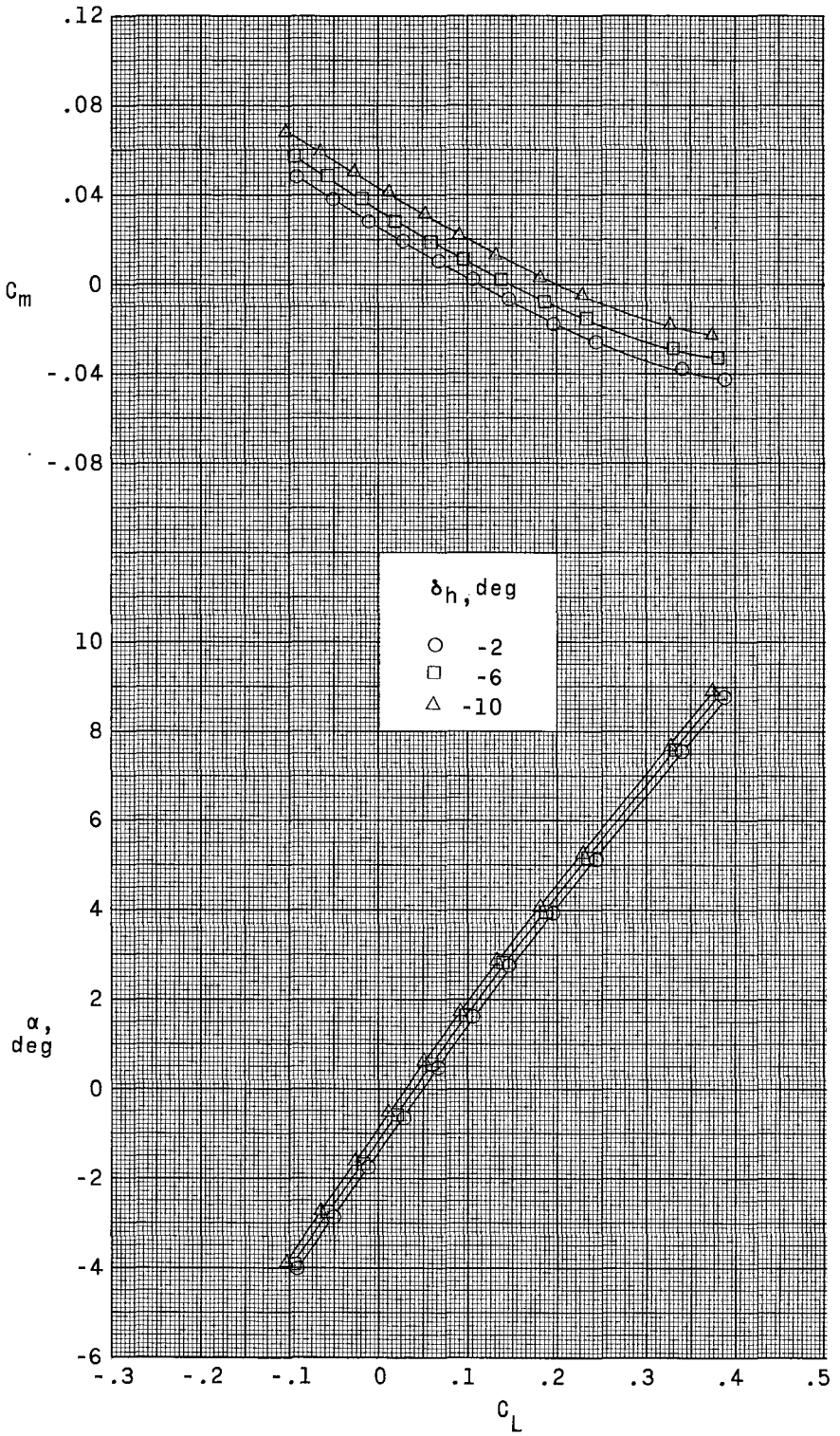

Figure 43.- Effect of horizontal-tail deflection on longitudinal aerodynamic characteristics at Mach number 1.30. $\Lambda = 75^{\circ}$.

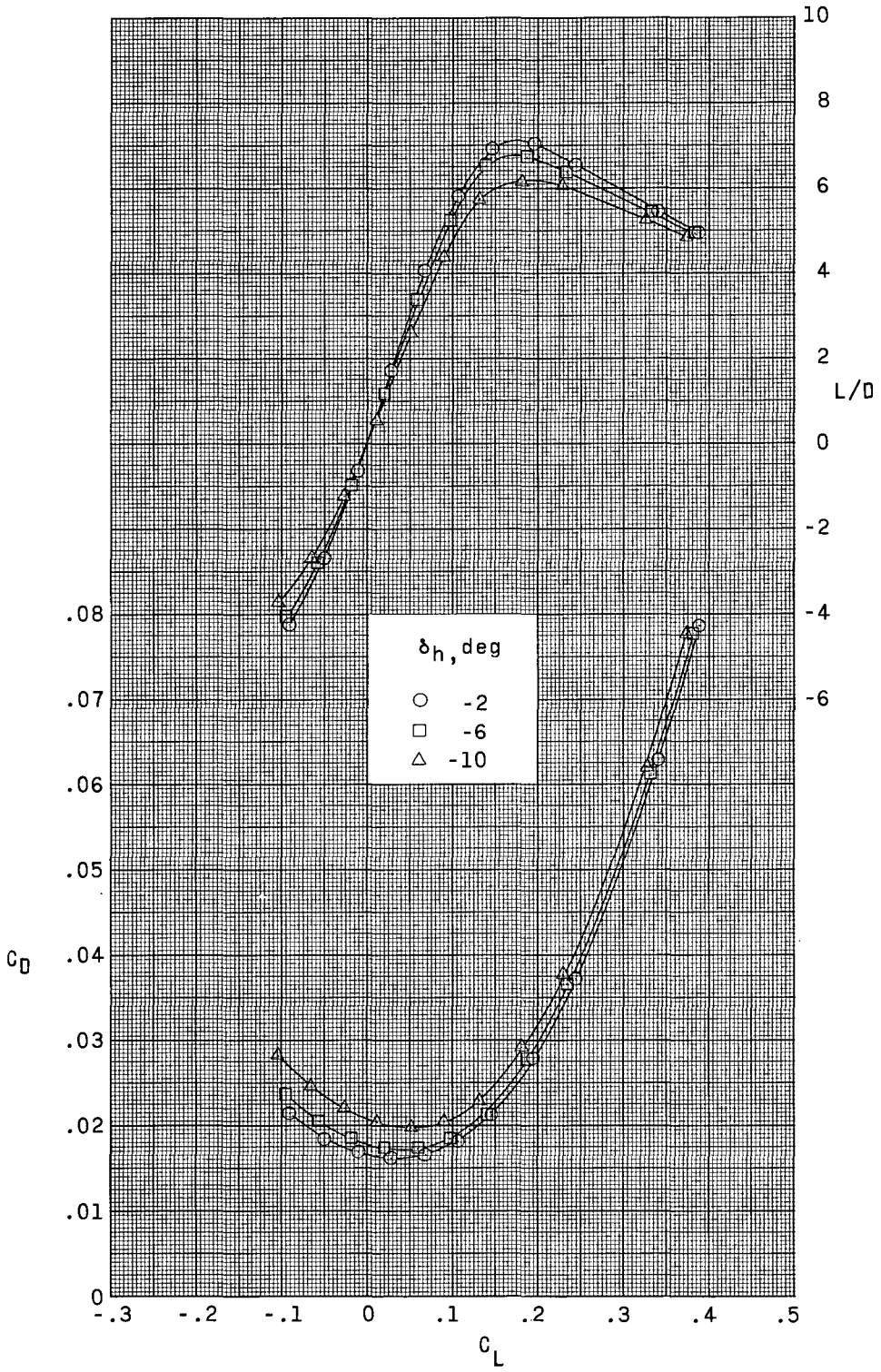

Figure 43.- Concluded.